NIST GCR 17-917-46v3

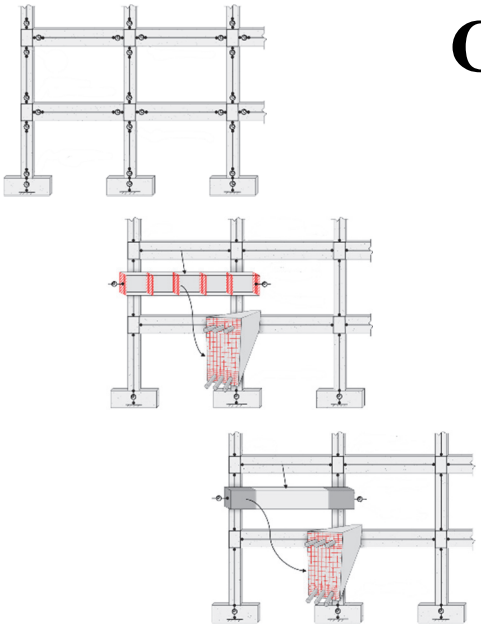

Guidelines for Nonlinear Structural Analysis for Design of Buildings

Part IIb – Reinforced Concrete Moment Frames

Applied Technology Council

This publication is available free of charge from:
https://doi.org/10.6028/NIST.GCR.17-917-46v3

nehrp

NIST
National Institute of Standards and Technology
U.S. Department of Commerce

Disclaimer

This report was prepared for the Engineering Laboratory of the National Institute of Standards and Technology (NIST) under Contract SB1341-13-CQ-0009, Task Order 13-497. The contents of this publication do not necessarily reflect the views and policies of NIST or the U.S. Government.

This report was produced by the Applied Technology Council (ATC). While endeavoring to provide practical and accurate information, the Applied Technology Council, the authors, and the reviewers assume no liability for, nor express or imply any warranty with regard to, the information contained herein. Users of information contained in this report assume all liability arising from such use.

Unless otherwise noted, photos, figures, and data presented in this report have been developed or provided by ATC staff or consultants engaged under contract to provide information as works for hire. Any similarity with other published information is coincidental. Photos and figures cited from outside sources have been reproduced in this report with permission. Any other use requires additional permission from the copyright holders.

Certain commercial software, equipment, instruments, or materials may have been used in the preparation of information contributing to this report. Identification in this report is not intended to imply recommendation or endorsement by NIST, nor is it intended to imply that such software, equipment, instruments, or materials are necessarily the best available for the purpose.

NIST policy is to use the International System of Units (metric units) in all its publications. In this report, however, information is presented in U.S. Customary Units (inch-pound), as this is the preferred system of units in the U.S. engineering industry.

Cover image – Three model idealizations (concentrated hinge, distributed plasticity, and fiber hinge) of a typical reinforced concrete moment-resisting frame system.

NIST GCR 17-917-46v3

Guidelines for Nonlinear Structural Analysis for Design of Buildings

Part IIb – Reinforced Concrete Moment Frames

Prepared for
U.S. Department of Commerce
Engineering Laboratory
National Institute of Standards and Technology
Gaithersburg, MD 20899-8600

By
Applied Technology Council
201 Redwood Shores Parkway, Suite 240
Redwood City, CA 94065

This publication is available free of charge from:
https://doi.org/10.6028/NIST.GCR.17-917-46v3

April 2017

U.S. Department of Commerce
Wilbur L. Ross, Jr., Secretary

National Institute of Standards and Technology
Kent Rochford, Acting NIST Director and Under Secretary of Commerce for Standards and Technology

Participants

National Institute of Standards and Technology

Steven L. McCabe, Acting NEHRP Director and Group Leader
Jay Harris, Research Structural Engineer
Siamak Sattar, Research Structural Engineer
Matthew S. Speicher, Research Structural Engineer
Kevin K. F. Wong, Research Structural Engineer
Earthquake Engineering Group, Materials and Structural Systems Division, Engineering Laboratory
www.NEHRP.gov

Applied Technology Council

201 Redwood Shores Parkway, Suite 240
Redwood City, California 94065
www.ATCouncil.org

Program Management

Jon A. Heintz (Program Manager)
Ayse Hortacsu (Associate Program Manager)
Veronica Cedillos (Associate Project Manager)

Program Committee on Seismic Engineering

Jon A. Heintz (Chair)
Michael Cochran
James R. Harris
James Jirsa
Roberto Leon
Stephen Mahin
James O. Malley
Donald Scott
Andrew Whittaker

Project Technical Committee

Curt Haselton (Project Director)
Wassim Ghannoum
Mahmoud Hachem
John D. Hooper
Santiago Pujol

Project Review Panel

Tony Ghodsi
Yuli Huang
Michael Mehrain
Farzad Naeim
John Wallace
Kent Yu (ATC Board Contact)

Working Group

Dustin Cook
Ian McFarlane
Hee Jae Yang

Preface

In September 2014, the Applied Technology Council (ATC) commenced a task order project under National Institute of Standards and Technology (NIST) Contract SB1341-13-CQ-0009 to develop guidance for nonlinear dynamic analysis (ATC-114 Project). The need for such guidance is identified as high-priority research and development topic (Proposed Research Initiative 6) in NIST GCR 14-917-27 report, *Nonlinear Analysis Research and Development Program for Performance-Based Seismic Engineering*, (NIST, 2013), which outlines a research and development program for addressing the gap between state-of-the-art academic research and state-of-practice engineering applications for nonlinear structural analysis, analytical structural modeling, and computer simulation in support of performance-based seismic engineering. In addition, the NIST GCR 09-917-2 report, *Research Required to Support Full Implementation of Performance-Based Seismic Design* (NIST, 2009) also identified the need to improve analytical models for buildings and their components in near-collapse seismic loading.

To help fill this gap, the ATC-114 Project developed a series of reports that provide general nonlinear modeling and nonlinear analysis guidance, as well as guidance specific to the following two structural systems: structural steel moment frames and reinforced concrete moment frames. This Part IIb report, referred to as *Guidelines* herein, provide practical guidance for nonlinear modeling and analysis specific to reinforced concrete moment-resisting frames and their components. It is a companion to *Part I Guidelines* (NIST, 2017) that provides general guidance on nonlinear analysis. Other Part II companion reports provide further details for selected system types.

This Part IIb document was developed by the members of the ATC-114 *Reinforced Concrete Moment Frames* project team. ATC is indebted to the leadership of Curt Haselton, who served as the Project Director, and to the members of the Project Technical Committee, consisting of Wassim Ghannoum, Mahmoud Hachem, John Hooper, and Santiago Pujol, for their contributions in developing this report and guiding the technical efforts of the Project Working Group, which included Dustin Cook, Ian McFarlane, and Hee Jae Yang. The members of the Project Review Panel, who were charged with reviewing the report during the various stages of development and ensuring that technical results were accurate, are also gratefully acknowledged. These individuals consisted of Tony Ghodsi, Yuli Huang, Mike Mehrain, Farzad Naeim, John Wallace, and Kent Yu (ATC Board Contact). The

names and affiliations of all who contributed to this report are provided in the list of Project Participants.

ATC also gratefully acknowledges Steven L. McCabe (Contracting Officer's Representative), Jay Harris, Siamak Sattar, Matthew Speicher, and Kevin Wong for their input and guidance throughout the project development process. ATC staff members Veronica Cedillos and Carrie Perna provided project management support and report production services, respectively.

Ayse Hortacsu
Associate Program Manager

Jon Heintz
Program Manager

Table of Contents

List of Figures

List of Tables

Chapter 1
Introduction and Scope

This *Part IIb Guidelines* document is intended to provide practical guidance for nonlinear modeling and analysis specific to the design of reinforced concrete moment-resisting frames and their components. It is a companion to NIST GCR 17-917-46v1, *Guidelines for Nonlinear Structural Analysis for Design of Buildings, Part I – General* (NIST, 2017) that provides general guidance on nonlinear analysis that is applicable to several types of building structural systems. Readers are referred to *Part I Guidelines* for an overall introduction and for guidance on general topics. Although much of the guidance provided in this document is generally applicable to concrete moment frames, the modeling criteria emphasize the seismic behavior of modern special reinforced concrete moment frames that adhere to current building code provisions for regions of high seismicity.

This *Part IIb Guidelines* document is meant to provide comprehensive guidelines for nonlinear analysis of special reinforced concrete moment frame structures, but it intentionally does not repeat material from other established standards and reference documents. Beyond the general reference standards cited in *Part I Guidelines*, this document is intended to build on the following documents:

- ASCE/SEI 7-16, *Minimum Loads for Buildings and Other Structures* (ASCE, 2017a)
- ASCE/SEI 41-13, *Seismic Rehabilitation of Existing Buildings* (ASCE, 2014).
- ACI 318-14*, Building Code Requirements for Structural Concrete and Commentary* (ACI, 2014)
- ACI 369R-11, *Guide for Seismic Rehabilitation of Existing Concrete Frame Buildings and Commentary* (ACI, 2011)
- NIST GCR 16-917-40, *NEHRP Seismic Design Technical Brief No. 1: Seismic Design of Reinforced Concrete Special Moment Frames: A Guide for Practicing Engineers* (NIST, 2016a)
- NIST GCR 16-917-42, *NEHRP Seismic Design Technical Brief No. 3: Seismic Design of Cast-in-Place Concrete Diaphragms, Chords, and Collectors: A Guide for Practicing Engineers* (NIST, 2016b)
- NIST GCR 10-917-5, *NEHRP Seismic Design Technical Brief No. 4: Nonlinear Structural Analysis for Seismic Design, A Guide for Practicing Engineers* (NIST, 2010)

The intended audience for these *Part IIb Guidelines* is engineering practitioners, who are familiar with the concepts and limitations of nonlinear structural analysis, and who desire more detailed guidance on modeling of special reinforced concrete moment frame buildings. Similarly, the objective is not to cover basic principles of nonlinear analysis, but rather to provide nonlinear modeling guidance to practitioners who are already experienced with these topics. These *Part IIb Guidelines* are written considering the analysis software capabilities that are currently available to practitioners, but also with a view towards emerging techniques that will become available in the future.

Chapter 2 of this document provides an overview of expected structural behavior and failure modes for special reinforced concrete moment frame buildings and Chapter 3 provides many of the general modeling guidelines. Chapters 4-6 provide specific guidelines for concentrated hinge component models (Chapter 4), fiber-type models (Chapter 5), and continuum finite element models (Chapter 6). In addition, Appendix A of this document provides a brief overview of available resources that can be used in conjunction with this document to model nonductile reinforced concrete frames. An example application is provided in Appendix B to illustrate the use of these *Part IIb Guidelines* for a case-study building.

Chapter 2

Structural Behavior and Failure Modes

This chapter discusses the behavior and potential failure modes of concrete moment frames subjected to seismic demands. Identifying and understanding these issues is critical for an analyst to develop computational models that capture all relevant behavior.

2.1 Overview of Frame Behavior

Figure 2-1 illustrates the various components of a concrete moment frame, including the columns, beams, beam-column joints, and foundation elements.

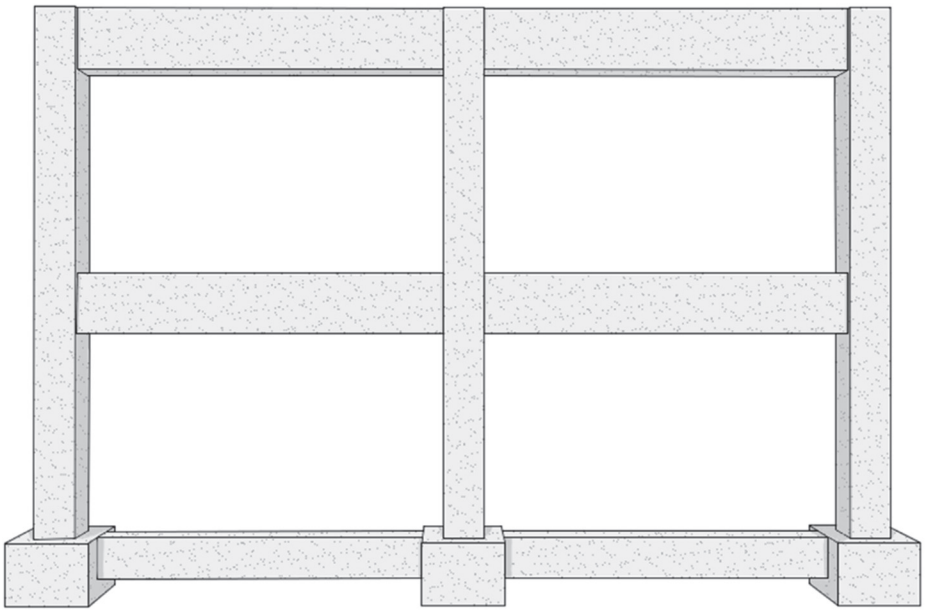

Figure 2-1 Overview of a typical reinforced concrete moment-resisting frame system and components.

In seismically designed moment frames, capacity design is employed to channel inelastic flexural deformations to the end hinge regions of beams, while limiting inelastic deformations in columns, joints, and foundations. A strong-column weak-beam design is employed to focus inelastic deformations in beams and protect columns, as well as beam-column joints from excessive damage. The strong-column weak-beam design approach, however, does not preclude inelastic deformations in columns, as higher mode effects and damage sequences can result in columns

experiencing significant inelastic demands. Foundations in seismically designed structures are designed to be stronger than the columns they support and force inelastic rotations in the columns.

Seismic detailing and capacity design principles are also intended to ensure ductile flexural yielding and preclude the less desirable failure modes such as shear and anchorage failures. Seismically detailed frame members will typically initiate loss of lateral strength at relatively large deformations, through flexural failure modes such as buckling and fracture of longitudinal bars, and crushing of the concrete core.

In non-seismically detailed frames, or in frames not adequately designed to resist their full seismic demands, any failure mode can be expected whether ductile or not. Premature failures can cause significant strength losses and structural instability that need to be addressed in analyses. Possible failure modes in non-seismically detailed frames include: anchorage failures of longitudinal bars, lap-splice failures, shear failures, interface shear failures, premature buckling of longitudinal bars, and crushing of the concrete core due to inadequate confinement. In rare instances, particularly in bridge construction, torsional failures may occur.

Over the past few decades, expected seismic hazard levels were increased across the United States, while the seismic design and detailing procedures have been greatly improved. In the 1980s, substantial improvements in the seismic design methodologies of concrete structures were introduced in the United States. Structures designed and built prior to that era typically do not have sufficient strength or adequate seismic detailing to limit seismically-induced deformations and ensure sufficient deformation capacity. On the other hand, structural systems designed to current hazard levels and design procedures are expected to withstand their expected seismic hazard levels with limited loss of lateral strength.

ACI 318-14, *Building Code Requirements for Reinforced Concrete* (ACI, 2014), specifies three seismic design levels for moment-resisting frames based on site seismicity: (1) Ordinary Moment Frames (OMF); (2) Intermediate Moment Frames (IMF); and (3) Special Moment Frames (SMF). OMF are designed with limited detailing and capacity design requirements for regions of low seismicity. For example, the shear strength of beams in OMF is not required to exceed the shear demand associated with the development of the probable moment strength at member ends. Older non-seismically designed frames built prior to the 1980s are typically detailed similarly to OMF. IMF have additional detailing and capacity design requirements over OMF, and are prescribed for regions of moderate seismic hazard. SMF are designed to achieve ductile responses up to the relatively large design drift levels (typically in the range of 3 to 4% of a story height). Consequently, if OMF or frames built prior to the advent of seismic detailing are overloaded during a seismic event, a wide range of strength-degradation modes can occur. If IMF or SMF are

overloaded, however, a limited subset of failure mechanisms can be expected. Table 2-1 indicates the likelihood of occurrence of phenomena causing strength degradation for frames whose characteristics fall into one of the three design levels discussed. It is important to recognize that these associations are approximate and only intended to provide guidance about what type of response is likely to be encountered. Ultimately, the specific characteristics of each structure must be evaluated to determine which modes of behavior are likely to occur and should be modeled in design.

ACI 318-14, ASCE/SEI 41-17, *Seismic Evaluation and Retrofit of Existing Buildings* (ASCE, 2017b), and ACI 369R-17, *Guide for Seismic Rehabilitation of Existing Concrete Frame Buildings and Commentary* (ACI, 2017), provide strength and detailing provisions to determine the weakest link in frame members that will likely fail first and generate the associated strength-degradation mode. ASCE/SEI 41-17 and ACI 369R-17 further provide modeling parameters for nonlinear analyses that define the lateral load versus lateral deformation response of frame members of all three frame categories. The modeling parameters provided in these documents account for the expected modes failure of members, however, some can be overly conservative and the documents do not define the cyclic parameters necessary to model the full hysteretic lateral behavior of frame members.

This document provides guidance on conducting nonlinear analyses of reinforced concrete frames satisfying the Special Moment Frame (SMF) designation of ACI 318-14. It also delivers guidance for defining the backbone, as well as cyclic lateral force versus lateral deformation relations for SMF. The following sections in this chapter discuss aspects of the seismic behavior of SMF that need to be considered in nonlinear analyses. Appendix A provides some general guidelines and references for modeling nonductile reinforced concrete frames.

2.2 Stiffness and Deformation of Components

Accurately modeling the lateral stiffness of structural systems is critical to achieving accurate estimates of the natural periods of vibration of a structure and the associated drift and force demands.

The stiffness of reinforced concrete members is highly dependent on loading history. Prior to flexural yielding or significant damage, flexural cracking spreads as lateral loads and drifts increase, and causes significant reductions in the effective lateral stiffness of members (Figure 2-2). Shear cracks also tend to widen resulting in the softening of the shear response as lateral force demands increase.

Table 2-1 Behavioral Effects to Consider in Nonlinear Analysis

Component	*Nonlinear Response Phenomena*	Structural System Types: *SMF*	*IMF*	*OMF / non seismic*
Beams of Moment Frames	Flexural yielding followed by **gradual lateral-strength** deterioration due to flexural failure modes, i.e., longitudinal bar buckling and/or concrete core deterioration	■	▨	▨
	Flexural yielding followed by **rapid lateral-strength deterioration** due to flexural failure modes, i.e., longitudinal bar buckling/fracture and/or concrete core deterioration		▨	■
	Flexural yielding followed by **rapid lateral-strength deterioration** due to brittle failure modes, i.e., shear failure, anchorage failure, splice failure, and/or sudden loss of confinement caused by ties opening or fracturing		▨	■
	Rapid lateral-strength deterioration prior to flexural yielding due to shear failure, anchorage failure, and/or splice failure		▨	■
	Beam elongation due to yielding and resulting effects on restraining slab	■	■	■
Columns of Moment Frames	Flexural yielding followed by **gradual lateral-strength deterioration** due to flexural failure modes, i.e., bar buckling and/or concrete core deterioration	■	▨	▨
	Flexural yielding followed by **rapid lateral-strength deterioration** due to flexural failure modes, i.e., longitudinal bar buckling/fracture and/or concrete core deterioration; more likely with higher axial load		▨	■
	Flexural yielding followed by **rapid lateral-strength deterioration** due to brittle failure modes, i.e., shear failure, anchorage, splice failure, and/or sudden loss of confinement caused by tie opening/fracturing; more likely with higher axial load		▨	■
	Flexural yielding followed by **axial-strength deterioration** due to flexural failure modes, i.e., longitudinal bar buckling/fracture and concrete core deterioration; more likely with higher axial load	▨	■	■
	Flexural yielding followed by **axial-strength deterioration** due to brittle failure modes, i.e., shear failure, anchorage failure, splice failure, and/or sudden loss of confinement caused by tie opening/fracturing; more likely with higher axial load		▨	■
	Rapid lateral-strength deterioration prior to flexural yielding due to brittle failure modes, i.e., shear failure, anchorage failure, and/or splice failure		▨	■
	Axial-strength deterioration prior to flexural yielding due to brittle failure modes, i.e., shear failure, anchorage failure, and/or splice failure		▨	■
Beam-Column Joints	**Gradual loss of shear stiffness** after beam and/or column flexural yielding	■	▨	
	Rapid loss of shear strength and stiffness after beam and column flexural yielding due to shear failure and/or anchorage failure		▨	■

Shading Legend	
	unlikely that phenomena will occur
▨	*uncertain whether phenomena will occur*
■	*very likely that phenomena will occur*

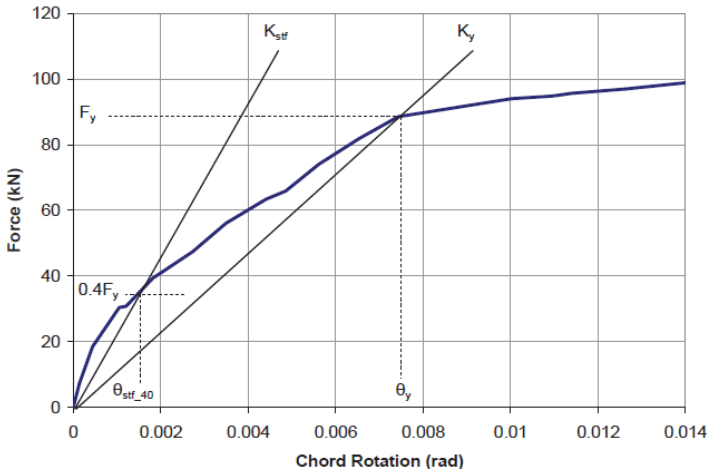

Figure 2-2 Stiffness degradation of a concrete column (data from Ingham et al., 2001 and figure from Haselton et al., 2008).

Current design standards, such as ACI 318-14 and ASCE/SEI 41-17, aim to provide near-yield stiffness estimates for concrete members. The stiffness provisions of ACI 318-14 and ASCE/SEI 41-17, as well as those of international standards from Europe, New Zealand, and Japan, were evaluated in light of the results from dynamic tests conducted on a full-scale four-story reinforced concrete building on the Japanese NIED/E-Defense shaking table (Nagae et al., 2015; Kwon and Ghannoum, 2016). The test building was subjected to multi-directional seismic excitations of increasing amplitude until near collapse damage states. The building structural system was complete including floor diaphragms, while the lateral force resisting systems consisted of moment frames in one direction and planar shear walls in the other. The studies referenced above demonstrated that all the standards evaluated produced stiffness estimates that were much higher than measured at first flexural yielding. Particularly, ACI 318-14 delivered stiffness estimates that were several times larger than the measured values. Limitations in stiffness estimates of design standards could mainly be attributed to inadequate treatment of flexural cracking, the longitudinal reinforcement ratio, and the flexibility due to bar-slip effects. The following subsections describe in more detail the various components governing the lateral stiffness of concrete frame members, while Chapters 4 and 5 provide rational procedures for modeling the lateral stiffness of concrete frames.

2.2.1 Beams and Columns

The stiffness of concrete beams and columns is primarily governed by: (1) the concrete modulus of elasticity, which is related to the concrete compressive strength; (2) the axial load, which affects the extent of concrete cracking; and (3) the longitudinal reinforcement ratio. Also affecting the apparent stiffness of concrete beams and columns are the anchorage conditions of longitudinal bars in adjacent members. Stresses in the longitudinal bars of beams and columns require a certain

distance within adjacent anchoring members to reduce to zero. This strain penetration results in the bars slipping at the interfaces between the framing and anchoring members equal to the integration of the strains over the penetration depth (Sezen and Seltzer, 2008; Ghannoum and Moehle, 2012a; Kwon, 2016) (see Figure 2-3).

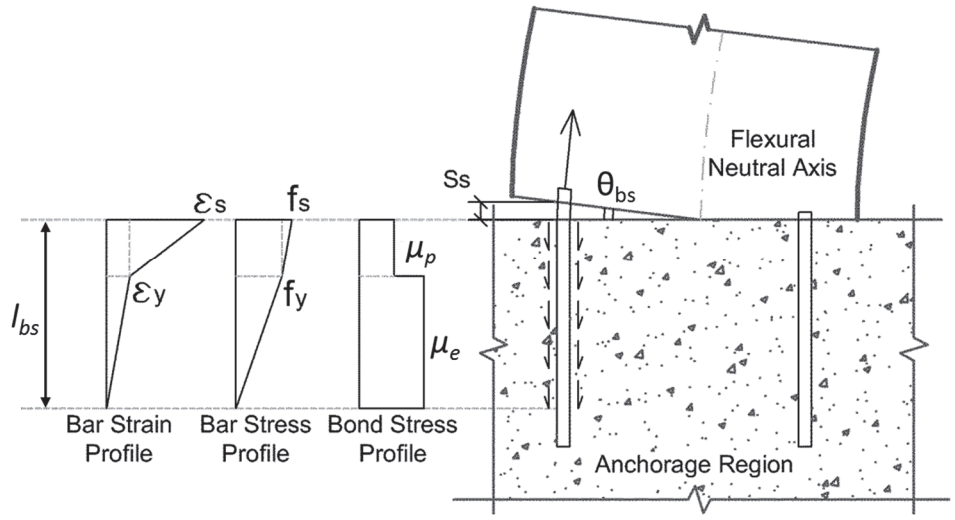

Figure 2-3 Bar slip at member interface due to strain penetration of longitudinal bars showing assumed uniform elastic and inelastic bond stress, μ_e and μ_p, and the resulting strain penetration depth, l_{bs}. (Adapted from Ghannoum and Moehle, 2012a)

Bar-slip deformations have limited effect on the internal stiffness of a member. However, they introduce rotations at the ends of members and result in an apparent reduction in member stiffness. The amount of bar slip is governed by the effective bond stresses between the bars and the surrounding anchoring concrete, while the bar-slip induced rotations are governed by the slip amount and the center of rotation.

Many studies have proposed relations to estimate the effective bond stresses around anchored longitudinal bars (Eligehausen et al., 1983; Lehman and Moehle, 2000; Alsiwat and Saatcioglu, 1992; Harajli, 2009). The studies have suggested that bond stresses can be approximated as constant prior to bar yielding and lead to essentially linear bar-slip rotational behavior. Furthermore, bond stresses have been shown to reduce in regions of inelastic bar strains, which results in gradual softening of the bar-slip behavior past bar yielding (Figure 2-3). Simple assumptions of constant elastic bond stress along the bar length are often used to calibrate the linear portion of bar-slip behavior (fib, 2013; Elwood and Eberhrad, 2009; Kwon, 2016). However, a wide range of elastic bond stress values have been proposed from 6 to 21 $\sqrt{f'_c}$ (in psi units) [0.5 to 1.75$\sqrt{f'_c}$ (in MPa units)], partly due to the wide range in experimental studies of anchorage conditions in adjacent members and bar deformation properties, and partly due to the difficulty in experimentally measuring bar-slip deformations. Nevertheless, based on a full-scale shaking table test (Nagae et al., 2015), Kwon

(2016) demonstrated that using the same elastic bond stress values of $9.6\sqrt{f_c'}$ (in psi units) [$0.8\sqrt{f_c'}$ (in MPa units)] was acceptable for anchorage in beam-column joints and foundations. This bond stress value is also recommended by a stiffness study that utilized close to 400 concrete column tests (Elwood and Eberhard, 2009) and by *fib Model Code for Concrete Structures 2010* (fib, 2013).

The center of bar-slip rotations has been postulated to range from the centroid of the compression steel to the flexural neutral axis. Recent advances in Digital Image Correlation have allowed the direct measurement of the center of bar-slip rotations in full-scale concrete columns (Sokoli et al., 2014). The measured center of bar-slip rotation was found to coincide with the theoretical location of the flexural neutral axis. Recommendations for incorporating bar-slip deformations into computational models can be found in Chapter 4 and Chapter 5 for various modeling approaches.

The effects of lap splices on the response of SMF are often limited to stiffening of segments containing them. Along the outer 20 longitudinal bar diameters of the splice length, element flexural rigidity can increase from its value at splice end to a value nearly 1.7 times larger. At splice ends, reinforcement strains have been observed to be 1.5 to 1.7 times the strains in comparable specimens without splices (Wang, 2014). The stiffness relation presented in Chapter 4 for frame members, Equation 4-2, accounts for the amount of longitudinal reinforcement. This relation can be used to account for the increased stiffness generated by the increased longitudinal reinforcement ratio within a splice length. In fiber-section models, increasing the longitudinal reinforcement within the splice region will result in a stiffening of the section at that location.

The main deformation components that need to be accounted for in structural analyses of beams and columns are therefore flexural, shear, and bar-slip deformations. Typically, flexural deformations are the largest. However, bar-slip deformation can reach up to 40% of the total lateral deformations (Sezen and Moehle, 2006; Elwood and Eberhard, 2009; Panagiotakos and Fardis, 2001). Shear deformations typically account for 5% to 10% of the total lateral deformations (Elwood and Eberhard, 2009), but can reach 15% in frame members with shear stresses close to the ACI 318-14 shear stress limit (Sokoli and Ghannoum, 2016).

2.2.2 Beam-Column Joints

For joints with light transverse reinforcement, shear cracking can cause significant shear deformations even prior to yielding of the longitudinal reinforcement (Mitra and Lowes, 2007; Kim and LaFave, 2007). Test results have also shown that the stiffness of the joint depends on the relative flexural strengths of the beams and columns (Leon, 1990; Beres et al., 1992). However, barring anchorage or shear-strength degradation, as should be the case in seismically designed frames, joint

deformations consist mainly of shear deformations, with strain penetration in longitudinal bars within the joints manifesting as bar-slip induced rotations at interfaces with beams and columns. Shear deformations in seismically detailed joints, however, typically have limited effect on the overall stiffness of concrete moment frames (Kwon and Ghannoum, 2016).

2.2.3 Stiffness Differences for Various Loading Levels

When defining a fixed lateral stiffness for concrete frame members expected to sustain flexural yielding, it is typical to use the secant stiffness to the point of first yield. However, if deflections or natural periods of vibration are required at service load levels, prior loading history should be taken into account. Member stiffness should be selected based on the maximum prior drift levels experienced (Kwon and Ghannoum, 2016) and not necessarily the drifts levels expected at service loads. In deflection sensitive applications, such as vibration analyses, analyzing the structural system at stiffness bounds covering the range of possible prior loading histories may be needed to identify the critical serviceability limits. Specific recommendations for selecting member stiffnesses are given in Chapters 4 and 5 for various modeling approaches. The provided stiffness recommendations in those chapters are based on recent research, and produce stiffness estimates in closer agreement with test data than those currently provided in design standards.

2.3 Strength and Ductility of Components

The various strengths (e.g., flexural, shear, or anchorage strengths), as well as the reinforcement detailing of concrete members, determine the weak link during seismic excitations, and the deformation ductility of members. This section discusses the various failures modes that can occur in concrete frames with emphasis on the behavior of components of special moment frames (SMF). The ACI 318-14 and ASCE/SEI 41-17 standards should be used to determine if members satisfy the SMF designation and are expected to exhibit sufficient ductility to be modeled as outlined in this *Guidelines* document.

2.3.1 Columns

Potential column behavior and failure modes include: (1) flexural softening due to longitudinal bar yielding; (2) spalling of concrete cover; (3) crushing of the concrete core; (4) shear failure either prior or subsequent to flexural softening; (5) loss of confinement from prying or fracture of transverse reinforcement; (6) longitudinal bar buckling and fracture; (7) lap splice failure; (8) bond failure across longitudinal bars; and (9) instability due to slenderness effects or excessive loss of strength. Anchorage failure of column longitudinal bars can also occur within adjacent members (e.g., joints and foundations). Columns in moment frames typically have a constant shear force diagram and maximum flexural demands at their ends. As such, the largest

inelastic demands (flexural or otherwise) tend to occur within plastic hinge regions at column ends whose length is generally on the order of the column section height (Priestley and Park, 1987).

Seismically detailed columns are designed to maintain a stable lateral strength with limited degradation up to a generally accepted threshold drift value of 4% of a story height. Capacity design principles are used to achieve stable flexural hinging while precluding the premature occurrence of less desirable modes of failure.

Bursting stresses related to bond can cause failure of lap splices with light confinement and lengths of up to 80 longitudinal bar diameters (Hardisty et al., 2015). Splice failure can limit the capacity of columns and beams to sustain deformation reversals in the nonlinear range of response (ASCE, 2017b). For this reason, lap splices are confined and located near inflection points in SMF, which virtually eliminates the risk of SMF members sustaining splice failures.

In some cases, nonstructural components can shift the location of hinging, as well as increase shear and local deformation demands on columns significantly. This is particularly the case for stiff partition walls in contact with columns. While it is preferable that such effects be eliminated by altering the details of nonstructural components, if such effects are anticipated, their effects on member behavior should be accounted for in simulation. This includes adjusting column clear span and hinge locations.

Shear failure can occur prior or subsequent to flexural yielding in frame members. If the estimated shear strength of a member is lower than its probable flexural strength, shear failure is expected prior to flexural yielding at relatively low deformation levels. However, if shear strength is slightly larger than flexural strength (less than 30% larger), then shear failure could occur after inelastic deformations in the hinge regions where the strength of shear transfer mechanisms degrade with inelastic deformations (ASCE, 2017b; ACI, 2017; Priestley et al., 1994; Sezen and Moehle, 2006; Ghannoum and Moehle, 2012b). Such shear failures can also occur in members that are seismically detailed, particularly when the transverse reinforcement design is governed by shear and not confinement requirements (Sokoli and Ghannoum, 2016). If shear strength is significantly larger than the flexural strength, members are not expected to sustain shear failures prior to flexural modes of failure. ACI 318-14 and ASCE/SEI 41-17 provide shear strength relations that can help ensure member shear strength exceeds the shear demands arising from flexural hinging.

Maintaining a stable and ductile response in flexure requires maintaining the integrity of the concrete core and the strength of the longitudinal bars. In cases where transverse reinforcement is insufficient, buckling of longitudinal bars can occur at

relatively low deformations, which can result in loss of lateral strength and premature bar fracture. Additionally, insufficient transverse reinforcement can lead to crushing of the concrete core in frame members at relatively low deformation demands, particularly in columns under high compressive axial loads. The quantity, detailing, and spacing of transverse reinforcement determine adequate confinement of the concrete core (Mander et al., 1988; Saatcioglu and Razvi, 1992; Razvi and Saatcioglu 1999) and stability of longitudinal bars (Pfister, 1964; Pantazopoulou, 1998). To provide adequate bracing for longitudinal bars and core confinement, transverse ties need to be properly anchored with 135 degree hooks extending sufficiently into the concrete core. Ties with 90 degree hooks tend to pry open when the concrete cover is lost in the plastic hinge regions. Columns can be expected to have a stable flexural response if their transverse reinforcement satisfies the provisions of ACI 318-14 for SMF. These provisions specify limits on the amount, spacing, and detailing of transverse reinforcement.

Anchorage failures can occur within the span of frame members due to inadequate lap-splicing or when bond demands are high along continuous longitudinal bars. Anchorage failures typically consist of bars splitting the surrounding concrete, which negatively impacts other strength mechanisms. In highly confined members, pullout of the bars from the surrounding concrete can occur with limited splitting. Mechanisms governing lap-splice failures are similar to those causing anchorage failures and manifest themselves typically through splitting of the concrete surrounding the splices (Orangun et al., 1977). To avoid anchorage failures in seismically detailed columns, ACI 318-14 requires that lap splices be removed from the plastic hinge regions and placed where flexural demands are lowest, typically around the column mid-span. Lap-splices are also required to be adequately confined with transverse reinforcement in seismically detailed columns.

Anchorage failures along continuous longitudinal bars can be expected within frame members if the distance between points of maximum and zero stress are shorter than the development length relations provided in ACI 318-14. Susceptible members typically have a relatively short span length, a steep moment gradient, and large bar diameters. It is noteworthy that the development or splice length limits provided in ACI 318-14 were derived from tests where the concrete surrounding the bars or splices was mostly intact prior to anchorage failure (Orangun et al., 1977). In cases where the surrounding concrete is damaged (e.g., at inelastic hinges or areas of severe shear cracking), the effectiveness of that concrete in resisting bond forces is weakened. It is recommended to subtract regions of anticipated large inelastic demands or damage from the available development or splice lengths when evaluating the potential for anchorage or splice failures (Ichinose, 1995; Sokoli and Ghannoum, 2016).

If adequately detailed, seismically detailed columns will only sustain longitudinal bar buckling and fracture or concrete core crushing at lateral drifts exceeding acceptable target levels, generally exceeding a story drift ratio of 4%. Simulating the lateral load versus strength response of seismically detailed columns therefore involves capturing the lateral stiffness prior to flexural yielding, the softening due to flexural yielding, and the subsequent lateral-strength degradation, whose initiation and rate of progression depend on the dominant failure mode and key column parameters (e.g., transverse reinforcement details and axial loads). The beneficial effects of confinement on core concrete strength gain and deformation capacity should be included in the model, particularly in fiber-section elements. Guidance on modeling concrete columns satisfying the SMF designation of ACI 318-14 is provided in subsequent chapters.

2.3.2 Beams

Beam behavior and modeling approaches are similar to those of columns. Notable differences between beam and column behaviors relate to the reinforcement layouts and the composite action of beams with slabs.

Concrete beams are ideally reinforced with a symmetric layout of longitudinal bars. Symmetric reinforcement layouts prevent sections from experiencing flexural compression failures prior to yielding of the tension steel at low axial loads. On the other hand, a higher ratio of the tension-to-compression steel affects the flexural mode of failure in beams from a ductile tension-steel yielding mechanism to a more brittle compression-concrete crushing. As a result, the addition of compression steel tends to improve the ductility capacity of beam sections (Corley, 1966). The ACI 318 design code has limited the amount of flexural tension steel in beams to preclude flexural-compression failures for several decades. In beams satisfying the SMF provisions of ACI 318-14, the top and bottom longitudinal reinforcement amounts are prescribed not to differ by a factor greater than two, which is intended to improve the ductility of sections. Nevertheless, top and bottom beam reinforcement amounts are seldom equal in beams, making beam flexural response unsymmetrical.

Beams and columns typically have differing layouts of transverse reinforcement. In beams, even those satisfying the ACI 318-14 provisions for SMF, the concrete core tends to be less well confined than in columns (Panagiotou et al., 2013). A main contributor is the typical lack of side longitudinal bars and the lack of horizontal cross ties in beams. Lighter transverse reinforcement layouts in beams compared with columns can also exacerbate the buckling behavior of longitudinal bars in compression.

The composite action of beams and slabs affects the strength and overall behavior of beams significantly. Slab steel running parallel to beams within an effective width

away from the web can significantly increase the flexural strength and affect the location of the flexural neutral axis depth in the beam.

Similar to seismically detailed columns, seismically detailed beams are only expected to sustain flexural failure modes at relatively large deformation demands. Simulating the lateral load versus strength response of seismically detailed beams therefore involves similar approaches as those used for columns, but also require accounting for the unsymmetrical stiffness, strength, and deformation capacities typically exhibited by beams. Guidance on modeling concrete beams that satisfy the SMF designation per ACI 318-14 is provided in subsequent chapters.

2.3.3 Beam-Column Joints

Beam-column joints are highly stressed components through which beam and column moments reverse, generating large bond demands and joint shear stresses. Joint strength and deformation capacities are influenced by the state of strain of the longitudinal bars in connecting beams and columns, as well as the bond demands around those bars within the joints. Beam-column joint behavior is also highly dependent on the joint aspect ratio (i.e., the ratio of joint height to length), the confinement of the joint either through transverse frame members or reinforcement, and the axial load (ACI, 2002).

Seismically detailed joints are designed to maintain a stable lateral strength with limited degradation up to the generally accepted threshold drift value of 4% of a story height. Capacity design principles are used to achieve a stable joint shear strength while precluding the premature occurrence of less desirable modes of failure, especially anchorage failures.

Joint shear strength is developed through direct shear transfer and compression strut action (ACI, 2002). The two modes of shear transfer rely on the presence of sufficient amounts of transverse reinforcement. ACI 318-14 specifies minimum amounts and spacing limits for joint transverse reinforcement to maintain the integrity of the joint shear strength and control shear cracking and deformations.

Anchorage failures of longitudinal bars could occur within short joints leading to splitting of the joint concrete and subsequent degradation of the joint strength. To remedy this, ACI 318-14 specifies a minimum length of 20 bar diameter for seismically detailed interior joints to prevent anchorage failures. Anchorage limits also exist for exterior joints.

Even though joints are expected to be damaged even in modern frames, laboratory testing (e.g., Hassan, 2011) suggests that joints with typical geometries and even relatively poor seismic detailing can maintain moderate axial loads even following significant loss of joint shear strength. Thus, modeling of loss of joint axial load

carrying capacity is not considered necessary for accurate simulation of frame response.

When transverse reinforcement and anchorage limits for seismically detailed joints are followed, shear and anchorage failures are not expected. Seismically detailed joints are able to maintain a stable strength capable of developing the flexural strength of framing members and limiting shear deformations. Therefore, for special moment frames, attempting to model yielding or deterioration of the joint is not necessary; the important aspect of the joint modeling is to account for the finite size of the joint (which adds stiffness to the frame) and account for the flexibility that is created by bond-slip into the joint (which is typically included in the calibration of the beam and column stiffnesses).

2.4 Floor Diaphragms

Floor slabs need to resist gravity loads as well as in-plane loads generated by lateral loading, such as wind, earthquake, and earth loads. Requirements and guidelines for design of concrete slabs can be found in the ASCE/SEI 7-16, ACI 318-14, and NIST GCR 16-917-42, *Seismic Design of Cast-in-Place Concrete Diaphragms, Chords, and Collectors: A Guide for Practicing Engineers* (NIST, 2016b). These requirements were developed to preclude inelastic behavior in diaphragms for in-plane actions and to ensure that inelastic out-of-plane deformations remain ductile during seismic loading. In-plane behavior of slab systems is typically modeled elastically (using a design method meant to protect the component), while the bending behavior should be modeled with nonlinear elements.

2.4.1 Bending Behavior

Bending behavior of diaphragms depends on several factors, including the presence and size of beams and drop panels, and the relative lengths of orthogonal spans. When concrete drop beams are present, beams and slabs act compositely in flexure over an effective width of the slab on either side of the beam. The composite action is often treated by simulating beams as T-shapes for both strength and stiffness evaluations. Various codes and standards prescribe different effective width of slabs to include in T-beams, with some distinguishing between the width to include for strength and the width to include for stiffness (e.g., ACI, 2014; ASCE, 2017b; and fib, 2013).

When concrete drop beams are present, composite action between the diaphragm and beams will generate flexural yielding in the diaphragm in the vicinity of beam plastic hinges. Typically, this behavior is accounted for in simulations by modeling beams as T-sections encompassing a portion of the diaphragm adjacent to the beam web. The T-beams typically have unsymmetrical flexural behavior and deformation capacities at which lateral-strength degradation initiates.

When concrete drop beams are not present, beams are concealed within the slab frame with the columns and walls. These concealed beams often have limited flexural stiffness and ductility capacity, and are sensitive to punching shear, due to the lack of confinement reinforcement and often limited transverse reinforcement. Concealed beams are typically modeled as rectangular beams with an effective width (ASCE, 2017b; Pecknold, 1975; Darvall and Allen, 1983; Hwang and Moehle, 2000; Dovich and Wight, 2005). The effective width of concealed beams can be different for bending stiffness or bending strength.

Modeling approaches for bending behavior of concrete diaphragms are discussed in Chapters 4 and 5 due to their interactions with the flexural behavior of beams and other framing members.

2.4.2 In-Plane Behavior

Slab diaphragms are proportioned to resist the maximum foreseeable in-plane loads without exceeding their elastic limit. Therefore, simulating the in-plane behavior of diaphragms, in most cases, entails achieving the appropriate in-plane stiffness.

Ensuring elastic in-plane behavior essentially involves ensuring elastic behavior of collectors and distributors within the diaphragms at the interface of vertical members, where lateral load transfers occur. Additionally, global equilibrium in the plane of a diaphragm generates tension and compression elements at diaphragm boundaries that are designed to remain elastic. Additional details on the design of concrete diaphragms can be found in NIST (2010b).

A more comprehensive review of in-plane diaphragm behavior and modeling approaches, which are typically decoupled from out-plane behavior, can be found in Section 3.7 of this *Guidelines* document and Section 2.5 of the *Part I Guidelines*.

Chapter 3

Nonlinear Modeling of Reinforced Concrete Frames and Components

Chapter 3 of the *Part I Guidelines* has provided general modeling guidance applicable to any type of structural system, and this chapter provides additional modeling guidelines specific to reinforced concrete special moment frame systems. This chapter provides general content applicable to any reinforced concrete frame component modeling approach (e.g., concentrated hinge type models, distributed fiber-type models, or continuum finite element models), and Chapters 4-6 provide additional guidance specific to each of the three component modeling options.

3.1 Overview of Three Frame Model Idealizations

This section briefly introduces the three idealized analysis models typically used for reinforced concrete frame structures and discusses the advantages and disadvantages of each method. More detailed discussions of how to use each approach are covered later in this chapter.

3.1.1 Concentrated Hinge Components Models

Concentrated hinge models are the ones most commonly used to simulate the overall response of reinforced concrete moment frames because they are fairly straightforward to calibrate and capture nonlinear behavior from the onset of yielding up through strength and stiffness degradation from rebar buckling and other effects. Figure 3-1 shows an idealized model of a frame where concentrated hinges are inserted at locations that are expected to yield during the analysis.

Components of the frame where inelastic behavior may occur should be modeled accordingly, and include the following:

- **Columns.** While special reinforced concrete columns are designed following the strong-column weak-beam provisions, this minimum criterion does not necessarily prevent column yielding. Unless it is demonstrated that the columns remain elastic, inelastic hinges should be included at both ends of columns. In this *Guidelines* document, it is recommended to place the inelastic hinges at column ends, just at the interface with the joints or foundation elements, as opposed to a finite distance into the column, which is related to the plastic hinge length. This is deemed to result in limited error in frame members and simplify modeling considerably. While inelastic flexural moment-rotation response is the

dominant effect, the flexural response should be adjusted for axial loads through some type of *P-M* yield surface relationship. The axial load level and level of confinement should be considered in defining hinge properties.

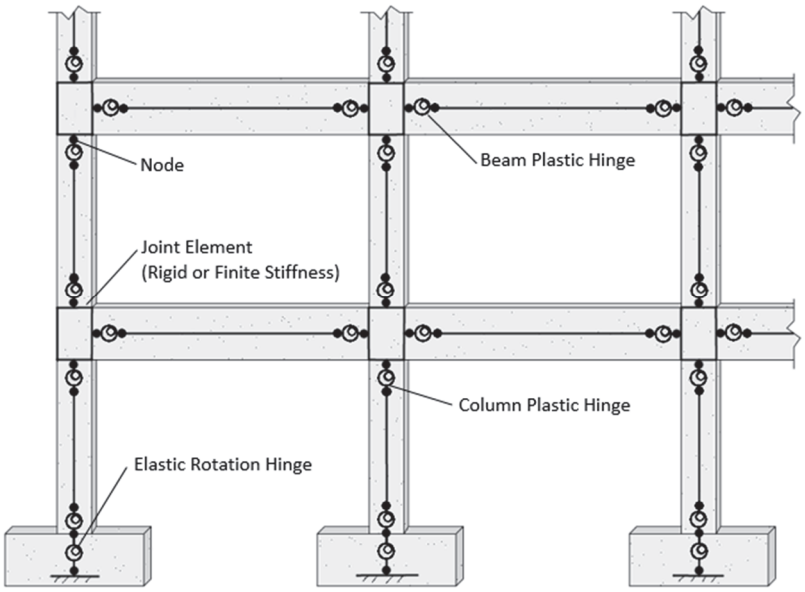

Figure 3-1 Overview of a typical reinforced concrete moment-resisting frame system, showing concentrated hinge centerline model idealization.

- **Beams.** Reinforced concrete beams are often composite with the floor slab, which affects the strength (e.g., negative bending strength), stiffness, and inelastic hinge properties. Where the slab contribution is significant, it should be considered in defining inelastic hinge properties. Similarly to columns, it is recommended to place beam hinges at beam ends, just at the interface of beam-column joints or other vertical members (e.g., walls).
- **Beam-Column Joints.** Joint connections in special reinforced concrete moment frames are capacity designed and are not expected to be the primary failure mode under seismic loading. Even so, the finite joint sizes can influence frame response and can be considered using rigid end offsets. Additionally, bar slip at the joint interface has been shown have an important effect in adequately capturing the stiffness behavior (which can be handled either explicitly or approximately).
- **Bar-Slip Effects.** Bar-slip effects can be accounted for by reducing the effective elastic flexural stiffness of beam and column elements or of the joints they frame into. It is essential not to double count bar slip effects by softening both frame members and joints for bar slip. Details on implementing this approach can be found in Chapter 4. Alternatively, zero-length rotational elements that capture softening due to bar slip can be used at the interface between frame members and members anchoring their longitudinal bars, such as joints, walls, or foundations.

Details on implementing this approach can be found in Section 5.4.1 as it is the preferred one for use with fiber-type beam and column members.

- **Splices.** In modern seismically-designed frames, splice failures are not anticipated. If splice failure is suspected for a building being modeled, force demands could be checked to confirm whether a spring is needed to model inelastic response.
- **Column Base Fixity.** The fixity of the column base depends on what supports the column. If the column is supported by a basement wall, then a fixed end condition is appropriate. If the column is supported by a footing, then the rotational flexibility of the footing could be included in the model through use of an elastic rotational spring. In all cases where column longitudinal bars are anchored in adjacent members (including hooked and headed anchorage), the effects of bar slip needs to be considered as described above.
- **Slabs.** In cases where slabs are not supported by beams, slab elements spanning between vertical elements can be used to account for the stiffening effects of the slab on a frame and monitor the force and deformation demands on the slab and slab-to-column connection. Details on modeling slabs can be found in Sections 3.6 and 4.5 of this *Guidelines* document.

Further details on characterizing inelastic hinges for columns, beams, joints, and slabs are provided in Chapter 4.

3.1.2 Fiber-Type Components Models

Fiber-type elements can be used to simulate the flexural behavior of frame members, including those of slab elements. When using fiber-type frame elements, beam-column joints, slab-column joints, and bar slip effects can be introduced as described for the concentrated hinge models.

Fiber-type idealizations typically capture the distribution of yielding through member cross sections. Inelastic yielding along the member length is generally represented by one of the following two formulation types:

- **Distributed Inelasticity Fiber Elements**. In this modeling approach, several fiber cross-sections are modeled throughout the length of the element. In this approach, the number of fiber sections and their locations, which are typically determined by numerical integration rules, implicitly define a plastic hinge length for the element over which inelastic deformations are concentrated. Figure 3-2a shows this distributed plasticity modeling approach, where the element includes inelastic sections at multiple integration points along the element length.
- **Concentrated Inelasticity Fiber Elements**. In this modeling approach, a single fiber cross-section is used for each end of the element and the user defines a

plastic hinge length to relate curvature to rotation. The middle of the element model is then composed of an elastic element. Figure 3-2b shows this fiber hinge approach, where inelastic sections only exist at the element ends and where the plastic hinge length is predetermined.

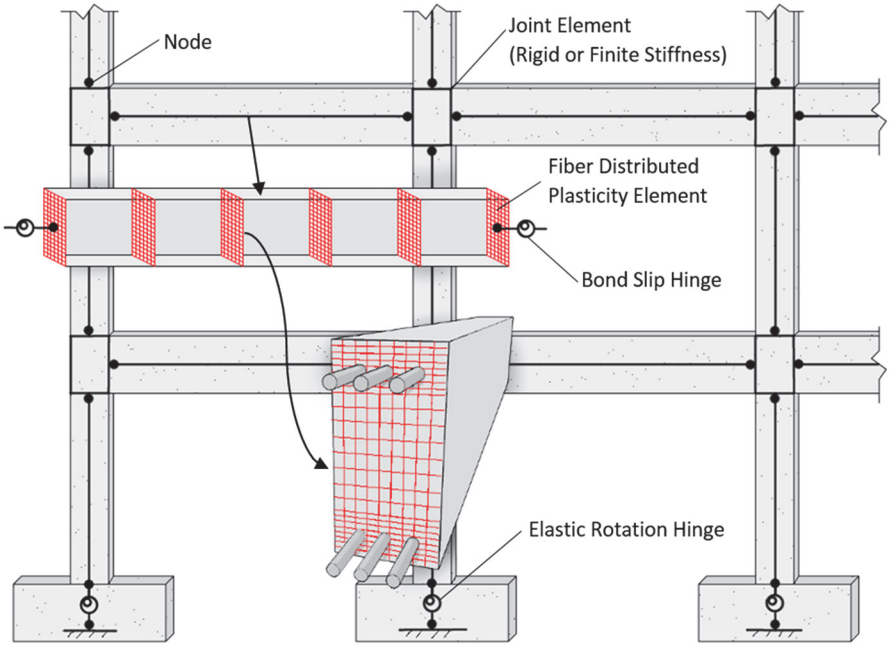

(a)

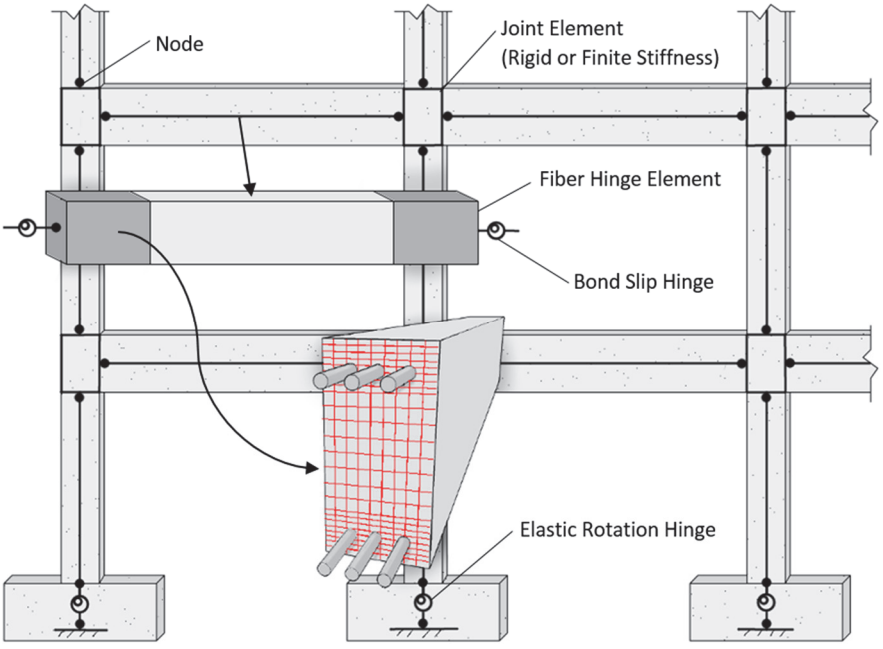

(b)

Figure 3-2 Overview of a typical reinforced-concrete moment-resisting frame system, showing the fiber-type model idealization.

Further details on fiber-type elements are provided in Chapter 5.

3.1.3 Continuum Finite Element Components Models

Continuum finite element models are not typically utilized for modeling seismic response of reinforced concrete frame structures. This is discussed further in Chapter 6.

3.2 Column and Beam Modeling

The modeling guidelines for column and beam components are specific to which component modeling approach is taken and specific guidance is provided in Chapters 4-6.

3.3 Column Splices

Column splices in seismically designed moment frame systems are generally considered to be designed with sufficient strength to sustain forces imposed by the frame. Where this is the case, the column splices are generally not modeled. If this is in question for the frame being analyzed, the force demands on the column splice can be checked; if it is a possible failure mode, then the splice can either be deemed as a deformation-controlled component (and nonlinearly modeled) or be deemed as a force-controlled component and with appropriate acceptance criteria to ensure that the demands are well below the capacity of the splice. If there is a question regarding a column splice being a potential controlling failure mode, ACI 369R-17, *Guide for Seismic Rehabilitation of Existing Concrete Frame Buildings and Commentary* (ACI, 2017) and ASCE/SEI 41-17, *Seismic Evaluation and Retrofit of Existing Buildings* (ASCE, 2017b) provide guidance on evaluating the strength of splices and selecting nonlinear modeling parameter and acceptance criteria for splices.

3.4 Beam-Column Joint Panel Zones

Under earthquake loading, beams and columns typically experience moment reversals at beam-column joints, which results in joint softening and increased frame flexibility. Modern seismic design provisions are intended to limit damage in joints, and focus flexural yielding in beams at the face of the joint panel zone with limited yielding in columns; however, system response may be such that columns exhibit significant inelastic response at the joint face. As discussed in Section 2.2.2 of this *Guidelines* document, the flexibility of seismically detailed beam-column joints originates mainly from the slip of longitudinal bars within the joint panel region and to a lesser degree from shear deformation of the joint panel regions. Given that seismically detailed joints are not expected to undergo significant damage or degradation, modeling them can effectively be reduced to capturing their secant

stiffness to first yield of adjacent frame members. The following sections provide recommendations for practical modeling of joint response under earthquake loading.

Celik and Ellingwood (2008) provide a review of the most common approaches for joint modeling. Two approaches are considered in this report because they are numerically robust and allow for computationally efficient modeling. The approaches are: (1) adjusting the stiffness of beam and column offsets within the joint panel regions; and (2) introducing a rotational hinge at the beam-column intersection. Figure 3-3 illustrates these two approaches. These models can be used to account for joint panel shear deformations, with bar-slip flexibility introduced directly through rotational hinges at beam and column ends (Figure 3-3b), or indirectly through adjusted beam and column effective stiffnesses. Further details on characterizing beam-column joint models are provided in Chapter 4.

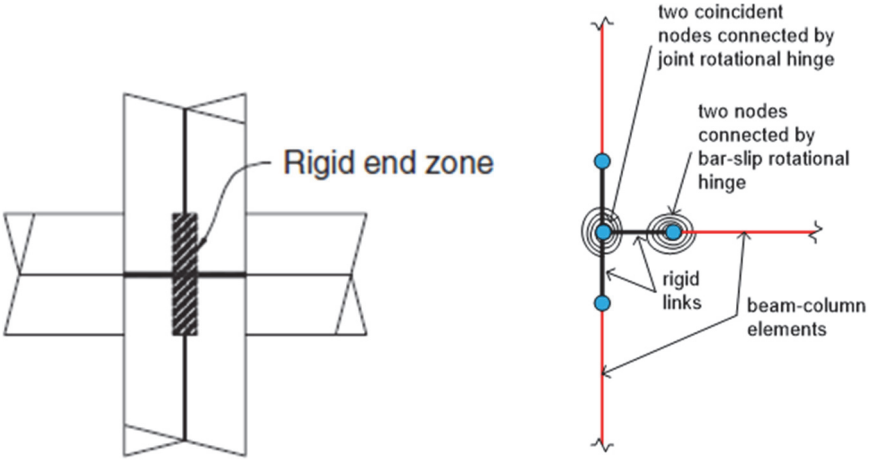

Figure 3-3 Recommended element configurations for modeling (a) stiffness adjustment of beam and column offsets (Elwood et al., 2007), and (b) joint center rotational spring in a planar frame (Celik and Ellingwood, 2008).

3.5 Floor Diaphragms and Collectors

The typical diaphragm in a reinforced concrete moment frame building is a reinforced concrete slab, which is typically post-tensioned and can either be a flat plate or include a gravity beam under the slab. Guidelines for modeling these types of floor diaphragms and collectors are covered in Section 3.6 of *Part I Guidelines*.

3.6 Secondary Gravity System Components

The general requirements for treatment of the gravity system can be found in Section 3.11 of the *Part I Guidelines*. This section provides supplementary information for how to model the gravity system particular to reinforced concrete frames.

3.6.1 Gravity Columns, Beams, and Joints

In most cases, gravity columns and other components of gravity frames (i.e., joints and beams) should be idealized using the same techniques used for components of lateral load resisting moment frames, and these items are covered in Sections 3.2 through 3.4. Alternatively, more simplified modeling approaches would be used for the gravity system components, but the modeling should be able to adequately represent the behavior or the gravity system and provide information for assessing acceptance criteria for gravity system components.

3.6.2 Slab-Column Connections

Slab-column gravity framing can be idealized by including the slab in the model using plate or shell elements with a reduced out-of-plane bending stiffness to account for cracking or by modeling the slab as an "effective beam." Figure 3-4 shows a simple model that is typically used for slab-column connections and based on work by Kang et al. (2009). This model is recommended for its simplicity, its ability to track unbalanced moments transferred to columns, and its compatibility with ACI 369R-17 and ASCE/SEI 41-17 modeling parameters and acceptance criteria for slab-column connections. The model includes elastic slab-beam elements with concentrated hinges at their ends. The model is also comprised of rigid links spanning the connection dimensions including column capitals. The slab-beam rigid elements are connected to the column rigid elements by a single torsional spring that captures the nonlinear behavior of the slab-column connection.

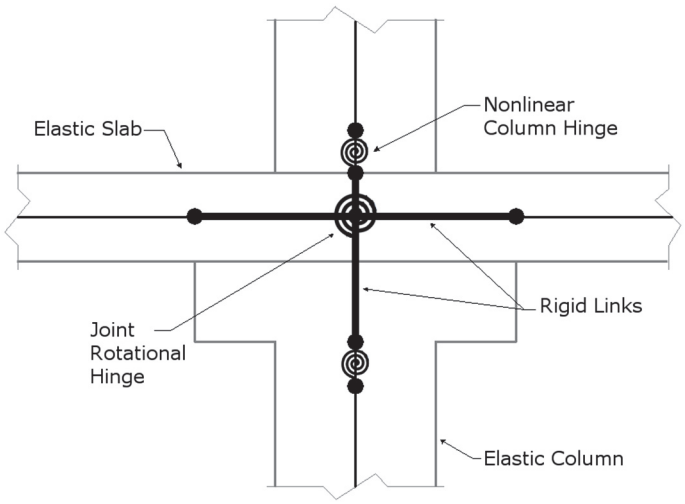

Figure 3-4 Idealized slab-column joint model.

In this modeling approach, slab-beams are modeled using elastic line elements having an effective flexural stiffness as presented in Section 4.5.2. The slab-beam concentrated hinges are defined as rigid plastic, with flexural strength and hardening

properties as presented in Section 4.5.1. The rotational slab-column connection spring is modeled using a typical backbone relationship as shown in Figure 3-5 that is effectively rigid before yield. The rotation at strength loss for the torsional spring is based on the onset of punching shear and is discussed in Section 4.5.3. The post-failure residual strength and rotation at final strength loss for this modeling approach can be found in Table 10-15 of ASCE/SEI 41-17; the residual strength ranges from 0.0 to 0.4 for slabs with continuity reinforcement (being higher for lower shear cases and for post-tensioned slabs). The post-failure degrading slope of the torsional spring can be conservatively assumed as being relatively steep, per ASCE/SEI 41-17.

Further detail on how to characterize the various components of the slab-column connection model are provided in Section 4.5.

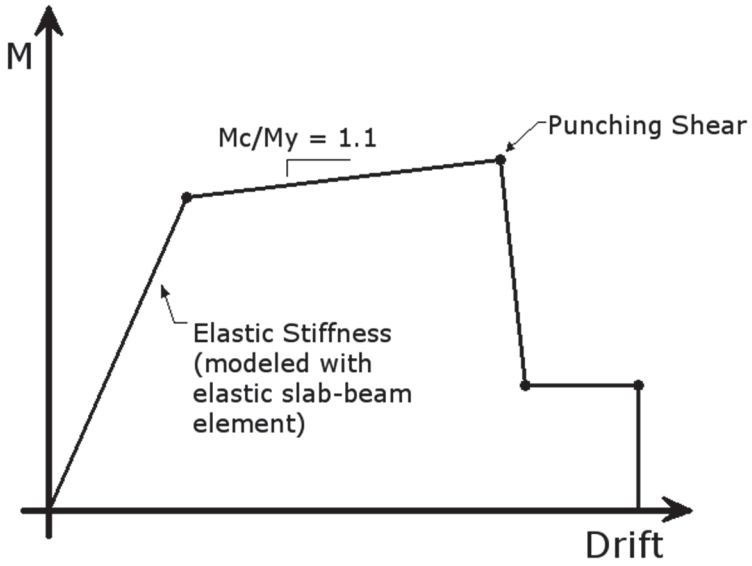

Figure 3-5 Slab-column connection backbone curve.

3.7 Modeling of Damping

Modeling recommendations for damping are covered in Section 3.7 of the *Part I Guidelines*.

Chapter 4

Concentrated Hinge Component Models

4.1 Overview of Concentrated Hinge Model

Concentrated hinge models are often used to represent the behavior of beam and column frame members. In such models, an elastic line element is used to simulate the elastic stiffness of a member, and zero-length rotational springs are added at each end to capture the inelastic deformations of the members (Figure 4-1). This approach has the advantage of being simple to implement and is computationally efficient. For beams and columns, generally little error is introduced in this approach when lumping inelastic deformations that occur over a finite plastic hinge region at member ends. This approach, however, is more difficult to implement if the location of inelastic deformations is unknown during the model-building phase, or if they do not occur at member ends. In most analytical software, the force-deformation relations of the elastic element and concentrated hinge are defined during the model-building phase and do not adjust to evolving boundary conditions. The effects of varying axial loads on column strength and stiffness cannot be captured during analyses and the force-deformation relations are typically defined based on the average boundary conditions expected during analysis.

For seismically designed beams and columns, the lateral load versus lateral displacement behavior follows the general shape of the curves shown in Section 2.3.2 of the *Part I Guidelines*. To simulate this behavior using concentrated hinge models, the moment-rotation relation attributed to the zero-length rotational springs can be idealized as illustrated in Figure 4-2 (where the force demand, M, is the moment in the beam and the deformation quantity, θ, is rotation*)*. A monotonic curve is defined for spring elements including specification of: yield strength and rotation, M_y, θ_y; capping strength and rotation, M_u, θ_p; and post-capping rotation, θ_{pc}, and an associated residual strength. The rotational spring behavior would follow the envelope curve if it were pushed monotonically. However, when concrete frame members are cycled laterally, degradation in strength and deformation capacities occur in the inelastic deformation range. To simulate those degradations, the envelope relation can be adjusted during analysis based on cumulative dissipated energy or cumulative deformations. Under many cycles, the response could even reach the first-cycle backbone. The following sections provide guidance on selecting

the modeling parameters for concrete columns and beams in concentrated hinge models.

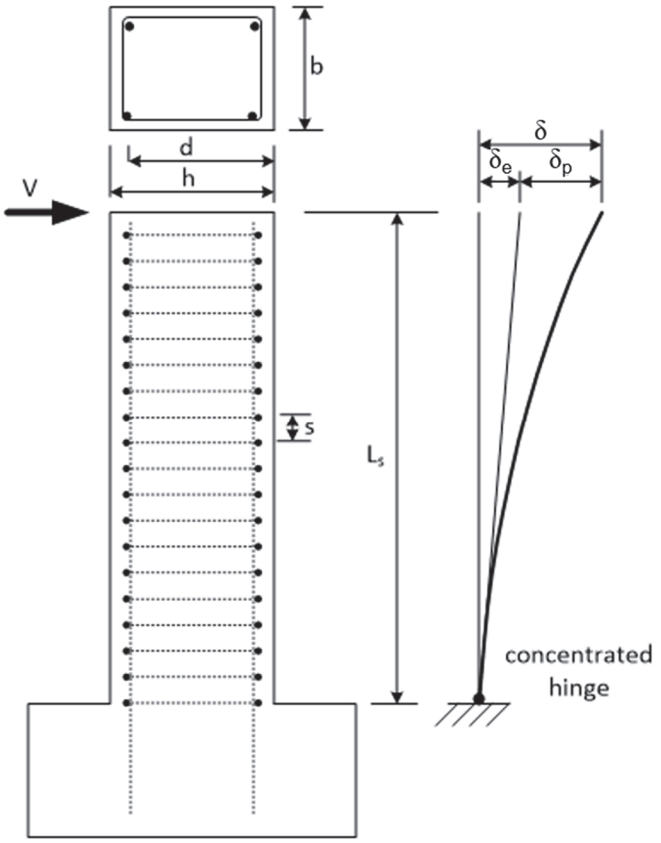

Figure 4-1 Idealized cantilever model of reinforced concrete beam-column with concentrated hinge at member end. Adapted from Haselton et al. (2016).

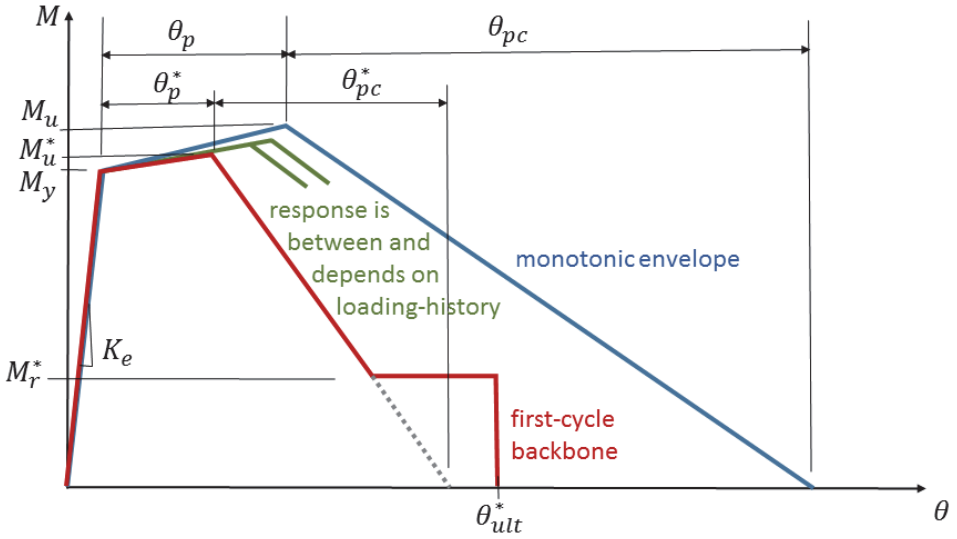

Figure 4-2 Idealized tri-linear end moment versus chord rotation response of equivalent cantilever column. Adapted from Figure 2-5 in *Part I Guidelines* (NIST, 2017).

The objective of the more advanced modeling approach outlined in Figure 4-2 (and the supporting equations in the later sections) is to model the beam or column in such a way that the response can be predicted for any generalized loading protocol. With this modeling approach, the element model would follow the Figure 4-2 "monotonic" curve if the element was pushed with a monotonic load, the element model would follow the Figure 4-2 "first-cycle backbone" curve if pushed with a cyclic load that had many damaging symmetric cycles of loading, and the element model would follow the Figure 4-2 "between" curves when subjected to a typical earthquake loading (since a typical loading is cyclic but typically has fewer cycles that test data used to calibrated the "first-cycle envelope" curve). Figure 4-3 shows sample test data for three nominally identical reinforced concrete column specimens, showing the behavior for monotonic loading and two cyclic loading protocols. This shows that the monotonic versus cyclic behavior is similar when there are a small number of cycles but are very different then there are many cycles of loading. The recommended modeling approach would enable modeling of a component under any of these loading protocols. The modeling approach, and additional illustrative experimental test data, are further described in Section 4.2.3.6.

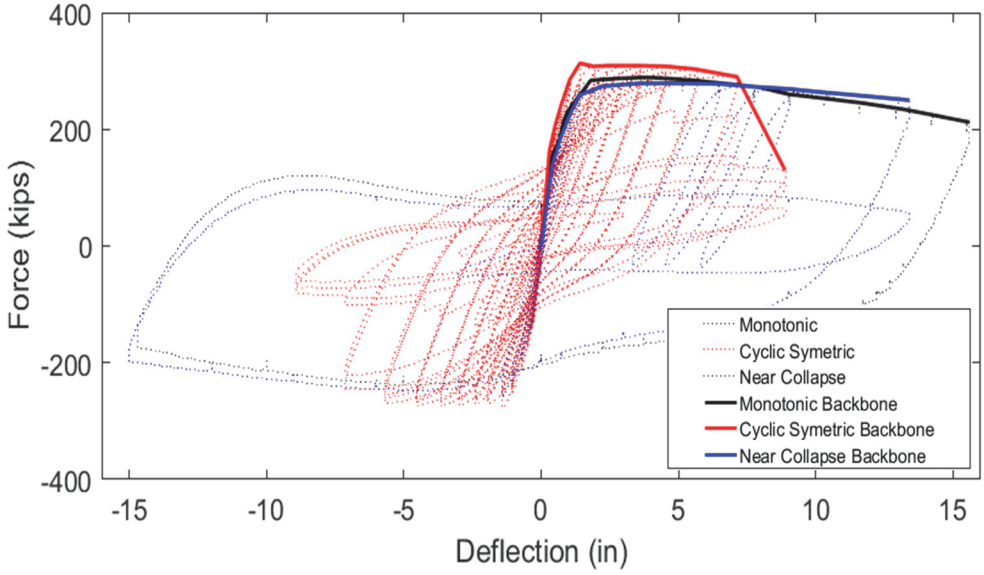

Figure 4-3 Loading protocols for specimens: (a) monotonic push in each direction; (b) ACI 374 symmetric cyclic (ACI, 2005); (c) near-collapse loading protocol (after Nojavan et al., 2014, 2016).

4.2 Modeling of Moment Frame Columns

4.2.1 Lateral Stiffness

In the concentrated hinge modeling approach, the lateral stiffness of a member is defined through the elastic stiffnesses of the line element and the rotational springs at its ends. If the elastic stiffness of a member is fully captured by the elastic line

element, then the elastic stiffness of the rotational springs should be input as essentially rigid. However, defining an essentially rigid stiffness to a rotational spring may cause numerical convergence issues. In such cases, the spring elastic stiffness can be reduced while the elastic element stiffness is increased such that the desired lateral stiffness of the member is preserved.

As discussed in Chapter 2, the lateral stiffness of concrete frame members is comprised of flexural, shear, and bar-slip deformations. Flexural and bar-slip deformations typically comprise the majority of the lateral deformations, with shear deformations accounting for less than 10% of total deformations in most cases and can be introduced in the shear stiffness of the elastic line element. Flexural and bar-slip deformations can be treated separately, with the flexural stiffness of the line element capturing flexural deformations and the elastic stiffness of the concentrated hinge capturing bar-slip deformations. This approach, however, is more commonly used in fiber-type models than in concentrated hinge models. Alternatively, empirical relations can be used to adjust the flexural stiffness of the line element to capture flexural and bar-slip deformations. In conjunction with either of these approaches, an elastic shear rigidity of $0.4E_cA_w$ can be used as prescribed in ASCE/SEI 41-17, *Seismic Evaluation and Retrofit of Existing Buildings* (ASCE, 2017b), where the concrete modulus of elasticity (E_c) is based on ACI 318-14, *Building Code Requirements for Reinforced Concrete* (ACI, 2014).

4.2.1.1 Moment-Curvature Approach

In this approach, flexural and bar-slip deformation are treated separately, with the flexural stiffness of a frame member derived from moment curvature analysis. Elastic beam theory gives the effective flexural stiffness of an elastic section at a given load as the moment divided by the curvature (i.e., $E_cI_{effective} = M / \varphi$).

If the secant stiffness to the point of first yield is desired, the moment and curvature values at that first yield can be used. The point of first yield can be defined where the longitudinal steel first reaches the yield strain or the concrete compressive strain reaches a value of 0.002. If the secant stiffness at a lower service load is desired and members have not been subjected previously to higher loads, the moment and curvature values at that load level can be selected. An advantage of using a moment-curvature approach to evaluate member stiffness is that the method intrinsically accounts for member geometry (e.g., circular or T-shaped sections), as well as the layout and amount of longitudinal reinforcing bars. However, the moment-curvature approach only accounts for flexural deformations and does not account for deformations due to bar-slip. Bar-slip deformations can be introduced in this approach as discussed in Section 5.4.

4.2.1.2 Empirical Equations

Simplified empirical equations are typically used to determine the flexural stiffness of line elements in concentrated hinge models. The following recommended equations account for the component deformations coming from flexure, bar-slip, and shear. It is noteworthy that this approach only accounts for the linear portion of the bar-slip behavior, leaving inelastic bar-slip softening to be accounted for in the concentrated hinge element. The flexural hardening ratio provided in Section 4.2.3.1 accounts for inelastic bar-slip softening.

Elwood et al. (2007) proposed an equation for column effective flexural rigidity that accounts for the stiffening effect of compressive axial load (P), based on an extensive column test database (Berry et al., 2004). This equation has been incorporated into ASCE/SEI 41-13, *Seismic Evaluation and Retrofit of Existing Buildings* (ASCE, 2014), and is as follows:

$$\frac{E_c I_y}{E_c I_g} = 0.3 + \left(\frac{P}{A_g f'_c} - 0.1 \right) \tag{4-1}$$

where:

$$0.3 \le \frac{E_c I_y}{E_c I_g} \le 0.7$$

Equation 4-1 provides the secant stiffness at first yield (K_y in Figure 2-2), but does not capture the substantial additional stiffness that occurs under pre-yield levels of loading, and does not include the effects of other parameters known to contribute to stiffness, such as the longitudinal reinforcement ratio. If a more detailed estimate of effective stiffness is desired, one could use empirical equations developed by Kwon (2016), which are based on moment-curvature analyses, a database of over 200 column tests, and shake table test data. Boundary conditions related to anchorage of longitudinal bars in adjacent members (e.g., footing, joints) can alter the bar-slip component of deformation. However, based on a full-scale shaking table test (Nagae et al., 2015), Kwon (2016) demonstrated that Equations 4-2 and 4-3 are equally valid for columns framing into foundations and/or beam-column joints. In these equations, the effective flexural rigidity of beams and columns is given as a function of the peak prior lateral drift ratio (DR), the compressive axial load ratio, and the longitudinal tension-steel reinforcement ratio (ρ_T). The effective flexural rigidity, which accounts for the component deformations coming from flexure, bar-slip, and shear, is given by:

$$\frac{E_c I_{eff}}{E_c I_g} = 0.003 \mathrm{DR}^{-0.65} + \gamma \le 0.8 \mathrm{DR} \le 0.012 \tag{4-2}$$

where:

$$\gamma = (-50\rho_T + 2.5)\left(\frac{P}{A_g f'_c}\right)^{(-20\rho_T + 2.15)} + (15\rho_T + 0.05) \quad (4\text{-}3)$$

Figure 4-4 illustrates the changes in the effective flexural rigidity of beams and columns as a function of the peak prior drift ratio experienced, compressive axial load ratio, and longitudinal tension-steel reinforcement ratio.

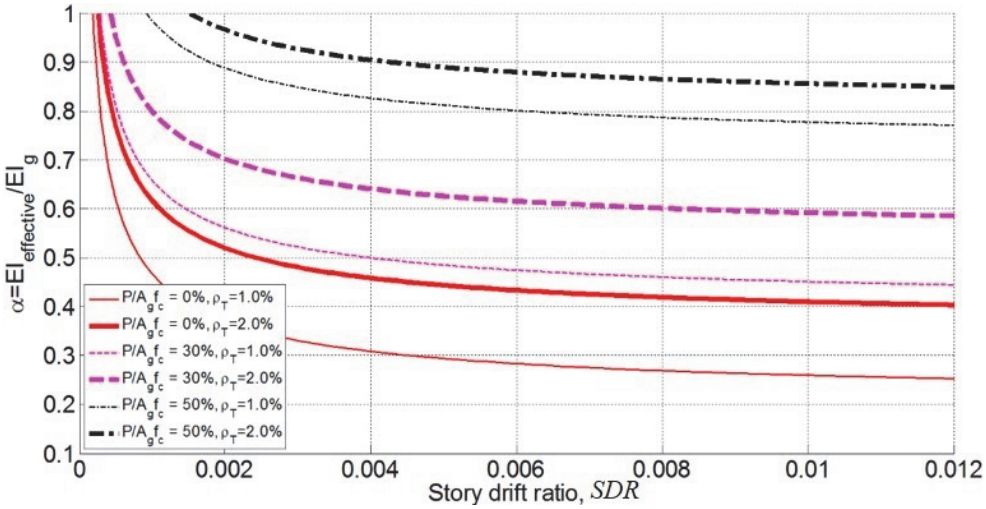

Figure 4-4 Lateral stiffness reduction factor versus maximum prior lateral story drift ratio (SDR) for various axial load ratios and tension-steel reinforcement ratios.

The lateral stiffness produced by Equation 4-2 does not vary greatly beyond a story drift ratio of 0.006 (see Figure 4-4), so the secant stiffness at first yield (K_y in Figure 2-2) can be estimated using a drift ratio of DR = 0.008 (since first yield typically occurs at drift ratios between 0.006 and 0.01 for concrete frame members). The stiffness at first yield should be used in any member expected to yield, which is likely the case for most members in a frame subjected to DBE or MCE_R ground motions. A lower drift ratio value may be used in members at higher floor levels that experience limited forces or deformations even during high intensity ground motions. For service load levels, a value of DR = 0.002 could be used to provide an upper bound on member stiffness; this presumes that the component does not have any stiffness loss from being previously subjected to a larger drift (e.g., from a past earthquake) and if a larger previous drift has been experienced, then that larger drift should be used in the stiffness calculation.

The flexural rigidity equations discussed in this section provide mean estimates for member secant stiffness and are associated with a large degree of variability. If a variability value is needed, a coefficient of variation of 0.45 is appropriate for either stiffness equation (Kwon, 2016).

4.2.2 Flexural Yield Strength

4.2.2.1 Uniaxial Loading with Constant Axial Force

For a set axial load, and loading in one direction, the nominal flexural strength of column and beam frame members can be computed using the strain compatibility approach (assuming that sections remain plane), and an equivalent rectangular compressive stress distribution under ultimate loads with a concrete crushing strain of 0.003 (ACI, 2014). When expected steel yield strength and concrete strength are used, this stress block approach results in a flexural strength close to the observed strength from column tests, with a median ratio of predicted strength to observed strength of 1.02 and σ_{LN} of 0.23 (Haselton et al., 2016).

4.2.2.2 Loading in Two Directions and/or with Variable Axial Load

Column members often have variable axial load and may also simultaneously be subjected to a bending moment about both axes. The combination of axial force and biaxial moment complicates the determination of the flexural strength, or yielding point, as the strain compatibility approach results in different yield strengths depending on the assumed axial force. To account for this complication of coupled axial and moment behavior, the strength of a column section can be defined as a *P-M* or *P-M-M* surface. Depending on the preference of a designer and software capabilities, the yield surface is defined either by providing multiple yield points on the *P-M-M* or by more fully defining a *P-M-M* surface. Figure 4-5 illustrates how such surfaces can be done in commercial software.

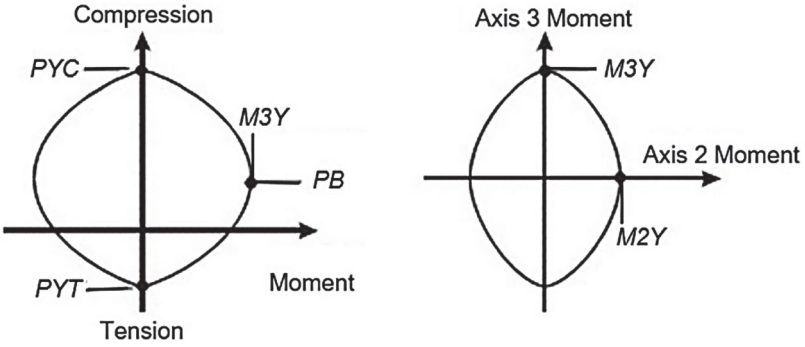

(a) *P-M* interaction at *M2Y* = 0 (b) *M-M* interaction at *P* = *PB*

Figure 4-5 Reinforced Concrete *P-M-M* surfaces in PERFORM-3D (CSI, 2016b).

It should be noted the post yield bending behavior (i.e., the shape of M-θ backbone curve) does not maintain the same shape for different flexural yield points along the *P-M-M* surface. Therefore, it may be required to define multiple backbone curves for varying intensity of the axial force and different moment angles. For example, a section with high compressive axial load will most likely results in some brittle crushing failure when bending moments are added and therefore the backbone curve

should properly reflect the failure shortly after the yield point; this is in contrast a delayed failure that would be observed for a column with light axial load and behavior that is closer to that of a beam element.

Defining the basic yield surface in common software may seem straightforward, but accurately capturing how the shape of M-θ backbone curve changes for various points on the P-M-M surface is a difficult process and creates more opportunity for errors in the analysis. Therefore, it is recommended that simpler M-θ backbone curves (without P-M-M) be used for a concentrated hinge component model. If directly modeling P-M-M behavior is desirable, then it is recommended that a fiber-based P-M-M hinge be used (with associated fiber modeling guidelines provided in Chapter 5).

4.2.3 Nonlinear Modeling Parameters

Unless noted otherwise, the recommended nonlinear modeling parameters provided in this section are from Haselton et al. (2016), which based their work on a dataset of 255 tests conducted on rectangular reinforced concrete column. The vast majority of tests in the dataset were pseudo-static cyclic tests in which columns were under constant compressive axial load. Only 27 monotonic tests were available and included in the database. The column test data was obtained from the database compiled by Berry et al. (2004). An expanded version of the database is available online (Ghannoum and Sivaramakrishnan, 2012a, 2012b). The data include tests failing in either flexure or flexure-shear; the empirical equations are calibrated to reflect the effects of detail on the component behavior, although this data set likely produces slightly conservative component modeling results as compared with a flexure-only data set. Properties of the 255 column dataset are as follows.

- Rectangular columns failing in a flexural mode (220 tests) or in a combined flexure-shear mode (35 tests); columns failing in a brittle shear mode were excluded
- Cross-section width, b, ranging from 150 to 550 mm (6 to 22 in); cross-section height, h, ranging from 150 to 610 mm (6 to 24 in)
- Concrete compressive strength, f_c', ranging from 20 to 120 MPa (3 to 17 ksi)
- Steel yield strength, f_y, ranging from 340 to 520 MPa (49 to 75 ksi)
- Compressive axial load ratio, $P/A_g f_c'$, ranging from 0.0 to 0.7, where P is the axial load, and A_g is the gross concrete cross-sectional area
- Shear span ratio, L_s/h, of 1.5 to 6.0
- Longitudinal reinforcement ratio, ρ, ranging from 0.015 to 0.043, where ρ is the ratio of longitudinal steel area to gross concrete area, A_s/A_g

- Spacing of transverse reinforcement, s/d, ranging from 0.1 to 0.6, where s is the tie spacing along member length and d is the cross-section bending depth (measured from the centroid of tensile reinforcement to the extreme compression fiber)
- Transverse reinforcement ratio, ρ_{sh}, ranging from 0.002 to 0.02, where ρ_{sh} is the ratio of transverse steel to concrete areas, A_{sh}/sb
- All database test specimens had symmetric longitudinal reinforcement and most had square cross-sections

4.2.3.1 Post-Yield Hardening Stiffness

Haselton et al. (2016) report that the axial load ratio and concrete strength are statistically significant for the prediction of the hardening stiffness, M_u/M_y, however, the inclusion of both of the parameters only resulted in an R^2 statistic of 0.17, not justifying their use. Ultimately, the following constant ratio of M_u/M_y was found to provide an acceptably low uncertainty of $\sigma_{LN} = 0.10$. This ratio of M_u/M_y was calibrated to a dataset consisting mostly of cyclic tests. However, the proposed equation is recommended for both monotonic and cyclic loading because the limited number of available monotonic tests prevented distinguishing between the two loading types.

$$M_u/M_y = 1.13 \tag{4-4}$$

Because Equation 4-4 was derived directly from column global force-deformation relations that include bar-slip deformations, Equation 4-4 accounts for the inelastic bar-slip softening effects.

4.2.3.2 Plastic Rotation Capacity

In contrast to the mechanics-based stiffness and strength equations, the equation to determine deformation limits, θ_p, is largely based on empirical evidence. Equation 4-5 can be used to determine the monotonic-curve rotation capacity (measured in radians) between yield and the peak moment resistance.

$$\theta_p = 0.155(0.16)^{v}(0.02 + 40\rho_{sh})^{0.43}(0.54)^{0.01c_{units}f'_c} \tag{4-5}$$

As the experimental data used to develop Equation 4-5 are limited to tests of columns with symmetrical reinforcement, the equation only applies to sections with symmetric reinforcement. Therefore, to model members with non-symmetric reinforcement, Equation 4-5 can be multiplied by the following correction term (Fardis and Biskinis, 2003), based on the ratio of the normalized reinforcement ratios of compressive, ρ', and tensile, ρ, steel:

$$\theta_p(\text{non-symmetric}) = \left[\frac{\max\left(0.01, \frac{\rho' f_y}{f_c'}\right)}{\max\left(0.01, \frac{\rho f_y}{f_c'}\right)}\right]^{0.225} \theta_p(\text{symmetric}) \quad (4\text{-}6)$$

4.2.3.3 Post-Capping Rotation Capacity

The parameters considered in the development of an equation for predicting post-capping rotation capacity are those that most influence deformation capacity, namely axial load ratio, transverse steel ratio, rebar buckling coefficient, stirrup spacing, concrete strength, and longitudinal steel ratio. In contrast to the calibration of other parameters where data from over 250 tests were used, there are only 15 tests suitable for calibration of the post-capping rotation, such that a post-capping slope was clearly evident in the measured data. Considering the trends of the limited data, the proposed equation is based on the axial load ratio, v, and transverse steel ratio, ρ_{sh}. As this equation was created based on limited test data, 0.10 was selected as a conservative upper bound for θ_{pc}. More recent research on large-scale ductile columns shows that this 0.10 upper bound is highly conservative (Nojavan et al., 2016). The equation for monotonic post-capping rotation is as follows:

$$\theta_{pc} = (0.76)(0.031)^{v}(0.02 + 40\rho_{sh})^{1.02} \leq 0.10 \quad (4\text{-}7)$$

4.2.3.4 Cyclic Behavior and Energy Dissipation

Once the envelope monotonic moment-rotation curve is defined in a concentrated hinge model (Figure 4-1), the cyclic behavior and degradation parameters need to be specified for nonlinear dynamic analyses (see Figure 2-5 of the *Part I Guidelines*). The nonlinear modeling parameters discussed here were calibrated using modeling parameters extracted from an experimental database. However, as most tests in the database were conducted using cyclic loading protocols, monotonic envelope parameters were inferred by projecting from the experimental data using the Ibarra et al. (2005) peak-oriented analytical model. The calibrated monotonic envelope parameters proposed by Haselton et al. (2016) are therefore best used with the damage accumulation algorithms of the Ibarra et al. analytical model to achieve strength and stiffness degradation due to cyclic damage progression. Cyclic energy dissipation can be quantified using a reference energy dissipation capacity based on the capping plastic rotation (Ibarra et al., 2005):

$$E_t = \lambda' M_y \theta_p \quad (4\text{-}8)$$

Past research has shown that cyclic degradation is highly dependent on the axial load level with cyclic energy dissipation capacity decreasing with increased axial load (CEB, 1996). The following equation reflects this trend

$$\lambda' = 30(0.3)^{v} \quad (4\text{-}9)$$

The energy dissipation capacity was calibrated using the Ibarra et al. (2005) peak-oriented analytical model (using the calibration approach described in Appendix C of the *Part I Guidelines*). Haselton et al. (2016) introduced energy-based degradation to the strength, post-capping strength, unloading stiffness, and reloading stiffness hysteretic parameters. The Ibarra et al. damage algorithms use a damage parameter (β_i) by which these hysteretic parameters are adjusted at each drift excursion (i):

$$\beta_i = \left(\frac{E_i}{E_t - \sum_{j=1}^{i} E_j} \right)^c \tag{4-10}$$

where (from Ibarra et al., 2005) E_i is the hysteretic energy dissipated in excursion i, E_j is the hysteretic energy dissipated in all previous excursions, E_t is the reference hysteretic energy dissipation capacity (which is a calibrated parameter based on component detailing), and c is the exponent defining the rate of deterioration. The value of c can be taken in the range of 1.0 to 2.0. Haselton et al. (2016) used a value of c = 1.0 when calibrating the modeling parameter relations.

Each time the element crosses the point of zero load, the Ibarra model reduces the strength, post-capping strength, and unloading stiffness parameters by the factor (1 - β_i). The model also increases the reloading stiffness parameter by the factor (1 + β_i).

The Ibarra et al. material model is implemented in the open source analytical software OpenSees (McKenna et al., 2000). Even so, the cyclic degradation relations presented in this section can be used with any software possessing a peak-oriented material model with energy-based damage accumulation rules that are in agreement with the presented rules.

4.2.3.5 Relationships between the Monotonic and Cyclic Backbone Curves

The rotation capacities provided in Section 4.2.3.2 estimate the monotonic loading curve, and the relationship between this curve and other backbone definitions has been described in Chapter 2 of the *Part I Guidelines* (NIST, 2017). Per *Part I Guidelines* Chapter 2, the monotonic rotation capacities are not directly comparable to cyclic backbone curves used in documents such as ASCE/SEI 41-17, which are intended to represent the degraded cyclic envelope. If cyclic degradation is not introduced explicitly in analyses as discussed in Section 4.2.3.4, a reduced moment-rotation backbone curve can be applied to implicitly account for degradation (see cyclic backbone in Figure 4-2 and Figure 4-3). Preliminary studies to relate the two (PEER/ATC, 2010) suggest that the monotonic values can be adjusted to obtain equivalent cyclic backbone properties as follows:

$$\theta_{p,cyclic} = 0.7\theta_p \tag{4-11}$$

$$\theta_{pc,cyclic} = 0.5\theta_{pc} \quad (4\text{-}12)$$

Figure 4-3 previously showed test data for a full-scale reinforced concrete column specimen to illustrate this difference between a monotonic backbone and cyclic backbone curves computed from two different cyclic loading protocols. In the absence of more detailed information like shown in Figure 4-3, the above equations can be used to approximate the cyclic backbone curve from the estimated monotonic curve.

4.2.3.6 Modeling Approach to Capture Response to Any Generalized Loading-History

As previously discussed in Section 4.1, the objective of the Section 4.2 modeling approach is to model a beam or column in such a way that the response can be predicted for any loading history. If the model is created per the recommendations in this document, the same component model should respond correctly when monotonically pushed and also respond correctly when cyclically loaded with any type of cyclic loading protocol. To illustrate this, test data are presented for a series of identical full-scale reinforced concrete columns recently tested under various loading protocols (data and figures are after Nojavan et al., 2014, 2016).

Figure 4-6 shows the five different loading protocols used for testing, ranging from monotonic loading to cyclic loading with many cycles, and also including a protocol that was developed to represent near-collapse loading behavior on a building. Figure 4-7 shows the test data results from the nominally identical test specimens subjected to the five different loading protocols; this shows that the component results differ substantially when the component is subjected to the variable loading protocols. Figure 4-7 also shows the computational results obtained from the model described in Section 4.2, calibrated individually to each set of test data (to provide the best possible fit that the model could provide), showing that the generalized model can capture reasonably well the response under all of these types of loading protocols. Figure 4-8 then shows the cyclic backbone curves for each protocol, computed as the "first cycle" envelope curve (which connects the peak responses at the first cycle of loading for each subsequent loading increment). This shows that the cyclic protocol can substantially reduce the envelope curve when there are many cycles of loading, but that the backbone curve for many of the cyclic loading protocols (which have fewer cycles) are similar to the monotonic curve.

The data in these figures illustrates what behavior a well calibrated component model should be able to capture.

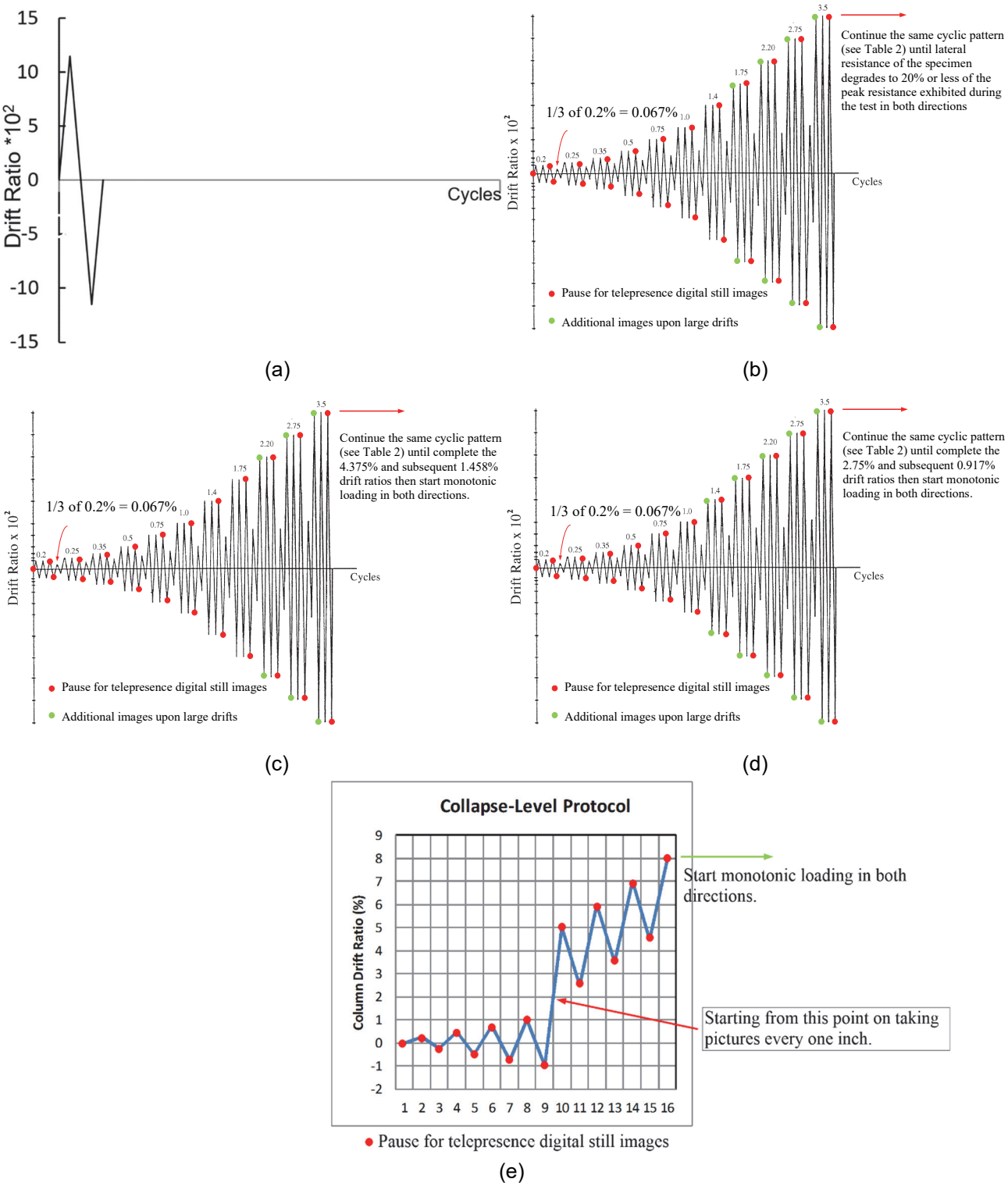

Figure 4-6 Loading protocols for specimens: (a) monotonic push in each direction; (b) ACI 374 symmetric cyclic; (c) ACI 374 symmetric cyclic followed by final monotonic push # 1; (d) ACI 374 symmetric cyclic followed by final monotonic push # 2; and (e) a near-collapse loading protocol (after Nojavan et al., 2014, 2016).

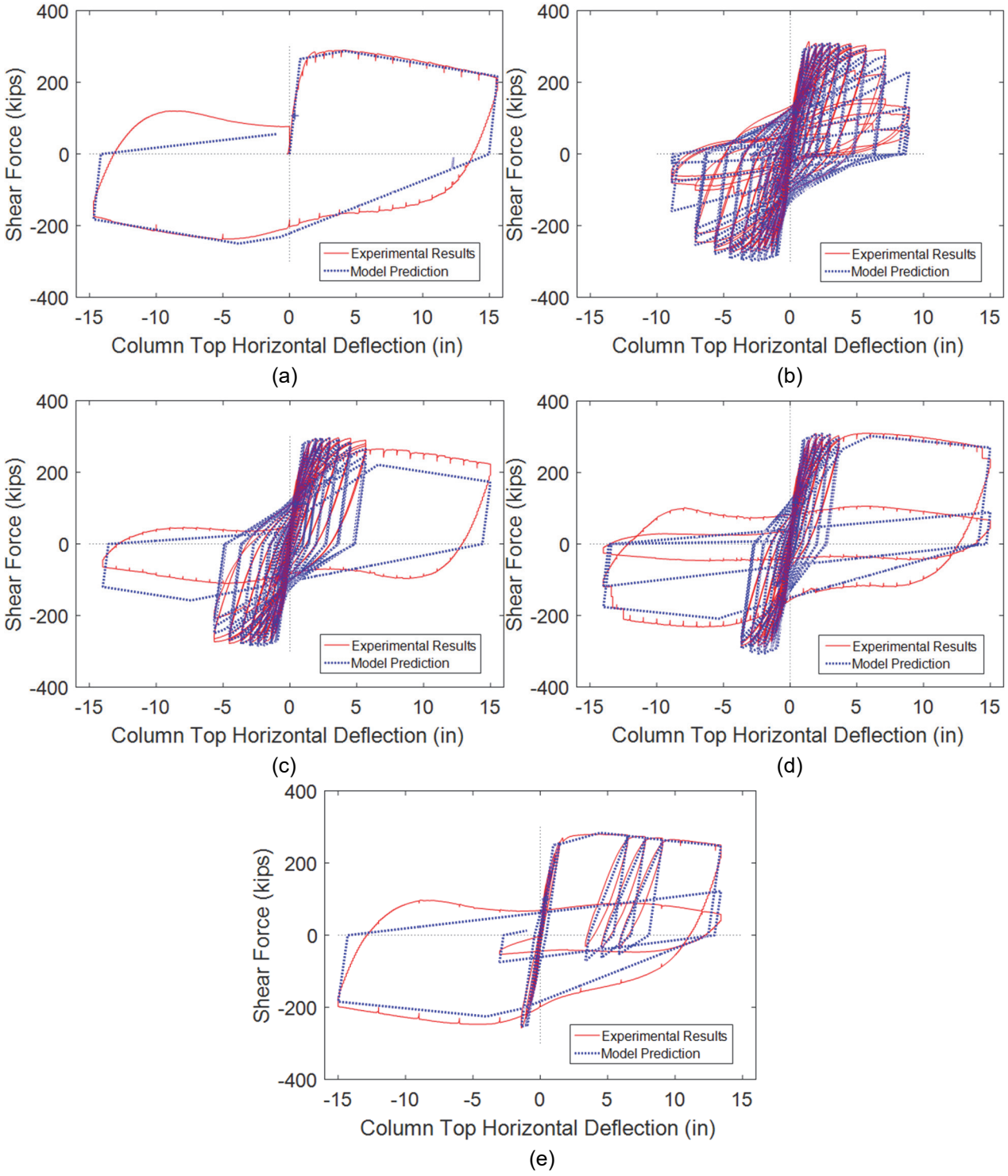

Figure 4-7 Experimental test data and calibrated model predictions (after calibration) for the following loading protocols show in Figure 4-4: (a) monotonic push in each direction; (b) ACI 374 symmetric cyclic; (c) ACI 374 symmetric cyclic followed by final monotonic push # 1; (d) ACI 374 symmetric cyclic followed by final monotonic push # 2; and (e) a near-collapse loading protocol (after Nojavan et al., 2014, 2016).

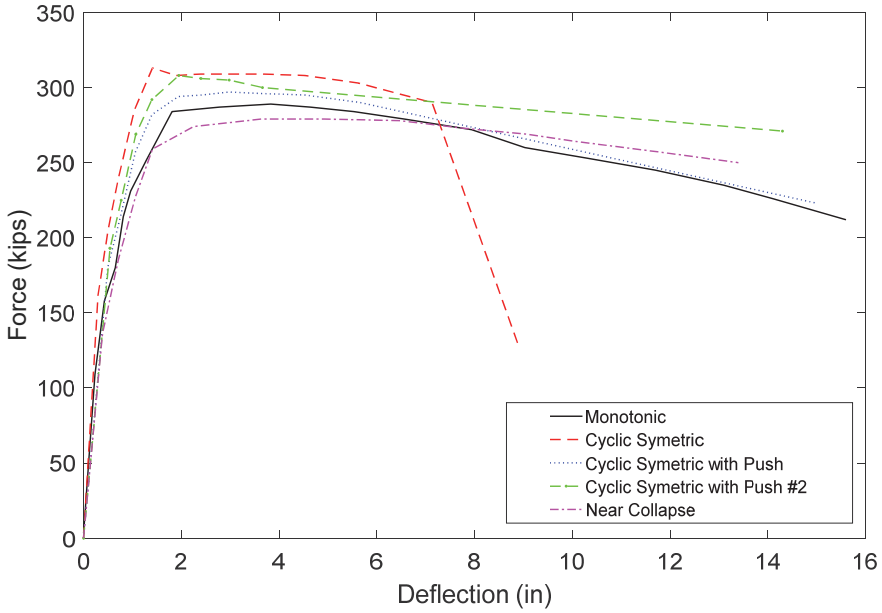

Figure 4-8 Cyclic envelop curves for identical columns subjected to various loading protocols (from Nojavan et al., 2014).

4.2.3.7 Uncertainties in the Component Modeling Parameters

The relations for the modeling parameters proposed by Haselton et al. (2016) were derived empirically based on a compiled database of experiments. The median and logarithmic standard deviation values for the ratio of predicted response parameters to the experimentally derived parameters are presented in Table 4-1. The values in Table 4-1 are not needed for most nonlinear analysis because the focus of the modeling is to have a mean-based model (per *Part I Guidelines*). However, these values are useful if one wanted to conduct probabilistic analyses of structural response or a sensitivity study.

Comparisons between modeling the parameters for columns by Haselton et al. (2016) and ASCE/SEI 41-13 can be found in Haselton et al. (2016).

Table 4-1 Prediction Uncertainties and Bias in Proposed Equations (Haselton et al., 2016)

Equation	Median (predicted / observed)	σ_{LN}
Post-yield Hardening Stiffness: M_c/M_y (Eq. 4-4)	1.01	0.10
Plastic Rotation Capacity: θ_p (Eq. 4-5)	1.02	0.61
Post-capping Rotation Capacity: θ_{pc} (Eq. 4-7)	1.00	0.72
Cyclic Energy Dissipation Capacity: λ' (Eq. 4-9)	1.08	0.60

4.3 Modeling of Moment Frame Beams

In the case where drop beams are not present, or when the web of the beam extending beyond the slab is less than the thickness of the slab (h_s), a portion of the slab spanning between vertical elements can be treated as an effective beam (or slab-beam) and assigned an elastic element with nonlinear rotational hinges at its ends. Torsional connecting spring elements can be added to connect the slab-beam rotation hinges and the vertical elements. The torsional elements can be used to simulate the punching shear failure mode. ACI 369R-17, *Guide for Seismic Rehabilitation of Existing Concrete Frame Buildings and Commentary* (ACI, 2017), and ASCE/SEI 41-17 provisions for slab-column moment frames specify the effective width (b_{eff}) of the slabs to include in strength and stiffness evaluations. ACI 369R-17 and ASCE/SEI 41-17 also present nonlinear modeling parameter for the slab-beam with the *a* parameter corresponding to θ_p and the *b* parameter corresponding to θ_{pc}. The reader is referred to Section 3.6 for additional details on how to model flat slab systems.

For the case where substantial drop beams are present (i.e., where the web of the beam extending beyond the slab is greater than the thickness of the slab, h_s), modeling the lateral behavior of beams is done similarly to that of columns. However, the composite action between beams and slabs in flexure need to be taken into account when evaluating beam strength and stiffness.

ACI 369R-17 and ASCE/SEI 41-17 specifies the effective width of slab on each side of the beam web (or effective flange width) for both strength and stiffness calculations to be taken equal to the smallest of the provided flange width, eight times the flange (or slab) thickness, half the distance to the next web, and one-fifth the beam span length.

Once the effective width of the slab acting compositely with a beam is determined, beam modeling parameters can be determined based on column parameters but using a T-section as follows:

- **Elastic stiffness.** The moment-curvature approach as well as the empirical stiffness reduction relations can be used to estimate beam elastic stiffness. Because the response of T-beams is not symmetric with respect to bending direction, the average of the negative and positive bending flexural stiffnesses can be used to define the stiffness of the beam elastic line element.
- **Moment strengths.** Yield and peak moment strengths can be determined as for columns, but should include the slab steel within the effective flange width.
- **Plastic rotation capacity.** Beam plastic rotation capacity can be estimated using Equation 4-5 with adjustments made based on Equation 4-6 for non-symmetric

reinforcement layouts. The slab steel within the effective flange width should be included in the reinforcement ratios when using Equation 4-6.

- **Post capping rotation capacity and hysteretic strength degradation.** There is limited experimental evidence available to determine these properties for beams.

4.4 Modeling of Beam-Column Joints

Two approaches are considered in this report because they are numerically robust and allow for computationally efficient modeling. The approaches are: (1) adjusting the stiffness of beam and column offsets within the joint panel regions; and (2) introducing a rotational hinge at the beam-column intersection.

4.4.1 Stiffness Adjustment of Beam and Column Offsets

Birely et al. (2012) evaluated the accuracy of several commonly prescribed joint-offset stiffness recommendations, including those from ASCE/SEI 41-13. The evaluations were performed considering test data from 45 interior beam-column joint sub-assemblages, and as such, coupled beam, column, and joint stiffness models.

Reasonably accurate sub-assemblage stiffnesses where observed when the stiffness provisions of ASCE/SEI 41-13 were used. For SMF, in which column flexural strength exceeds that of beams by at least 20% at joints, ASCE/SEI 41-13 stipulates that column offsets within the joint panel should be modeled as essentially rigid, while those of the beams should be modeled as having the same elastic stiffness as the beams (Figure 3-3a). These joint modeling recommendations do not account for softening effects due the slip of beam and column longitudinal bars within the joint region. Therefore, the recommendations should be used in conjunction with the ASCE/SEI 41-13 beam and column stiffness provisions or other frame member models that include the effects of bar-slip within the joint-panel region. The ASCE/SEI 41-13 beam and column elastic stiffness provisions are presented in Section 4.2.2.2 (Equation 4-1) of this document, which remained unchanged in the ACI 369R-17 and ASCE/SEI 41-17 standards.

Birely et al. (2012) also considered beam and column member stiffnesses that are generally lower than those of ASCE/SEI 41-13 and more consistent with stiffness recommendations proposed by Kwon (2016) as provided in Section 4.2.1.2. If the beam and column stiffness provisions proposed by Kwon (2016) are used (Equations 4-2 and 4-3), it is recommended to model both column and beam offsets within joints as essentially rigid. In this case as well, the softening effects of bar-slip within the joint panel region are modeled implicitly through the reduced effective stiffnesses of beams and columns. This set of recommendations produced reasonably accurate stiffness of a full-scale four-story reinforced concrete building tested on a shaking table (Nagae et al., 2015; Kwon, 2016).

4.4.2 Rotational Hinge at the Beam-Column Intersection

This type of modeling approach includes rigid offset links to correctly model the geometry of the joint and locations of the interface between the joint and the beams and columns. A rotational hinge is provided at the center of the joint model to account for the shear behavior of the joint (Figure 3-3b). Spring models exist for both modern and older, non-ductile joints, though the research has focused more on older joints. A summary of available joint models is provided in Jeon et al. (2014) with several of the models defining a joint shear stress versus strain response that can be used for modeling. Celik and Ellingwood (2008) provide guidance on transforming a joint shear stress versus strain relationship to a joint moment versus rotation relationship for use with the rotational hinge and element configuration shown in Figure 3-3b.

However, given the reasonable accuracy obtained by adjusting beam and column offsets, and the added complexity of implementing and calibrating the hinge-type models, the former approach is recommended unless significant joint damage is anticipated and a more detailed modeling approach is warranted.

4.5 Modeling of Gravity System Connections

Section 3.6.2 provides an overview of how the slab-column system can be idealized and this section provides additional detail for how the slab-column model can be created when using the concentrated hinge modeling approach.

4.5.1 Slab-Beam Strength

If the slab-beam flexural strength is lower than the connection punching shear strength, inelastic response is assumed to concentrate at the hinges located at the ends of the slab-beam elements. The flexural strength of the hinges at slab-beam ends is estimated assuming that only the reinforcement within the column strip, as defined in ACI 318-14, is effective in resisting moments caused by lateral loads. The analysis should account for the effects of moments caused by gravity within the column strip by applying gravity loads before lateral demands are applied. A good reference is not available for the post-yield moment-strength hardening ratio (M_u/M_y), so the suggested value of $M_u/M_y = 1.13$ is recommended as for beams and columns (Equation 4-4).

The slab-column connection punching-shear behavior is modeled by a rotational spring that can transfer moment between the slab and the column, as shown in Figure 3-4. This spring can be idealized as a rigid-plastic spring of strength M_f/γ_f, where M_f is capacity of the connection to transfer moments through flexure (and should be computed using expected material properties) and γ_f is the fraction of the moment assumed to be transferred through flexure in conventional design. The value of γ_f can

be computed as follows using Equation 8.4.2.3.2 of ACI 318-14, where b_1 is the column dimension in the direction of loading and b_2 is the column dimension in the orthogonal direction.

$$\gamma_f = \frac{1}{1+\left(\frac{2}{3}\right)\sqrt{\frac{b_1}{b_2}}} \tag{4-13}$$

For interior slab-column connections, M_f is limited by the strength of reinforcement (top and/or bottom) within 2.5h from column faces perpendicular to the direction of moment M_f, where h is the slab thickness. For exterior slab-column connections, Moehle (2015) recommends assuming γ = 1.0 and calculating M_f for a yield line "along the inside face of the column and extending at 45º angle to the slab edge." This yield line is not to extend beyond 1.5h from column faces perpendicular to the direction of M_f.

4.5.2 Slab-Beam Stiffness

Estimates of the stiffness of the slab-column system are obtained with assumptions different from assumptions used to estimate strength. To estimate stiffness, the "effective width" of the slab is recommended by Hwang and Moehle (2000) as follows:

$$\text{effective width} = 2c + \frac{L}{3} \tag{4-14}$$

where L is the slab span perpendicular to the direction of bending and effective width and c is the column cross-sectional dimension in the direction of L.

For exterior columns and for bending moment parallel to the slab edge, this effective width should be reduced by 50%. These estimates of effective width were obtained assuming the slab-column joint is rigid.

Slab bending stiffness should be reduced to account for cracking. Bending stiffness of reinforced concrete slabs supported by square columns and having spans of similar length in both directions (with f'_c = ~ 4 ksi and f_y = 60 ksi) may be assumed to be a fraction β of the bending stiffness of the gross section (Hwang and Moehle, 2000) as follows:

$$\beta = 4\frac{c}{L} \geq \frac{1}{3} \tag{4-15}$$

Prestressed slabs should be expected to have reduced cracking and larger stiffness. ACI 369R-17 and ASCE/SEI 41-17 recommend β = 0.5 for post-tensioned slabs (Kang and Wallace, 2005).

4.5.3 Connection Plastic Rotation at Punching-Shear Strength Loss

The ACI 369R-17 and ASCE/SEI 41-17 standards provide modeling parameters for the plastic rotation at punching shear failure, which can be used in the torsional spring of the slab-column connection. The modeling parameters are provided in tabular from in the standards for prestressed and non-prestressed slabs. The table in the standards also distinguishes between slabs with and without continuity steel through a column connection, while the provided modeling parameters deliver estimates of mean response for slabs with continuity steel and mean minus one standard deviation for slabs without continuity steel. Elwood et al. (2007) discusses the development of the modeling parameters for slab-column connections, which are illustrated in Figure 4-9.

Once punching shear occurs there is an associated strength loss (as shown previously in Figure 3-5), with the post-punching behavior depending on whether the slab-column connection has bottom continuity reinforcing through the connection. The scope of this document is for modern buildings (which would have bottom continuity steel going through the joint), so a punching shear failure should result in strength loss but not a vertical instability problem for the building; therefore, provided that the strength loss is modeled, the occurrence of punching shear would be allowable and would not invoke a deformation-controlled acceptance criteria to be checked (see Section 6.3 of *Part I Guidelines* (NIST, 2017)). If continuity steel were not present, and the possibility of vertical instability existed, then the drift at vertical instability would need to be estimated and a deformation-controlled acceptance criterion would need to be enforced (or the default ACI 369R-17 and ASCE/SEI 41-17 values could be used, per Section 6.3 of *Part I Guidelines*).

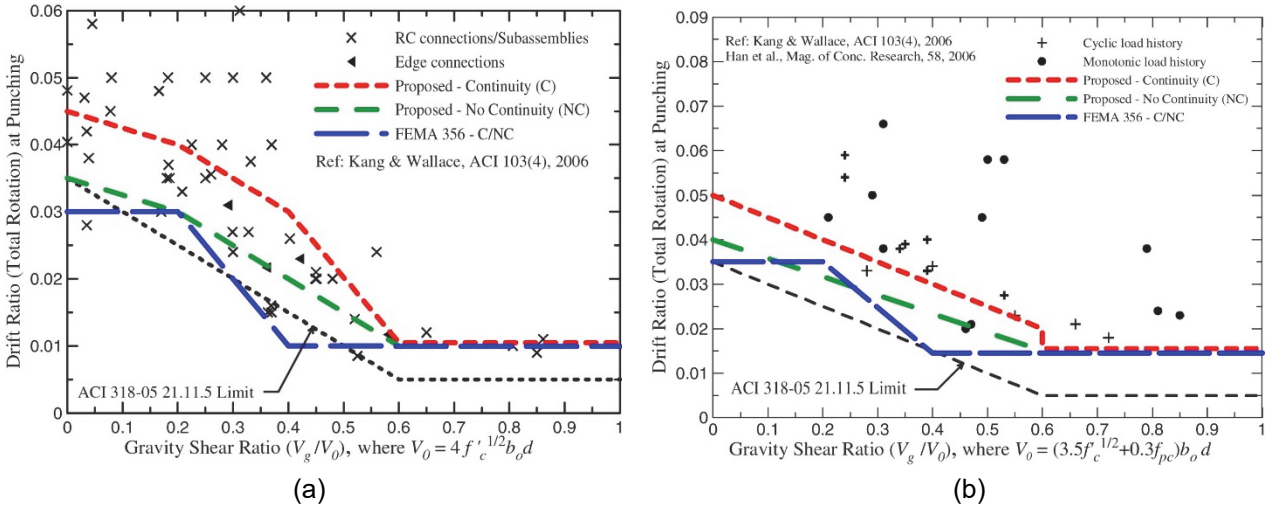

Figure 4-9 Drift ratio at punching shear failure versus ratio of shear caused by gravity to shear strength attributable to the concrete $V_0 = V_c$ (Elwood et al., 2007).

Chapter 5

Fiber-Type Component Models

5.1 Overview

As discussed in Section 2.4 in *Part I Guidelines*, and discussed in further detail in Section 3.1.2 of this *Guidelines* document (with specific reference to Figure 3-2), fiber-type components can be used to provide an intermediate level of detail between concentrated plastic hinge components and detailed continuum models. In this approach, a cross section is discretized into fibers describing the section geometry each having a uniaxial nonlinear material model. Fiber sections may be assigned to one or more sections (integration points) along the length of the frame element. At each section, the stresses are integrated over the fibers resulting in the overall forces acting on the cross section. The primary two types of fiber models are those that have concentrated inelasticity (with all of the inelasticity at a discrete plastic hinge, which requires the plastic hinge length to be defined) versus models that have distributed inelasticity (where a plastic hinge length is not set and some type of numerical integration is performed over the element length to convert strains to rotations and displacements).

The following are some of the advantages of using fiber section models for reinforced concrete moment frames:

- They provide an accurate representation of section properties including geometry, material properties (steel, concrete), including the possible use of complex uniaxial material constitutive models, which allows an increased level of accuracy in describing section response.
- It is possible to model sections of virtually any shape including custom geometries, T-beams, and columns of different shapes.
- The number of degrees of freedom per element and the number of overall elements are usually unchanged compared to using concentrated hinge models, which means that the size of the stiffness matrix and overall problem size is about the same, as long as sections do not use an excessive number of fiber elements, which is usually unnecessary.
- These models rely on first principles of fiber stress-strain response, which allows them to automatically handle *P-M* and *P-M-M* interaction of beams and columns.

- These models can capture axial growth and lengthening effects associated with flexure and curvature (due to crack opening) and neutral axis shift. For restrained members, the axial lengthening can generate significant axial forces that would have been otherwise ignored with other types of models. This is especially important when these forces act on other force-controlled members.
- Fiber models can be used to model some special modes of behavior, such as fracturing connections, and compression-only behavior.
- These models can accurately represent *P-M* and *P-M-M* interaction effects on strength and stiffness, which can be very important for accurately estimating maximum shears in members with varying axial loads such as columns and link beams. It also avoids underestimation or overestimation of concurrent element forces (moment and axial forces) acting on a section. Even though some concentrated hinge models account for *P-M* force interaction, the axial and bending stiffnesses are usually assumed to stay constant in those models, which can lead to significant differences in stiffness that can affect force and deformation distribution. For example, a column experiencing an increase in axial load will experience both increased strength and stiffness and attract substantially more shear force. This effect cannot be accurately predicted by concentrated hinges.

Using fiber-type component models for reinforced concrete moment frames have some limitations and challenges, including:

- They entail an increased computation cost for the state determination at the section level, which depends on the number of fibers used per section, and the complexity of the uniaxial material models. However, satisfactory results can usually be achieved with a relatively small number of fibers, which keeps the computation increase to a minimum.
- It assumes that plane sections remain plane, which is not true especially at large strains.
- Shear and torsion are usually assumed to be elastic, though it is usually simple to introduce uncoupled nonlinear shear springs. It is difficult to model interaction between shear and axial/bending behavior. Section 5.4.2 discusses modeling of shear behavior.
- While the fiber-based formulation relies on first principles and is very accurate in representing section axial and bending actions, the typical fiber models cannot handle rebar bond slip. Section 5.4.1 provides guidance on incorporating bond slip directly into the fiber model.
- The fiber-based models typically are also not able to represent rebar buckling and fracture behavior. Even when fiber-type models attempt to account for buckling

and fracture behavior in the steel stress-strain model, this often leads to numerical issues due to strain localization. If high levels of nonlinear degradation are being modeled, including modes like rebar buckling and fracture, then a more phenomenological and empirically-calibrated concentrated hinge model should be used (see Chapter 4).

- It is difficult to directly model complex pinching and degrading behavior, especially in the presence of shear-flexure interaction, although some basic pinching behavior is captured by the fiber-section formulation, especially when the steel uniaxial model includes the Bauschinger effect. Those effects can be included by modifying the fiber constitutive models to affect overall section behavior, although it could be difficult to calibrate such a model to reproduce very complex behaviors.
- Axial lengthening can lead to unexpected results when used with rigid diaphragms and other similar constraints; care should be taken to not impose axial constraints to a fiber model, otherwise the use of fiber elements should generally be avoided if such constrains are present in the model.

The reader is also referred to Section 2.4, *Part I Guidelines*, for additional discussion of the benefits and limitations of fiber models.

5.2 Fiber-Section Modeling

With fully distributed plasticity element models, the fiber section locations and integration weights are usually selected to match optimal integration algorithms, and the user may not have the ability to control the integration weights at key locations, such as at the ends of the element. This may result in effective plastic hinge length for the end sections that is driven by the weight of the integration algorithm and the number of integration points, rather than by physical empirical data. While such a model might provide reasonable overall response, the local deformation and curvatures may be inaccurate. Alternatively, using an element with a finite length hinge zone (plastic hinge model) can partially resolve this limitation, since the analyst is able to provide the actual plastic hinge length over which the curvature and axial strain of the fiber section are integrated, resulting in better consistency between the global and local deformations. When using such techniques, it is recommended to calibrate the plastic hinge assumption, and monitor its performance during the analysis using monitoring gages (when supported by the analysis software).

It is also important to understand the software's assumption about where the fiber section is located, especially for plastic hinge models. With some software, it might be possible to explicitly specify the location the fiber section where the moment is evaluated, such as at the edge of the plastic hinge zone (e.g., at the column face or centerline) or an offset location, for example at the middle of the plastic hinge. Note

that some software (e.g., PERFORM-3D) will only allow a single integration point, where the fiber section will be located at the middle of plastic hinge segment. For beams, this can lead to a larger maximum beam moment at the face of the column than expected, and the difference will depend on the length of the plastic hinge zone and the moment gradient in the hinge. Other software, such as OpenSees (McKenna et al., 2000), allow the user to specify the actual location of the fiber section within the plastic hinge length.

For fiber models that require definition of a plastic hinge length, it can be estimated using a wide range of available equations and recommendations (not fully enumerated here). A simple rule of thumb is to use a plastic hinge length $l_p = 0.5h$, where h is the depth of the section, which is reasonably accurate for moment frames with typical dimensions. Other more detailed expressions (e.g., Priestley and Park, 1987; Berry and Eberhard, 2008) have been proposed based on analyzing databases of reinforced concrete column test data. Their proposed expressions are functions of multiple parameters including member length, l, bar diameter, d_b, steel yield strength, f_y, and concrete strength, f_c'. One such proposed expression by Berry and Eberhard (2008) is as follows (psi units):

$$l_p = 0.05l + 0.008 d_b f_y / \sqrt{f_c'} \tag{5-1}$$

When the plastic hinge length is unknown or difficult to estimate, fiber-section models with distributed plasticity can be used to estimate the extent of yielding along the element. This can be especially valuable for beams and columns where yielding may not be directly predictable, such as in members with large gravity forces and moments, as well as members where the strength varies significantly along the length. This approach generally works well for hardening components, but if softening is experienced at the section level, numerical localization can occur and the estimated length of the yielding can become highly dependent on the integration scheme (number and weights of integration points). When distributed plasticity is used and the plastic hinge length is known, one possible modeling approach is to specify end elements with a specified length and reduced number of integration points (one or two) in order to explicitly control plastic hinge length, which can be used as an alternative to the plastic hinge model implementation discussed above. This can be particularly helpful with members exhibiting softening behavior. Alternatively, the number of integration points can be set such that the integration weights of the end fiber sections approximately match the plastic hinge length to element length ratio (Hachem et al., 2003). This typically requires the use of three to five integration points depending on the member slenderness. When using elements with displacement-based formulations, there may also be a need to use multiple elements along the member's length in order to better estimate the curvature distribution, due to the linear-curvature assumption in each element. For a typical

moment-frame beam, using three elements, two at the plastic hinges and one for the rest of the beam, is common, though some element types require up to five integration points.

The accuracy of the section response depends on the number of fibers used to discretize the section, which in turn can affect the accuracy of the overall analysis. While increasing the number of fibers improves the accuracy of the predicted behavior, the improvement diminishes quickly as the number of fibers exceeds 5 to 10 concrete fibers in each direction, and almost no improvement is observed beyond 10 to 20 fibers along each direction in most cases. While using more fibers improves accuracy, it also increases the computational cost which, depending on the number of fiber elements in the model, can result in a significant penalty to the analysis. It is recommended to use the fewest number of fibers that result in a reasonable accuracy in the fiber section response, which is best determined by analyzing different discretizations of a section until an optimal discretization is found. In practice, the optimal number of fibers typically ranges from 4 to 10 fibers in each direction of the section. For beams, this generally results in a small number of fibers (for example 10 unconfined and 10 confined concrete fibers along the depth, for a total of 20 fibers). A square column might use 6×6 = 36 fibers for the confined concrete core, and 4×5 = 20 fibers for the cover along the circumference for a total of 56 fibers. The size of the fibers may be varied in order to obtain a higher accuracy with a smaller number of fibers. For example, smaller fibers may be used near the outer edges of the member where the strains are highest, and larger fibers used near the middle. Smaller fibers near the edges of the component, in the region where the unconfined concrete will spall, can also help with convergence because it causes the force change to be more gradual as the cover spalls. In contrast, slightly larger fiber sizes may be used for cover concrete fibers that are not as critical for the overall accuracy of the response. Steel bars are typically represented using one fiber per bar. Bundled bars or bars that are close to each other may be represented using a single fiber with the total area of the bars.

5.3 Fiber Material Modeling

A uniaxial material is assigned to each fiber in the section. In typical reinforced concrete section, three uniaxial material models are usually used to model steel reinforcement, confined concrete and unconfined concrete.

5.3.1 Steel Reinforcement

Typically, the steel stress-strain curve should have the following:

- Initial modulus representing elastic response; this modulus is also used for unloading from a plastic state

- Modeling of the post-yield plateau and/or strain hardening modulus

In addition, it is helpful to capture some or all of the following:

- Bauschinger effect, where the plastic deformation of a material in one direction affects the subsequent response in the opposite direction; this can affect the cyclic response of the member and help with accurate simulation of pinching and unloading behavior
- Cyclic isotropic hardening of the material
- Bond-slip behavior
- Bar buckling and fracture behavior
- Reduction of ultimate (fracture) strain due to low-cycle fatigue

Bond-slip behavior can be modeled directly within the steel constitutive model (in an approximate manner), or modeled separately using special fiber end-sections or rotation springs (Section 5.4.1). Bar buckling rarely governs with well-detailed concrete frame members, and is more commonly observed with older concrete structures with large stirrup or hoop spacing. Bar buckling or low-cycle fatigue can still occur under large cyclic demands, but it is rare for a single earthquake to generate enough large cycles for this to be a concern.

Figure 5-1 shows a commonly used steel stress-strain model by Menegetto and Pinto (1973) that includes the Bauschinger effect. Some structural analysis software support such highly nonlinear models, while other software offer simple bilinear models with kinematic or isotropic hardening (preferred). The basic input parameters for such models are usually the yield stress (f_y) and modulus of elasticity (E_s). The analysis should typically use the expected reinforcement yield stress, which may be approximated as $f_{ye} = 1.2f_y$. Some models require the strain at onset of hardening (ε_{sh}) which can range from 0.005 to 0.015 with a typical value of 0.01, strain hardening modulus (E_{sh}) which can range from $0.021E_s$ for $f_y = 60$ ksi to $0.042E_s$ for $f_y \geq 90$ ksi (ACI, 2003), or ultimate strain at fracture (ε_{su}) which can be taken as 0.12 for #10 bars and smaller and 0.09 for #11 bars and larger, but is recommended to be reduced to 0.09 and 0.06, respectively, in order to limit the likelihood of early fracture due to buckling or low-cycle fatigue (Caltrans, 2006). The values for ε_{sh}, E_{sh}, and ε_{su} can vary with the grade and size of the steel reinforcement and Table 5-1 provides a simple set of recommendations for how ε_{sh} and E_{sh} vary with steel yield strength. The modeling of strain hardening is important for predicting monotonic and cyclic post-yield strength gains, and its omission can be unconservative since it can result in an underestimation of force demands on force-critical member actions.

Table 5-1 Steel Reinforcing Hardening Onset Strain ε_{sh} and Modulus E_{sh} (ACI, 2003)

F_y (ksi)	ε_{sh}	E_{sh}/E_s
60	0.0086	0.021
75	0.0035	0.025
≥90	0.0035	0.042

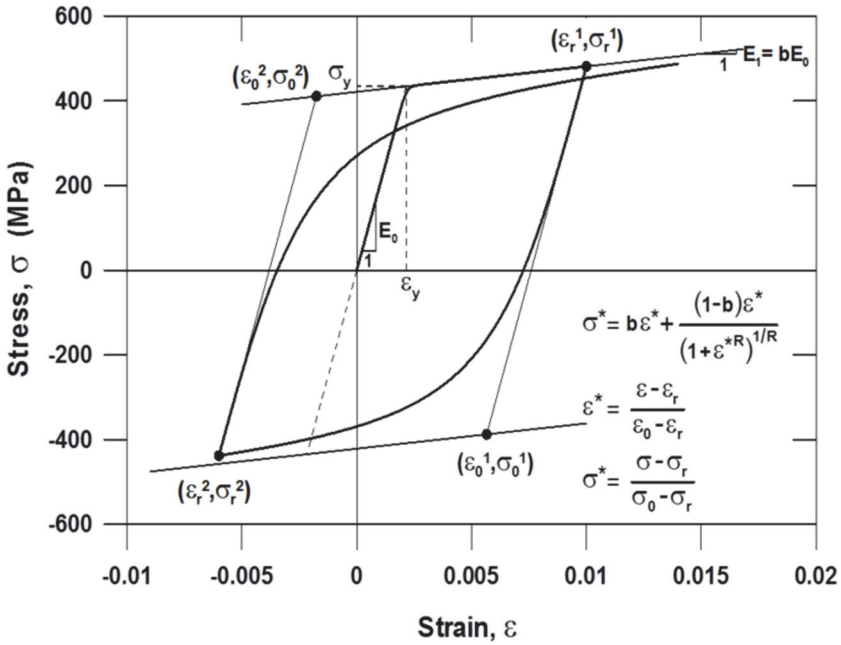

Figure 5-1 Cyclic stress-strain model for steel (Menegetto and Pinto, 1973). Note that the notation shows E_s as E_0 and E_{sh} as E_1.

5.3.2 Confined and Unconfined Concrete – Compressive Stresses

The concrete stress-strain curve typically exhibits a hardening stress-strain segment followed by a softening segment. The negative slope can be steep for unconfined concrete, reflecting a very small ultimate strain capacity, whereby confined concrete can exhibit very stable response up to relatively large strains. There are several models that can be used for modeling concrete uniaxial behavior (e.g., Mander et al., 1988; Chang and Mander, 1994; and Popovics, 1973). While the required accuracy of the model generally depends on the specific modeling requirements, the following are some good model qualities to have:

- Gradual changing initial modulus
- Ability to specify the value of the post-peak descending modulus to represent different levels of confinement
- Ability to specify the concrete maximum compressive strength and corresponding strain

- Ability to specify the maximum tensile strength and corresponding strain
- Adequate modeling of cyclic behavior reflected through loading and unloading rules

The unconfined concrete strength, used to determine the concrete stress-strain model, should be taken as the expected concrete compressive strength, which can be estimated as $f'_{ce} = 1.3\, f'_c$. Mander et al. (1988) and other studies (e.g., Park et al., 1982; Sheikh and Uzumeri, 1982; Ahmad and Shah, 1982; Kappos, 1991; Saatcioglu and Razvi, 1992; Razvi and Saatcioglu, 1999) provide recommended values and equations for estimating key parameters of confined and unconfined concrete stress-strain curves including the peak confined concrete stress (f'_{cc}), peak unconfined and confined strains (ε_{co} and ε_{cc}), spalling strain (ε_{sp}), and ultimate confined strain (ε_{cu}). Typical ε_{co} values for unconfined concrete range from 0.002 to 0.003, and is usually taken as 0.002. The spalling strain, ε_{sp}, is generally not too critical for understanding behavior, but can usually be taken as $2\varepsilon_{co}$. The values for ε_{cc} and ε_{cu} are largely dependent on the level of confinement, but typical values of ε_{cc} generally range between 0.004 and 0.01. Values for ε_{cu} can go up to 0.05 or larger for highly confined columns.

Figure 5-2 shows a stress strain model for confined and unconfined concrete for monotonic stress-strain in compression (Mander et al., 1988). A full implementation for response history analysis requires additional details about tension behavior (discussed in the next section), in addition to loading/unloading and cyclic degradation rules for cyclic behavior. Common structural analysis software typically do not have the capability to model exactly the backbone shape, and the response is usually approximated using a bilinear or trilinear backbone. In general, trilinear models are sufficiently accurate for practical application, and are preferred over bilinear models.

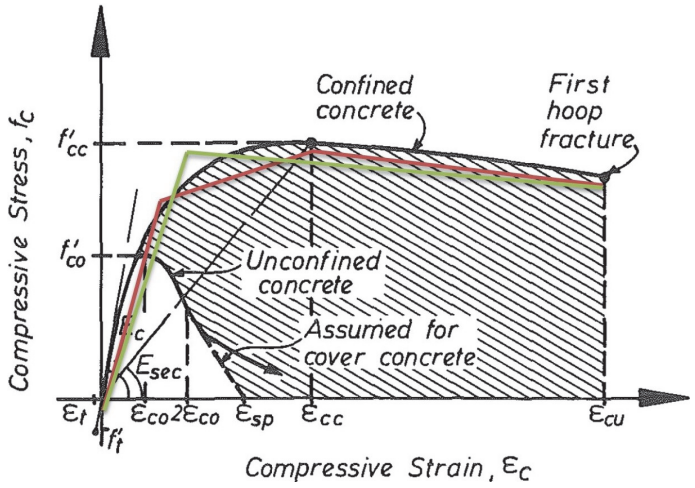

Figure 5-2 Stress-strain model for confined and unconfined concrete (Mander et al., 1988), with simplified bilinear and trilinear approximations.

$$f_c = \frac{f'_{cc} xr}{r - 1 + x'} \tag{5-2}$$

$$x = \frac{\varepsilon_c}{\varepsilon_{cc}} \tag{5-3}$$

$$r = \frac{E_c}{E_c - E_{\text{sec}}} \tag{5-4}$$

$$E_c = 57{,}000\sqrt{f'_{co}} \text{ (psi)} \tag{5-5}$$

$$E_{\text{sec}} = \frac{f'_{cc}}{\varepsilon_{cc}} \tag{5-6}$$

$$\varepsilon_{cc} = \varepsilon_{co}\left[1 + 5\left(\frac{f'_{cc}}{f'_{co}} - 1\right)\right] \tag{5-7}$$

$$f'_l = \frac{1}{2} k_e \rho_s f_{yh} \tag{5-8}$$

where f'_{cc} and ε_{cc} are the maximum confined concrete stress and corresponding strain, respectively, and f'_{co} and ε_{co} are the unconfined concrete strength and corresponding strain. ε_{co} may be taken as 0.002.

f'_l is the effective lateral confining stress on the concrete, as defined in Equation 5-8, along a given direction. Note that it is possible to have different confining stresses f'_{lx} and f'_{ly} along the x and y directions of a section, respectively. ρ_s and f_{yh} are the transverse reinforcement ratio and yield strength, respectively.

k_e is the confinement effectiveness coefficient that is defined by Equation 5-9 as follows and Figure 5-3 for rectangular sections.

$$k_e = \frac{\left(1 - \sum_{i=1}^{n} \frac{(w'_i)^2}{6 b_c d_c}\right)\left(1 - \frac{s'}{2 b_c}\right)\left(1 - \frac{s'}{2 d_c}\right)}{1 - \rho_{cc}} \tag{5-9}$$

where ρ_{cc} is the ratio of the area of longitudinal reinforcement to area of the core of the section, and parameters w'_i, b_c, d_c and s' are defined in Figure 5-4. Other expressions of k_e for general and circular sections are provided in Mander et al. (1988).

f'_{cc} can be computed from f'_{co}, f'_{lx} and f'_{ly} using Figure 5-3. When $f'_{lx} = f'_{ly}$, f'_{cc} may be computed using Equation 5-10.

$$f'_{cc} = f'_{co}\left(-1.254 + 2.254\sqrt{1 + \frac{7.94 f'_l}{f'_{co}}} - 2\frac{f'_l}{f'_{co}}\right) \tag{5-10}$$

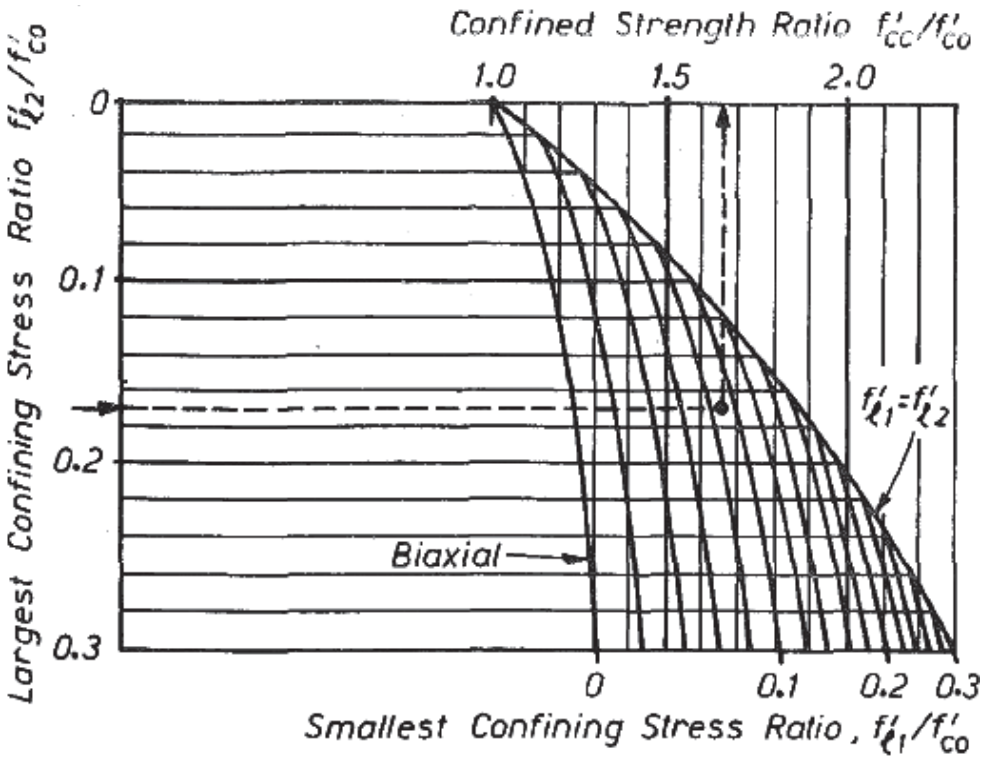

Figure 5-3 Confined core for a rectangular hoop reinforced section (Mander et al., 1988).

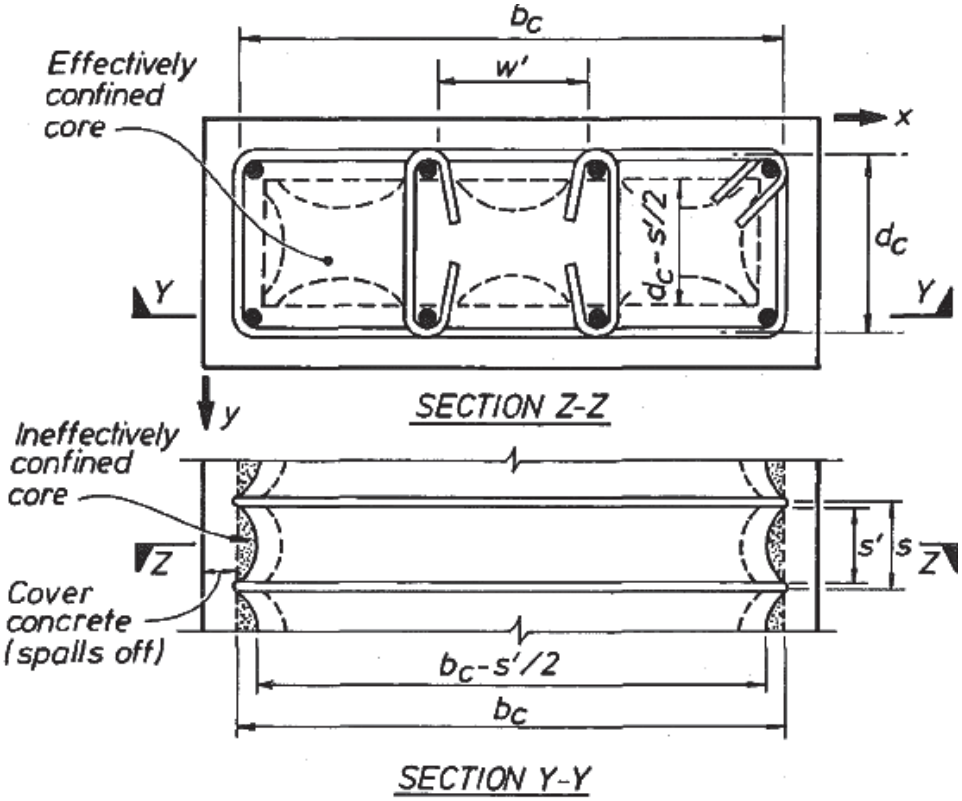

Figure 5-4 Confined strength determination from lateral confining stresses for rectangular section (Mander et al., 1988).

Mander proposes a fairly complex method for computing ε_{cc}, which relies on solving an energy balance equation; in contrast, Paulay and Priestley (1992) propose Equation 5-11 as a simpler and conservative estimate of the ultimate confined concrete strain, where ε_{su} is the ultimate tensile strain of the transverse steel.

$$\varepsilon_{cu} = 0.004 + 1.4\rho_s f_{yh} \varepsilon_{su} / f'_{cc} \tag{5-11}$$

5.3.3 Confined and Unconfined Concrete – Tensile Stresses

The tension portion of the concrete stress-strain curve is typically modeled either as pre-cracked (i.e., no tensile capacity) or as linear-elastic up to the tensile cracking stress, after which the concrete suddenly loses all of its capacity. The concrete tension strength generally does not have a significant impact on section strength, but can be important for predicting the uncracked stiffness, though it might lead to some overestimation of initial stiffness since it ignores cracking due to service loads, wind loads or shrinkage. This increase in stiffness might also lead to increased stiffness-based damping (βK damping, such as in Rayleigh damping), which can be partially addressed by reducing the concrete modulus or, by using fiber sections only in the plastic hinges and elastic members with cracked properties over the remainder of the element. Regardless of the modeling technique used, it is important to ensure that the members have realistic cracked stiffness at their expected deformation range, and also understand how fiber section stiffness affects overall damping, which can depend on the analysis software being used. After cracking, the concrete between the cracks continues to bond to the reinforcement, which increases the flexural and axial stiffness of the member through a phenomenon known as "tension stiffening." While the effect generally reduces with additional cracking, it can be important for estimating the effective stiffness at small deformations. The "tension stiffening" effect can be simulated by using a gradual descending branch for the concrete tensile stress-strain response. Figure 5-5 shows a simplified model which uses two parameters α_1, which describes the immediate stress loss after cracking and ranges from 0.4 to 0.7, and α_2 which is dependent on the reinforcement ratio and ranges from 12 to 22. Kaklauskas and Ghaboussi (2001) and Torres el al. (2004) provide recommendations for α_1 and α_2. Alternatively, values of $\alpha_1 = 0.5$ and $\alpha_2 = 14$ may be used for simplicity. A simplified version of the tension stiffening model without the sharp stress drop may be used in software that only supports bilinear stress-strain models. Overall, because the influence of concrete tension typically decreases at large deformations, their modeling might be more important under service level ground motions than under large intensity ground motions.

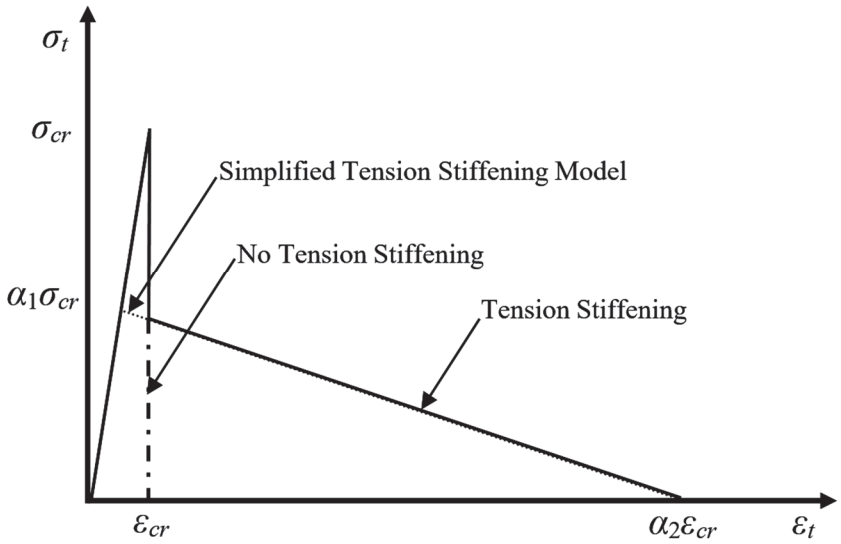

Figure 5-5 Concrete tension material models with and without tension stiffening.

5.3.4 Limitations of First-Principles Stress-Strain Modeling

While the fiber-based formulation relies on first principles and is very accurate in representing section axial and bending actions, it does not directly capture other modes of behavior such as bar slip, bar buckling and fracture. These behaviors are very complex and mostly defined through empirical data, with limited modeling guidance. It is possible to modify fiber behavior to partially or fully account for these behaviors, though it is critical that the resulting models be checked and calibrated against existing data. Alternatively, those behaviors can be modeled using discrete springs at the ends of the member. In general, overall model validation and calibration against experimental data are important and help in gaining confidence in the modeling approach.

5.4 Modeling Shear and Bond-Slip Deformations

The lateral deformations of concrete beams and columns can be separated into flexural, shear, and bar-slip deformations. As discussed in Section 4.2, integrating sectional moment-curvature relations over member length and introducing bar-slip rotational flexibility provides reasonably accurate estimates of overall member lateral stiffness. By their formulation, fiber-section elements produce only flexural deformations equivalent to integrating moment-curvature relations over member length. Therefore, fiber-section frame elements require the introduction of bar-slip and shear flexibilities.

It should be noted that published rotation capacities, such as those in ASCE/SEI 41-13, typically include total deformations and rotations, and hence the measured analytical deformations due to flexure, shear and bar slip should be combined prior to performing acceptance criteria checks.

5.4.1 Bond-Slip Deformations

As discussed in Chapter 2, slip of longitudinal bars from the anchoring members induces rigid-body rotations at the ends of framing members. The center of the bar-slip rotations has been shown to coincide with the flexural neutral axis (Sokoli et al., 2014). The added flexibility resulting from bar-slip rotations can be added to fiber-section beam and column elements through zero-length fiber-sections or elastic rotational springs at element ends.

If zero-length fiber-sections are used to model bar-slip, the fiber-sections should have the same geometry and discretization as the fiber-sections of the adjacent element. To maintain compatibility in the flexural neutral axis depth between the bar-slip fiber-sections and the adjacent element fiber-sections, all material model parameters of the zero-length sections should be identical to those of the adjacent frame elements, but with strain values multiplied by the scaling factor, $r_y = (S_y/\varepsilon_y)$; where S_y is bar slip at yield, as shown in Equation 5-12, and ε_y = longitudinal bar yield strain (Ghannoum and Moehle, 2012a).

$$S_y = \frac{l_{sp}\varepsilon_y}{2} \tag{5-12}$$

Although anchorage conditions in adjacent members (e.g., footings or joints) and bar properties can influence the bond stresses developed and the resulting bar-slip component of deformation, past studies have shown that assuming a uniform bond stress in the anchorage regions of $9.6\sqrt{f_c'}$ (psi) [$(0.8\sqrt{f_c'}$ (MPa)] can be used to compute a bar-slip flexibility that is reasonable for anchorage in footings and beam-column joints (Elwood and Eberhard, 2009; fib, 2013; Kwon, 2016). Due to a lack of more detailed studies that provide bond stress values for varying boundary conditions, this value is recommended for use at all beam and column interfaces, regardless of the anchoring member type (e.g., footing, wall, joint); so long as sufficient anchorage length is provided to prevent bond deterioration. This value is applicable for all traditional anchorage details, i.e., straight-bar, hooked-bar and headed-bar anchorage. Using this uniform bond stress, the effective strain penetration depth l_{sp} is given by Equation 5-13 at bar yield (Elwood and Eberhard, 2009):

$$l_{sp} = \frac{1}{38.4[3.2]} \times \frac{f_y}{\sqrt{f_c'}} d_b \text{ psi [MPa]} \tag{5-13}$$

Alternatively, instead of zero-length fiber-sections, discrete elastic rotational springs can be added at the ends of beam and column fiber-section elements to simulate bar-slip rotations. A yielding bond-slip spring in series with a fiber element will cause inelastic deformations to localize in only one of the two elements. Therefore, it is recommended to only introduce elastic bond-slip springs with a rotational stiffness,

K_{SE}, as specified in Equation 5-16, and to not allow the bond-slip spring to yield. This approach therefore leaves the inelastic bar-slip softening to be accounted for in the fiber elements through softening the steel-fiber hardening slope. However, there is insufficient evidence to provide recommendations for adjusting steel hardening properties, and given the wide range of steel hardening properties or reinforcing bars in the market (Ghannoum and Slavin, 2016), such refinement may not lead to improved accuracy.

The moment at first yield (M_y) can be related to the spring rotation (θ_{BS}) due to a bar-slip (S_y) as follows:

$$M_y = K_{SE}\theta_{BS} \tag{5-14}$$

Given that bar-slip rotation occurs about the flexural neutral axis, it can be related to the strain penetration depth and the member curvature at the bar-slip interface (ϕ_y) as follows:

$$\theta_{BS} = \frac{S_y}{C_C} = \frac{\varepsilon_y l_{sp}}{s} \times \frac{\phi_y}{\varepsilon_y} = \frac{\phi_y l_{sp}}{\varepsilon_y} \tag{5-15}$$

where:

C_C = distance from neutral axis to the center of the tension steel.

Hence the zero-length spring stiffness can be evaluated as:

$$K_{SE} = \frac{2M_y}{\varphi_y l_{sp}} \tag{5-16}$$

5.4.2 Shear Deformations

Shear deformations in concrete beams and columns are typically small and account for 5 to 10% of the total deformations. In fiber-section implementations, elastic shear stiffness is typically specified directly at the element level. For well detailed beams and columns that are flexurally dominated, a shear stiffness of $0.4E_cA_w$ may be used. If the element implementation does not account for shear deformation, or if shear nonlinearity is expected, shear deformations can be introduced through shear springs within the element or at element ends with a lateral stiffness corresponding to the equivalent elastic shear rigidity along the element length.

Chapter 6

Continuum Finite Element Component Models

Continuum finite element modeling (FEM) of reinforced concrete frame components is not common for purposes of earthquake resistant design of building structures, as the simpler approaches outlined in Chapters 4 and 5 are typically sufficient for purposes of seismic design. The FEM approach is more commonly used more complex analyses such as analysis for blast loading. Even so, it can be used for detailed studies of discontinuities, joints, panel zones, deep elements, and other cases of complex behavior. In such cases, idealizing the reinforced concrete composite as a continuum composed of connected small "finite" elements may provide information on stress distribution that may not be provided by the idealizations described in Chapters 4 and 5. For a brief history on the use of FEM analysis for reinforced concrete structures, the use of "continuum models" to represent reinforced concrete started in the 1960s (Nilson, 1968). Numerical representations of complex phenomena such as cracking and nonlinear stress-strain response were simplified through the use of the concept known as "smeared cracking." Kwak and Filippou (1990) compiled a comprehensive summary of work done on this subject until 1990. A critical review of uses of FEA in reinforced concrete was published by Vecchio and Palermo (2001). It discussed results from "prediction competitions." The review was published in a special publication on FEA edited by William and Tanabe (2001). The ability of current FEA software to reproduce reinforced concrete response was tested more recently through an experiment involving a beam with a depth well beyond the ranges of previous experience (Collins et al., 2015). Lowes and Filippou (2006) edited a compilation of papers on critical topics related to the use of FEA for reinforced concrete. A state-of-the-art report and guide for practicing engineers interested in detailed finite element analysis of reinforced concrete structures was published by the Fédération Internationale du Béton (fib, 2008).

In modeling reinforced concrete using FEM approaches, the problems of shear and bond have proven difficult and are mentioned here as a limitation and difficulty of the FEM modeling approach. Formulations estimating shear strength and deformation were developed for finite element analysis in the 1990s (Vecchio, 1989; Stevens et al., 1991). Idealizations of bond for use in FEA algorithms was done by Lowes et al. (2004).

Several current commercial software packages and open-source research packages (e.g. OpenSees, DIANA, and Abaqus) have FEM capabilities and, in the rare cases where a more complex model is needed beyond those outlined in Chapters 4 and 5, can be used for such analysis for the seismic design of reinforced concrete frame structures.

Appendix A

Modeling Nonductile Reinforced Concrete Frames

A.1 Overview

Non-seismically detailed concrete members tend to behave in a nonductile manner and are prone to loss of lateral and gravity load carrying capacities at relatively low drifts. In most damaging earthquakes around the world, the collapse of nonductile concrete buildings is often the major cause of fatalities.

As stated previously, the main focus of this document is to provide nonlinear modeling guidelines for seismically detailed concrete moment frames. However, much of the content of the document can be applied to systems not designed to withstand their full seismic demands and expected to sustain significant loss of strength during seismic events (e.g., simulating the stiffness of members or interface behavior such as bar-slip). Recommendations for determining deformations at loss of strength, as well as modeling the ensuing cyclic degrading behavior of nonductile members, are not provided in this document. This appendix provides a brief overview of available resources that can be used in conjunction with this document to model nonductile concrete frame members.

Simulating the seismic behavior of nonductile concrete structures entails adequately assessing the initial strength and stiffness of components, the drift capacity of components at which lateral strength loss is initiated, the ensuing rate of strength degradation, and the threshold damage level at which gravity collapse occurs. A challenge in such simulations is accounting for the often severe strength losses that occur and the related numerical convergence issues. Structural systems exhibiting strength degradation in discrete components will suffer a cascading sequence of component overloads leading to loss of strength, followed by redistribution of loads to adjacent members, which can lead to further overload and loss of strength in other components. If strength or deformation capacities of components are significantly over- or under-estimated, simulated failure sequences and structural damage can vary drastically. This behavior contrasts the stable and often hardening behavior of seismically detailed members, which results in lower outcome sensitivity to modeling assumptions.

The ACI 369R-17 standard, now the source document of concrete provisions for ASCE/SEI 41-17, provides important resources for building nonlinear numerical

models of reinforced concrete structural members, including beams, columns, beam-column joints, and slab-column connections. The standard provides strength and deformation modeling parameters covering the full range of concrete member behavior, from seismically detailed to seismically deficient members. Failure modes treated in the standard include shear failure, axial failure, and anchorage or splice failure. While ACI Committee 369 has been working on updating all lateral-force versus lateral-deformation backbone modeling parameters in the committee's standard to provide mean estimates of component behavior during cyclic loading, not all modeling parameters in the current 2017 version have been updated to achieve that objective. Mean estimates are given for modeling parameters of columns and slab-column connections with continuity reinforcement (Elwood et al., 2007; Ghannoum, 2017). Mean minus one standard deviation modeling parameters are provided for slab-column connections without continuity reinforcement (Elwood et al., 2007). Conservative estimates are given for beams and beam-column joints, which have remained virtually untouched from those in FEMA 356, *Pre-standard and Commentary for the Seismic Rehabilitation of Buildings* (FEMA, 2000). It is important to note that the backbone parameters provided in ACI 369R-17 were derived from experimental tests with mostly symmetric reversed cyclic loading protocols, with multiple cycles performed at incremental drift targets. As such, even parameters achieving mean cyclic behavior may be conservative in cases where members are pushed essentially monotonically to failure, such as in near-fault pulse motions. Furthermore, the cyclic behavior of components past the initiation of strength loss is not defined in the ACI 369R-17 standard.

Further guidance on how to use ACI 369R-17 and ASCE/SEI 41-17 procedures, modeling parameters, and acceptance criteria can be found in SEAOSC (2017) and the ATC-78-3 report, *Seismic Evaluation of Older Concrete Frame Buildings for Collapse Potential* (ATC, 2015). Additionally, models that explicitly treat cyclic degrading behavior in nonductile concrete members are available in the literature for some cases. An overview of the models that are most compatible with the guidelines presented in this document are provided below.

A.2 Modeling Columns

Leborgne and Ghannoum (2014a, 2014b), which built on work by Elwood and others, provide relations for simulating the complete cyclic lateral strength versus lateral deformation behavior of shear critical concrete columns. These relations, along with capabilities for adjusting the failure surface during analysis based on varying boundary conditions (e.g., axial load and plastic rotations), were implemented in a computational model in the open source analytical software OpenSEES (McKenna et al., 2000). A calibrated version of the model is also available in OpenSEES that only requires input of column basic material and

geometric properties to fully calibrate the lateral cyclic behavior of shear critical columns.

A.3 Modeling Beam-Column Joints

Celik and Ellingwood (2008) provide a review of the most common approaches for modeling of nonductile beam-column joints that include cyclic behavior. These approaches range from macro-elements with interface and joint panels calibrated to experimental data (Mitra and Lowes, 2007), to simpler models with rigid offsets at frame members connected by a central zero-length spring that simulate the shear and/or bar-slip behavior in joints, often referred to as scissor models (Alath and Kunnath, 1995). Jeon et al. (2014) assessed the accuracy and functionality of several leading beam-column joint models and recommend joint modeling parameters and cyclic behavioral rules compatible with the scissor joint modeling approach. The advantages and disadvantages of each available model for beam-column joints are discussed in Jeon et al. (2014). The model by Jeon et al. (2014) accounts for joint shear and anchorage failures within the central scissor rotational spring and was calibrated to account for bar-slip deformations within the joint. It should therefore not be used in conjunction with frame members whose stiffness was reduced to account for bar-slip flexibility. Hassan (2011) proposes a scissor modeling approach focused on exterior and corner joints. The scissor model by Hassan (2011) accounts for shear deformations only and provides all necessary nonlinear modeling parameters and cyclic behavioral rules. Hassan (2011) also provides a moment-rotation model that accounts explicitly for bar slip deformation and anchorage failure within joints that can be used in conjunction with the scissor model.

A.4 Modeling Slab-Column Connections

The effective slab width relations and cracking stiffness factors presented in Section 4.5 of this Guideline apply for slab-column connections in nonductile frames as they do for SMF. Deformations at initiation of punching shear failure can be obtained from ACI 369R-17 as discussed in Elwood et al. (2007). Guidance on modeling the degrading behavior past the initiation of punching shear failure can be found in Kang et al. (2009).

Appendix B

Reinforced Concrete Frame Example Building

B.1 Introduction

The following example documents the development of a computer model and a series of analyses to ascertain building behavior by implementing this *Guidelines* document and *Part I Guidelines*. The simple and discrete nonlinearity modeled is intentional and reflects the modeling a practicing engineer may select as part of their ASCE/SEI 7-16, *Minimum Loads for Buildings and Other Structures* (ASCE, 2017a), design to satisfy requirements of Chapter 16. As a simplification for this example, foundations are modeled with pinned supports and rotational springs to represent the mat foundation. For soil-structure interaction guidance refer to NIST 12-917-21, *Soil-Structure Interaction for Building Structures* (NIST, 2012).

B.2 Building Description

The example building is a five-story concrete office building located in San Francisco, California. The first three stories have overall plan dimensions of 120 feet by 80 feet as depicted in Figure B-1. Above the fourth floor, the floor plate setbacks a single bay for an overall plan dimension of 85 feet by 80 feet. A roof top garden is located at this fourth floor setback. Mechanical equipment is located on the roof. The fourth and fifth floor plans are shown in Figures B-2 and B-3, respectively. During the design development phase, a new project requirement for a large conference space in the first story at the south-east corner of the building necessitated the removal of a column at grid lines B4.

The seismic force-resisting system consists of two concrete moment–resisting frames in both the N-S direction and the E-W direction. It should be noted that one of the concrete moment-resisting frames in E-W direction has an out-of-plane offset where the concrete moment-resisting frame on Grid 5 at lower levels shifts to Grid 4 at level 4 to accommodate the building setback at that level. These frames are detailed as special moment-resisting frames due to the high seismicity and high demand for system ductility as required by ASCE/SEI 7-16.

Floor construction consists of 12 in. normal weight concrete flat plate with perimeter beams. The perimeter beams have a width of 24 inches and a depth below slab of 18 inches. A 12-inch-thick reinforced concrete slab is used in lieu of a post-tensioned

slab to avoid the inclusion of post-tensioning effects in the perimeter beams. A 2'-6" mat at grade supports superstructure loads and transfers them to the soil below.

The site is located on Soil Type D and per ASCE/SEI 7-16 the building is designed for Seismic Design Category D. The site's location in San Francisco is outside the near-fault zone and within the deterministic cap.

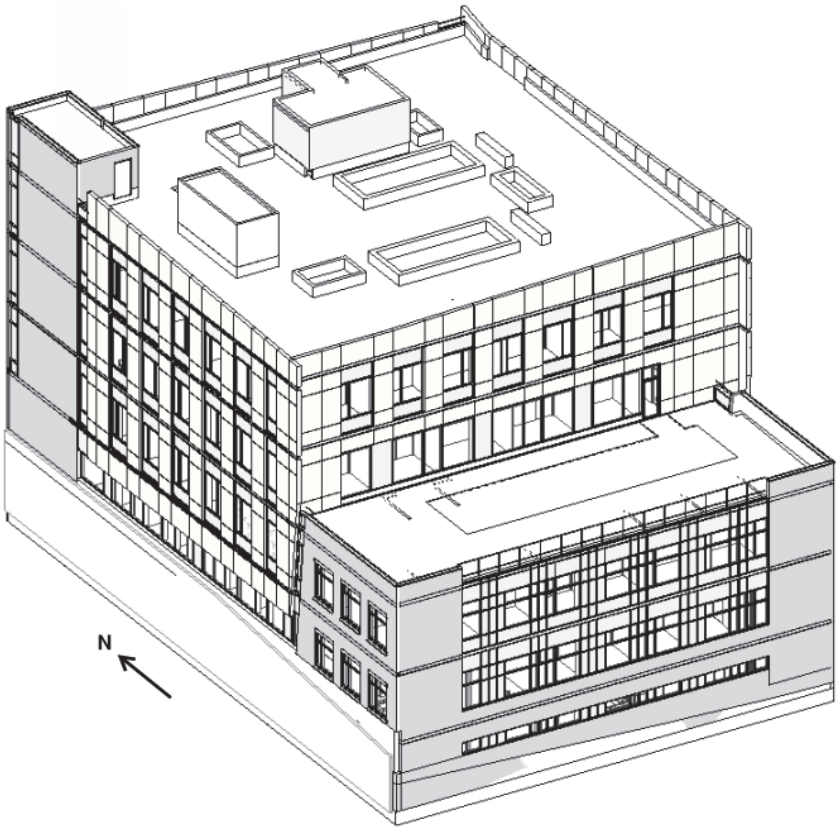

Figure B-1 Example building.

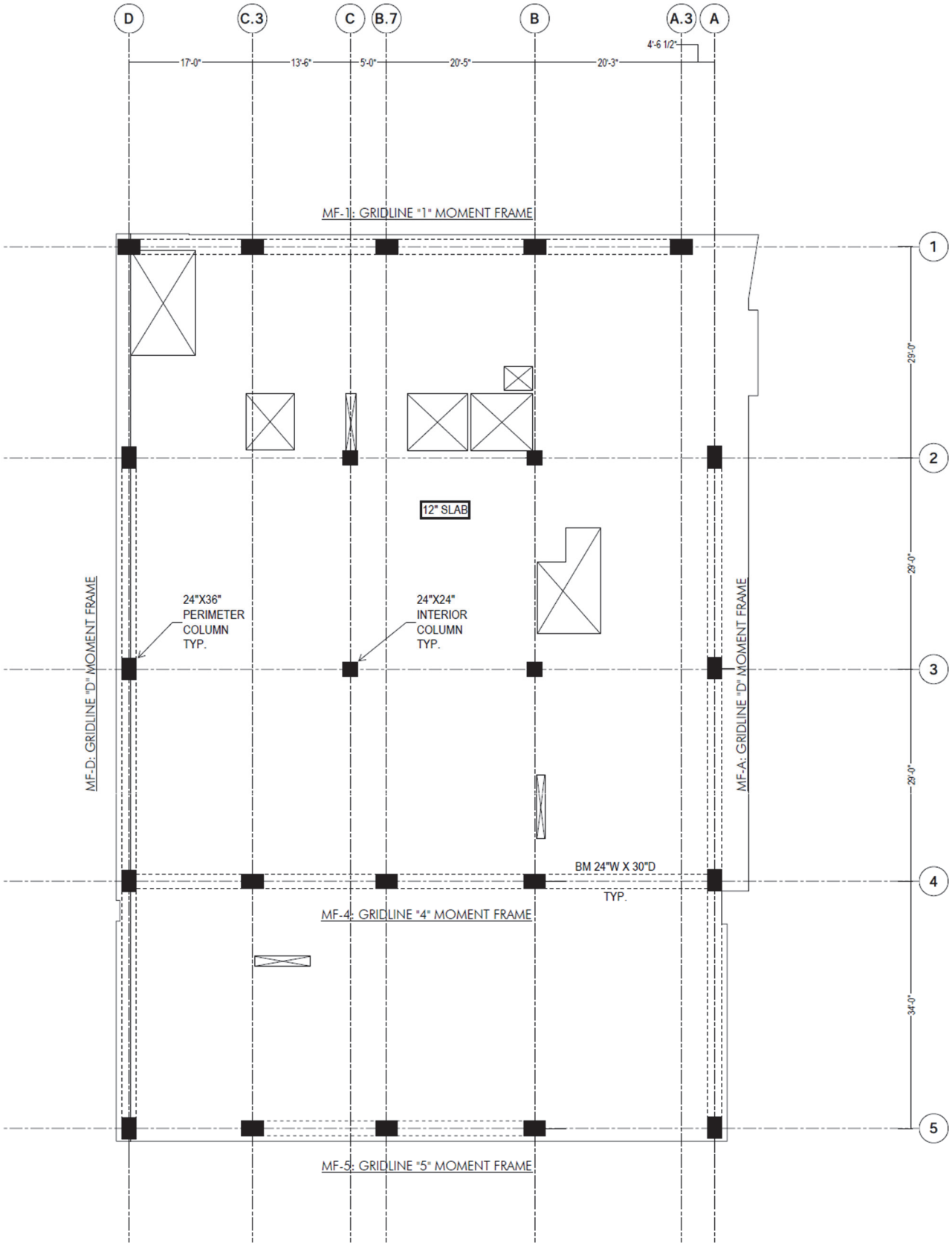

Figure B-2 Level 4 plan.

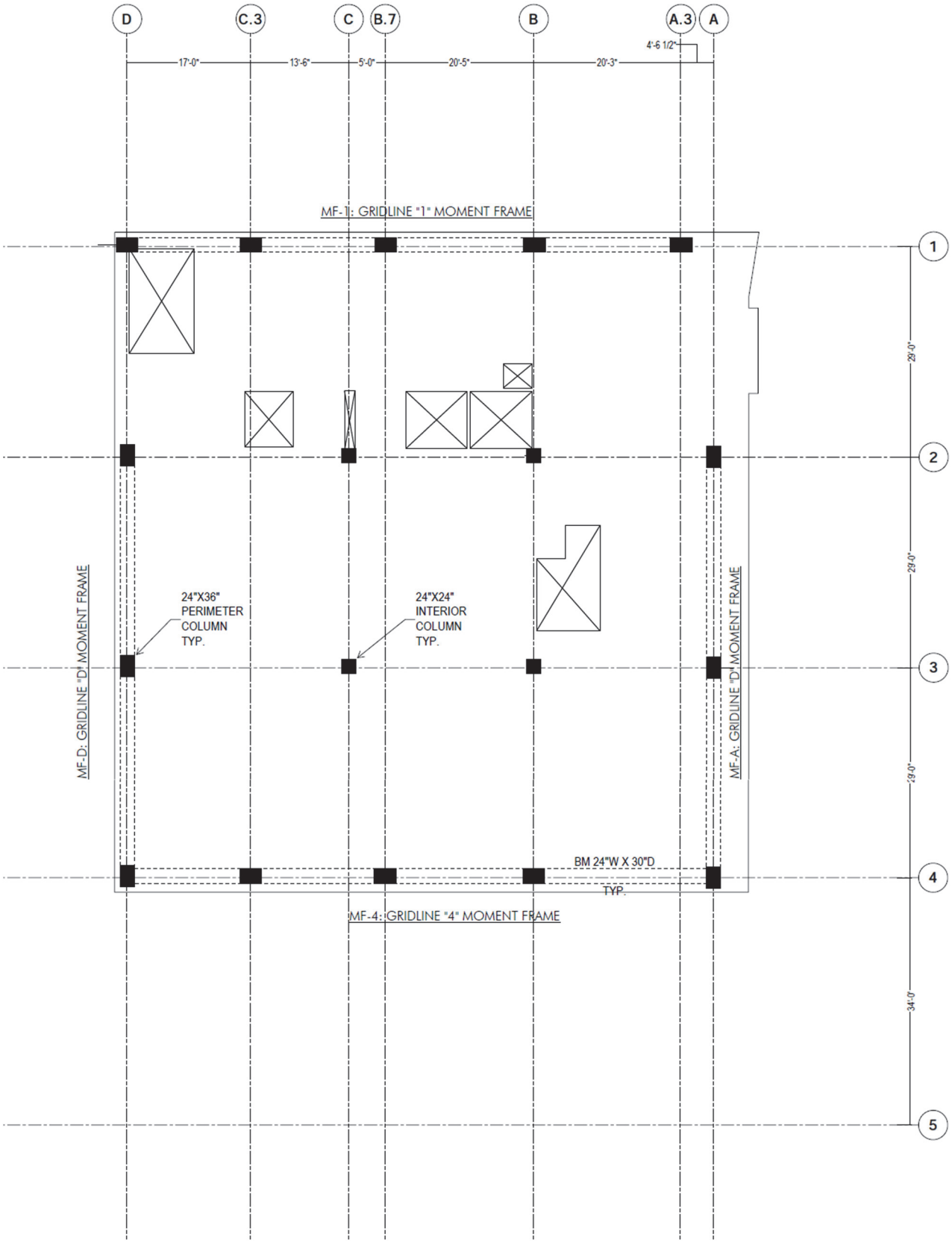

Figure B-3 Level 5 plan.

B.3 Linear Structural Analysis and Design of Building

The example building is proportioned and designed under elastic analysis per prescriptive requirements of ASCE/SEI 7-16 and ACI 318-14, *Building Code Requirements for Reinforced Concrete* (ACI, 2014). The elastic analysis and design process is not documented in its entirety as the interest of this guideline is focused on the nonlinear analysis and design. However, some important elastic modeling assumptions, analysis results, and structural designs are provided below.

B.3.1 Modeling Criteria

A three-dimensional mathematical model using ETABS (CSI, 2015) software is created for the linear elastic analysis. Of most significance in a concrete building is modeling realistic stiffness properties of the structural elements considering cracked sections in accordance with ASCE/SEI 7-16 Section 12.7.3, Item a. This example utilizes the following effective stiffnesses per ACI 318-14 Table 6.6.3.1.1(a).

I_{eff} = $0.35I_{gross}$ for beams

I_{eff} = $0.70I_{gross}$ for columns

I_{eff} = $0.25I_{gross}$ for slabs

B.3.2 Fundamental Periods

The computed periods and the modal response characteristics of the building for the first six modes are presented in Table B-1.

Table B-1 Computed Periods and Modal Response Characteristics

Mode	Period (sec)	Effective Mass Ratio *E-W*	Effective Mass Ratio *N-S*	Description
1	1.26	0%	80%	First Mode N-S
2	1.02	83%	0%	First Mode E-W
3	0.72	0%	0%	First Mode Torsion
4	0.40	0%	12%	Second Mode N-S
5	0.31	9%	0%	Second Mode E-W
6	0.24	0%	0%	Second Mode Torsion

B.3.3 Modal Analysis

The building is analyzed using the Modal Response Spectrum Analysis (MRSA) procedure of ASCE/SEI 7-16 § 12.9.1 and ETABS software. In accordance with ASCE/SEI 7-16 Section 12.9.1.4, the results of the MRSA are scaled such that the base shear of MRSA is no less than that of the Equivalent Lateral Force (ELF)

procedure. The computed seismic story shears and overturning moments for the building are shown graphically in Figure B-4.

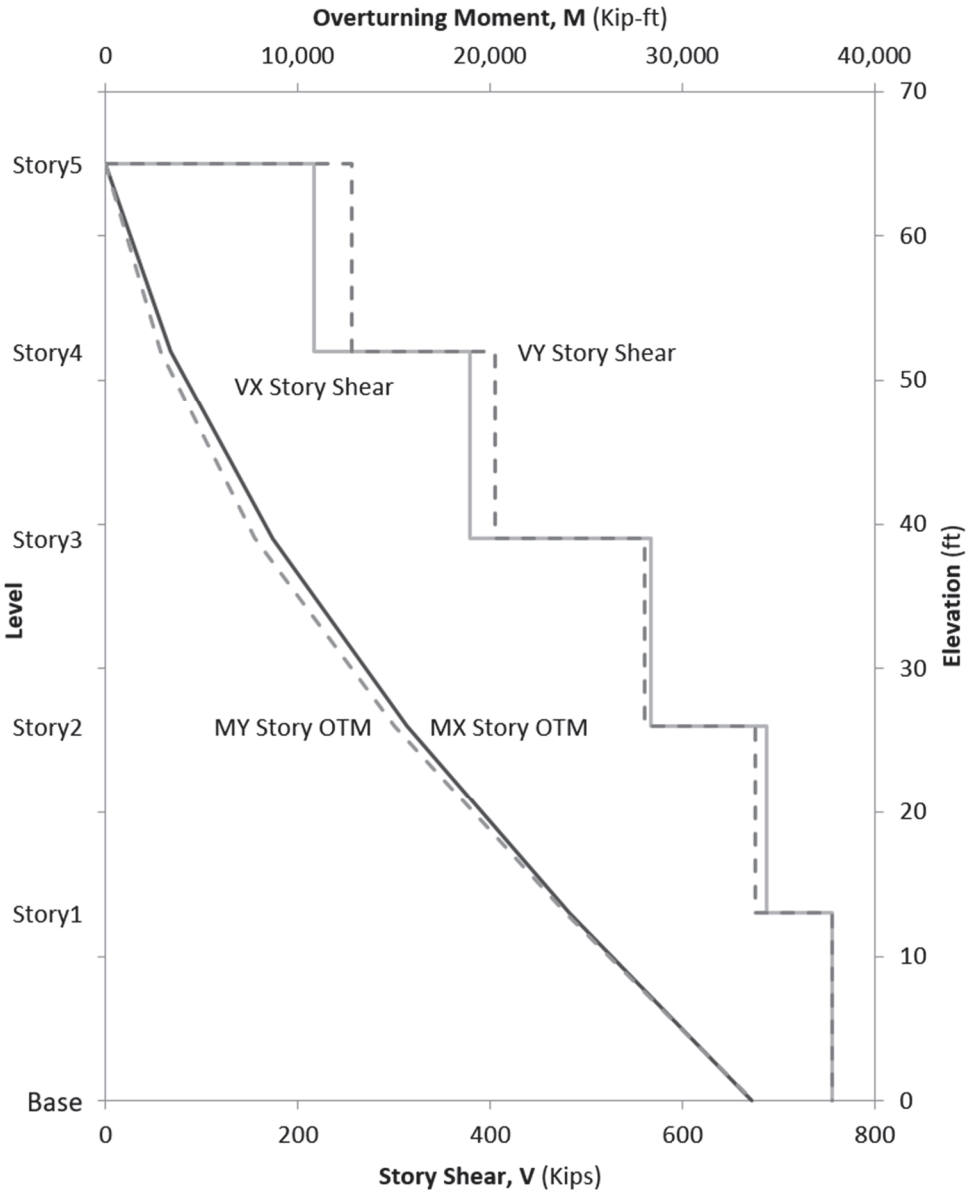

Figure B-4 Seismic story shears and overturning moments.

B.3.4 Drift Check

The Story drifts are computed in accordance with ASCE/SEI 7-16 Section 12.9.1.4.2 and then checked for acceptance based on Section 12.12.1. According to ASCE/SEI 7-16 Table 12.12-1, the story drift limit for this Occupancy Category II building is 2 percent of the story height. The story drifts are taken directly from the modal combinations in ETABS. A plot of the total deflection in both the N-S and E-W directions is shown in Figure B-5 and a plot of story drifts is in Figure B-6.

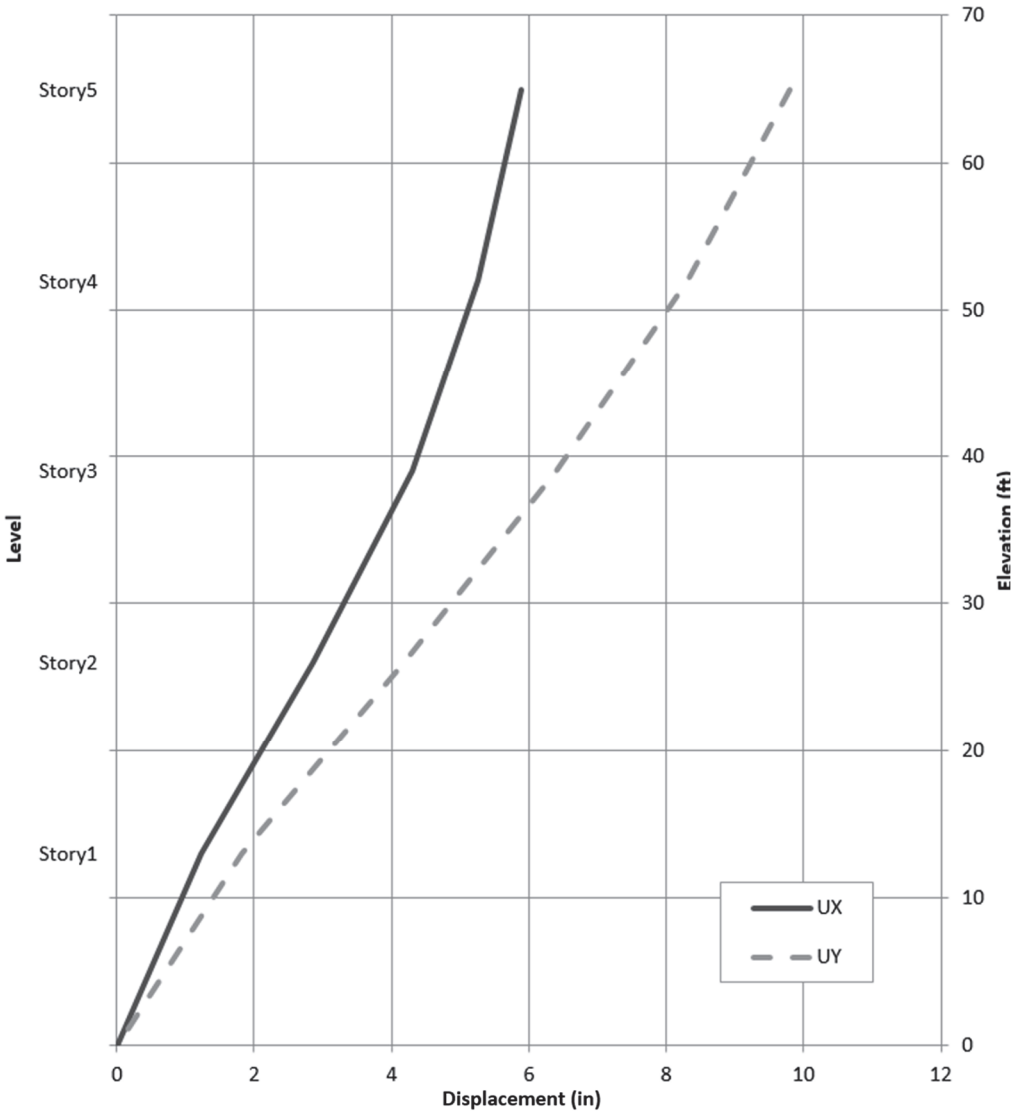

Figure B-5 Maximum story displacement.

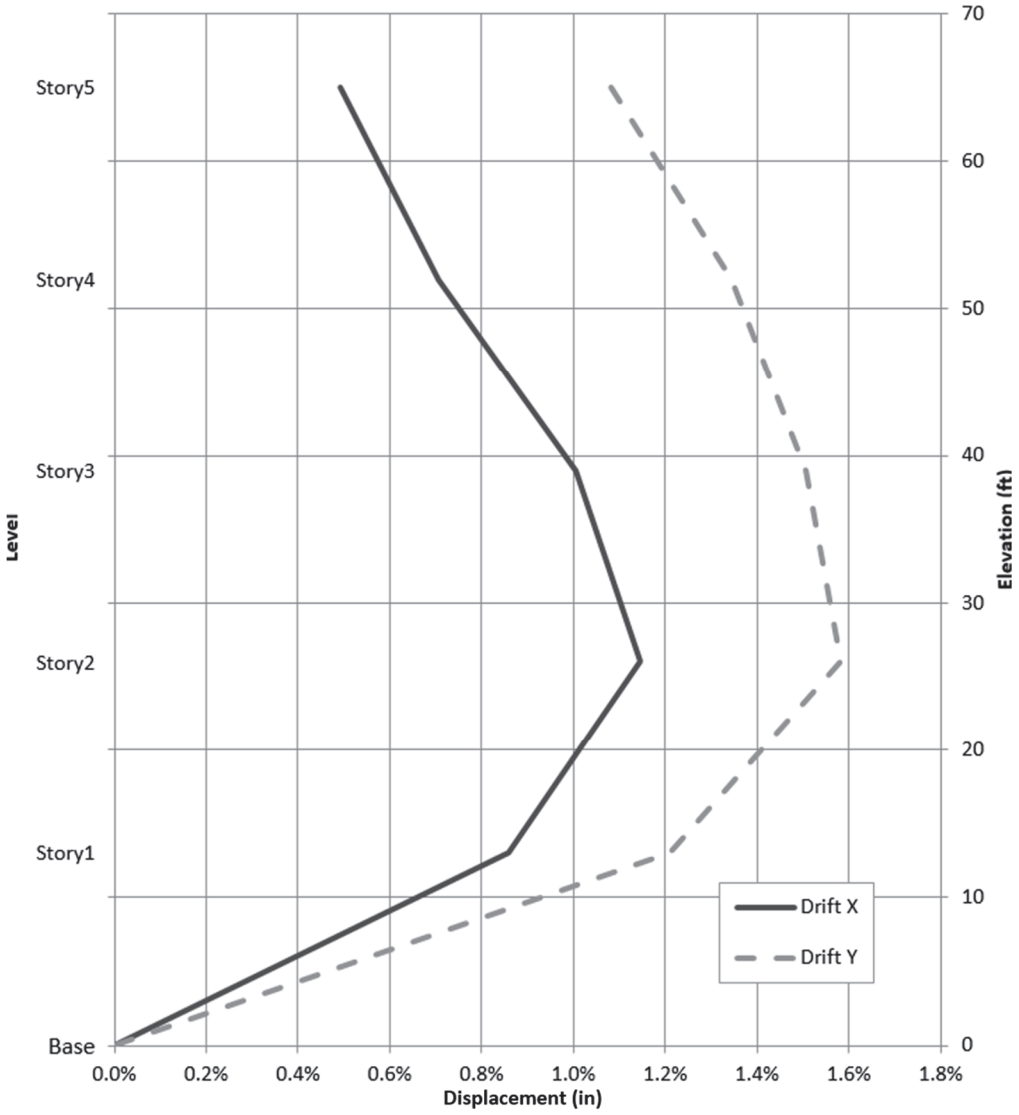

Figure B-6 Maximum story drift.

B.3.5 Structural Design of Primary Moment-Resisting Members

Based on the elastic analysis results, the design and detailing of the primary moment frame members, perimeter beams and columns, are representatively presented in this section. The design of these members are of interest as the reinforcing in beams and columns determines the backbone curves of the plastic hinges of beams and the fiber cross section of the columns. The beam and column reinforcing design for MF-D along grid D and MF-1 along grid 1 are scheduled in Table B-2 and Table B-3. The primary beams and columns of MF-D and MF-1 are identified in Figures B-7 and B-8.

Table B-2 Beam Design Schedule

Mark	Size	Bottom Bars	Top Bars
BM01	24×30	(4)-#6	(5)-#7
BM02	24×30	(4)-#7	(5)-#7
BM03	24×30	(4)-#7	(5)-#8
BM04	24×30	(5)-#7	(6)-#9
BM05	24×30	(5)-#7	(7)-#9
BM06	24×30	(5)-#8	(5)-#9
BM07	24×30	(5)-#8	(7)-#9
BM08	24×30	(5)-#8	(6)-#11

Table B-3 Column Design Schedule

Mark	Size	Reinf
C01	24×36	(12)-#8
C02	24×36	(12)-#10

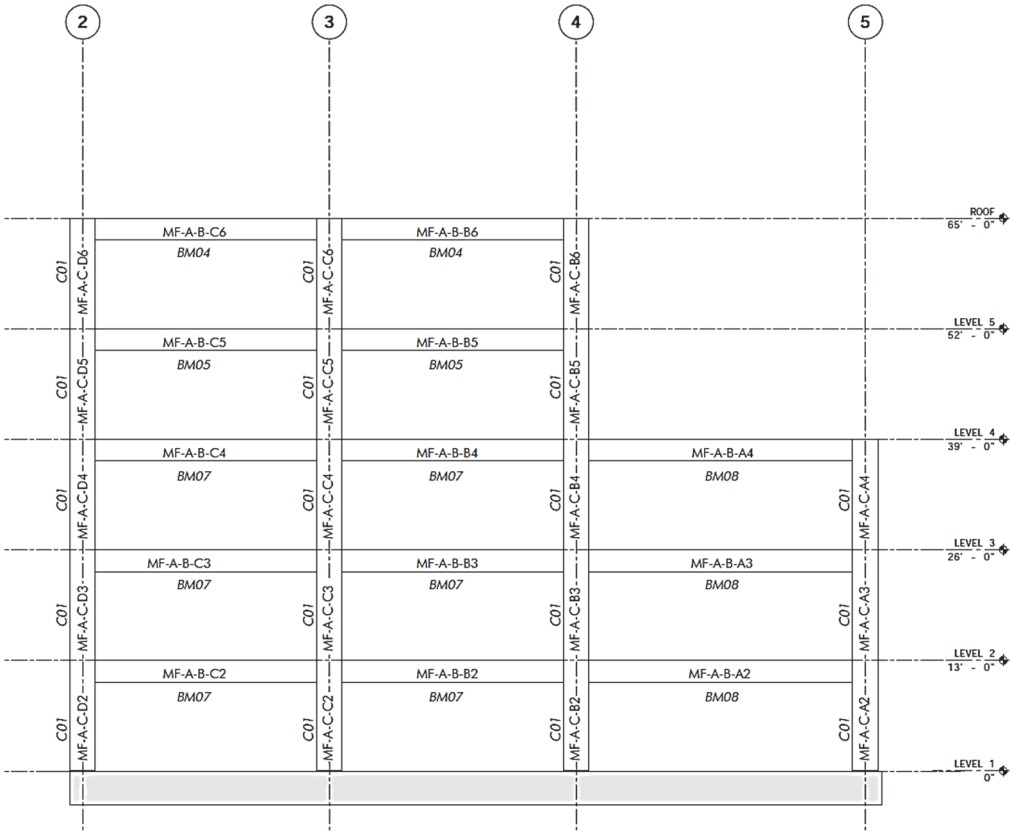

Figure B-7 MF-D beam and column marks.

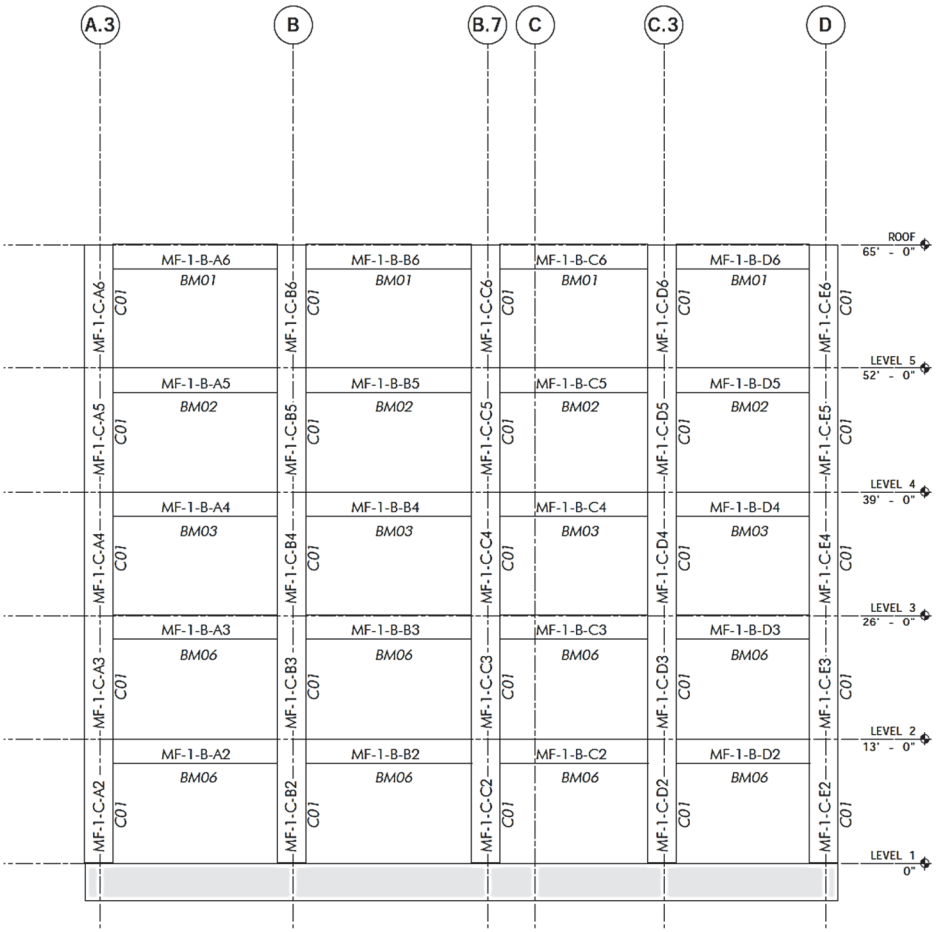

Figure B-8 MF-1 beam marks.

B.3.6 Structural Design of Secondary Moment-Resisting Members

As discussed in Section 3.6, the "gravity" system of the building also participates in resisting earthquake demands and contributes to the overall building stiffness. Therefore, the reinforcing design for floor slab is required to be modeled as a secondary slab-beam frame system with nonlinear hinges. The design of the top and bottom bars only at the column strips are of interest as the middle strips are generally considered not engaged in the moment frame action. The following describes the typical slab design over columns for the example building:

- Top Bars: #7 @ 10" o.c.
- Bottom Bars #5 @ 12" o.c.

Note that the design is given in the rebar intensity as the width of the slab-beam is determined later in Section B.4.5.

B.4 Nonlinear Modeling

B.4.1 Material Models for Fiber Hinges

The material stress-strain models for concrete and steel are developed for the implementation of fiber-section hinges. The stress-strain model for steel is based on a simple parametric definition. The parameters used to define the steel stress-strain model are as follows and the resulting curve is illustrated in Figure B-9.

F_{ye} = expected yield stress
= 66 ksi

F_{ue} = expected tensile stress
= 99 ksi

ε_{sh} = strain at onset of hardening
= 0.015

ε_u = ultimate strain capacity
= 0.090

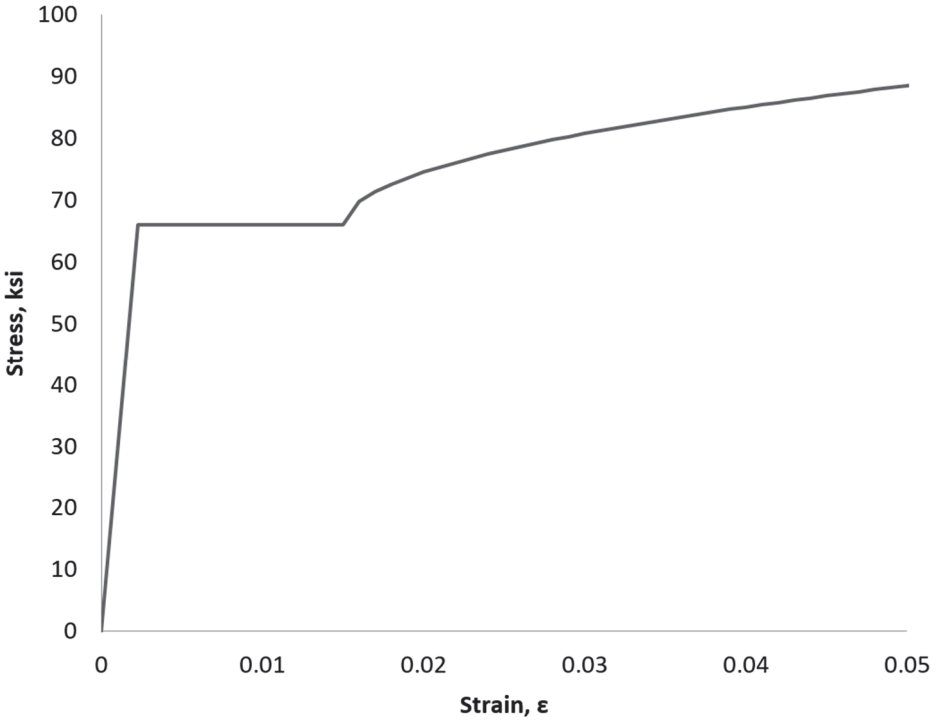

Figure B-9 Simple steel stress-strain curve.

The stress-strain model for confined concrete is based on the Mander parametric definition. The parameters used to define the concrete stress-strain model are as followed and the resulting curve is illustrated in Figure B-10.

- Expected confined compressive strength: 7.8 ksi

- Strain at confined compressive strength: 0.0022
- Ultimate confined strain capacity: 0.005
- Confinement bar yield stress: 66 ksi

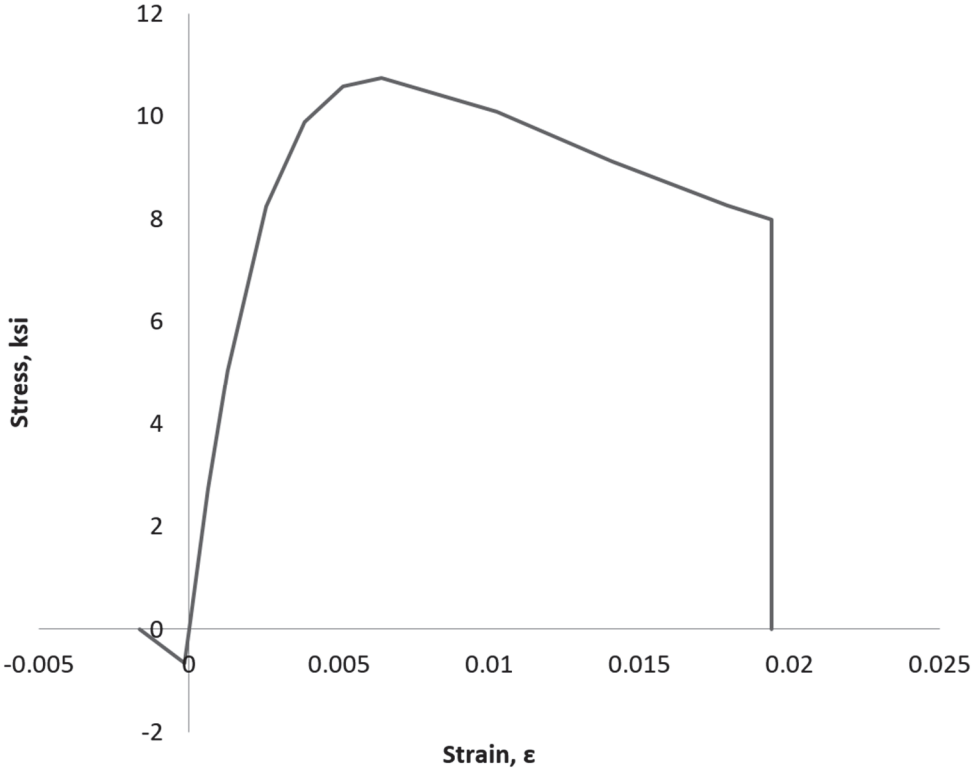

Figure B-10 Mander confined concrete stress-strain curve.

B.4.2 Beam

The primary moment frame beams are modeled using elastic line elements and zero-length rotational hinges to capture both the elastic deformation over the member length and inelastic deformations near the ends of the members. The discrete concentrated hinges are generally located at about 10% of the member length from the ends, but the additional distance needs to be considered as the software typically considers the analytical length, or center-to-center length, not the clear span length. In this example, to account for the software using center-to-center element lengths, a relative length factor of 0.20 is used instead of 0.10, so that the beam concentrated hinges are all properly located to approximately account for the joint panel zone area.

B.4.2.1 Beam Line Element

The effective stiffness of the line-element, which captures both the flexural rigidity of the beam outside the plastic hinges and the bar-slip effects, is determined using Equations 4-2 and 4-3.

A drift value of 0.008 was assumed, which results in an effective stiffness up to the approximate yield point of the beam component. Based on the equation above, an effective stiffness ratio in the range of 0.15 to 0.27 is determined. A few values larger than 0.30 are observed for the highly-reinforced beams at the transfer column region, but the single value of 0.21 is chosen and assigned to all moment frame beams to reasonably capture the effective stiffness reduction in all moment frame beams.

B.4.2.2 Beam Concentrated M3-θ Hinge

The concentrated nonlinear moment-rotation hinges for the beams are defined per Section 4.2.3. Four parameters, $\theta_{cap,pl}$, θ_{pc}, M_y, and M_c, are required to define the idealized tri-linear backbone curve. Figure B-11 illustrates a sample T-beam section B24×30×62 with (5)-#8 top and (5)-#7 bottom reinforcing.

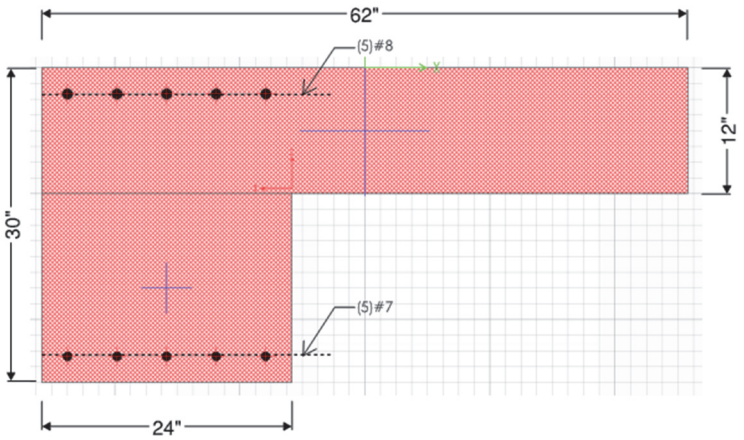

Figure B-11 Beam section: B24×30×62 with 5#8 on top and 5#7 at bottom.

The corresponding calculated backbone curve parameters are:

θ_p = 0.046

θ_{pc} = 0.096 ≤ 0.10

To account for the cyclic behavior, the backbone curve is modified with 0.7 and 0.5 factors applied to θ_p, and θ_{pc}, respectively (in accordance with Section 4.2.3).

$\theta_{p,cyclic}$ = 0.033

$\theta_{pc,cyclic}$ = 0.048

M_y^+ = 6100k-in

M_y^- = 7400k-in

The resulting idealized backbone curve of the moment-rotation is illustrated in Figure B-12. Note that this backbone curve shape does not match what is illustrated in Figure 4-2. The strength loss in the backbone relationship is modeled as an instantaneous drop, where the unloading happens as a single event, instead of the more gradual linear descent, where unloading is achieved through a series of multiple events. This is expected to be a conservative approach to modeling and was done simply due to the numerical constraints of the commercial software being used for this example. In this software, the modeling of gradual strength loss often causes numerical difficulties because the multiple events from one hinge could be intertwined with the events from other hinges as multiple hinges are competing to incrementally redistribute the loads to each other. This causes the nonlinear analysis to become unstable as the program tries to reduce time steps to an unreasonable minimal number to capture all these redistribution events. Based on this, the presumably-conservative backbone approach of Figure B-12 was used in place of the recommended approach of Figure 4-2.

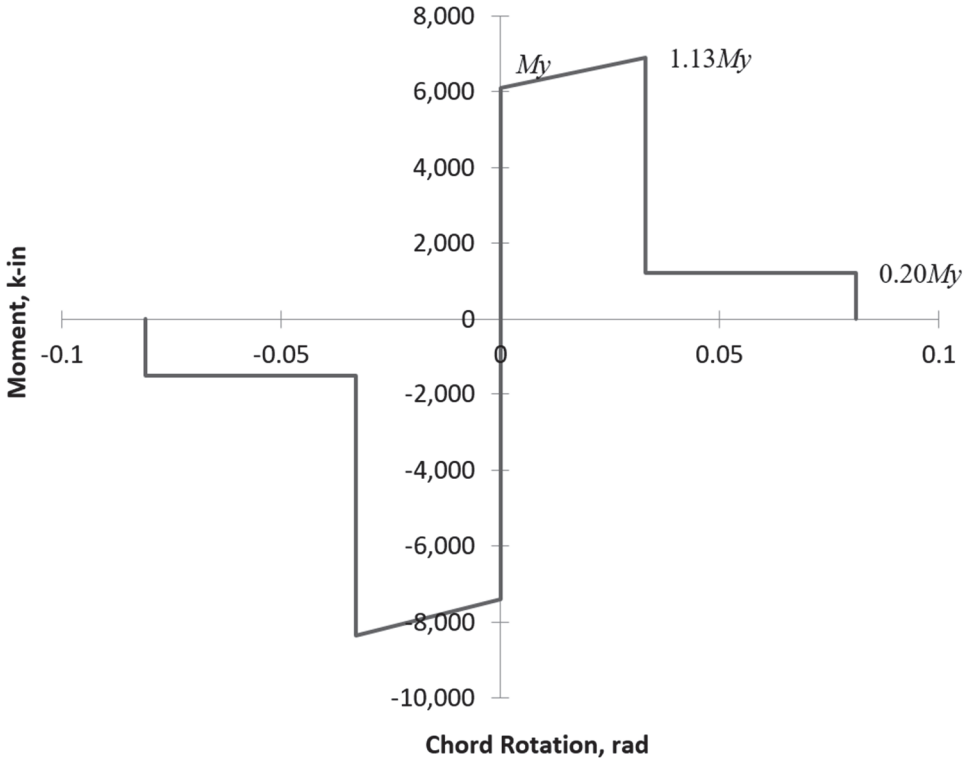

Figure B-12 Primary beam moment-rotation backbone curve.

B.4.3 Column

Similar to the beam assembly, columns are modeled using elastic line elements and zero-length plastic hinges to capture both the elastic deformation over the member length and inelastic deformations near the ends of the members. The discrete hinges are located at 0.20 relative length from the ends (with the rationale being consistent

with the previous discussion of beam), but unlike the beams, the columns employ concentrated fiber-section hinges in order to capture the *P-M-M* interaction.

B.4.3.1 Column Line Element

The effective stiffness of the line-element, which captures both the flexural rigidity of the column outside the plastic hinges and the bar-slip effects, is determined using Equations 4-2 and 4-3. Similar to beams, this equation assumes the drift ratio of 0.008. Based on the equation above and the assumption of 1.0% reinforcing and axial load ratio of 0.25, the effective stiffness factor of approximately 0.40 is determined.

B.4.3.2 Column Concentrated Fiber Hinge

The fiber section of a column concentrated hinge is defined using its rebar layout with concrete lumped into a reasonable number of fibers distributed within the section geometry. A given concrete section with a rebar layout is automatically converted to fiber-section in SAP2000 (CSI, 2016a). The original section definition input and the resulting fiber-section are illustrated in Figure B-13 and B-14, respectively.

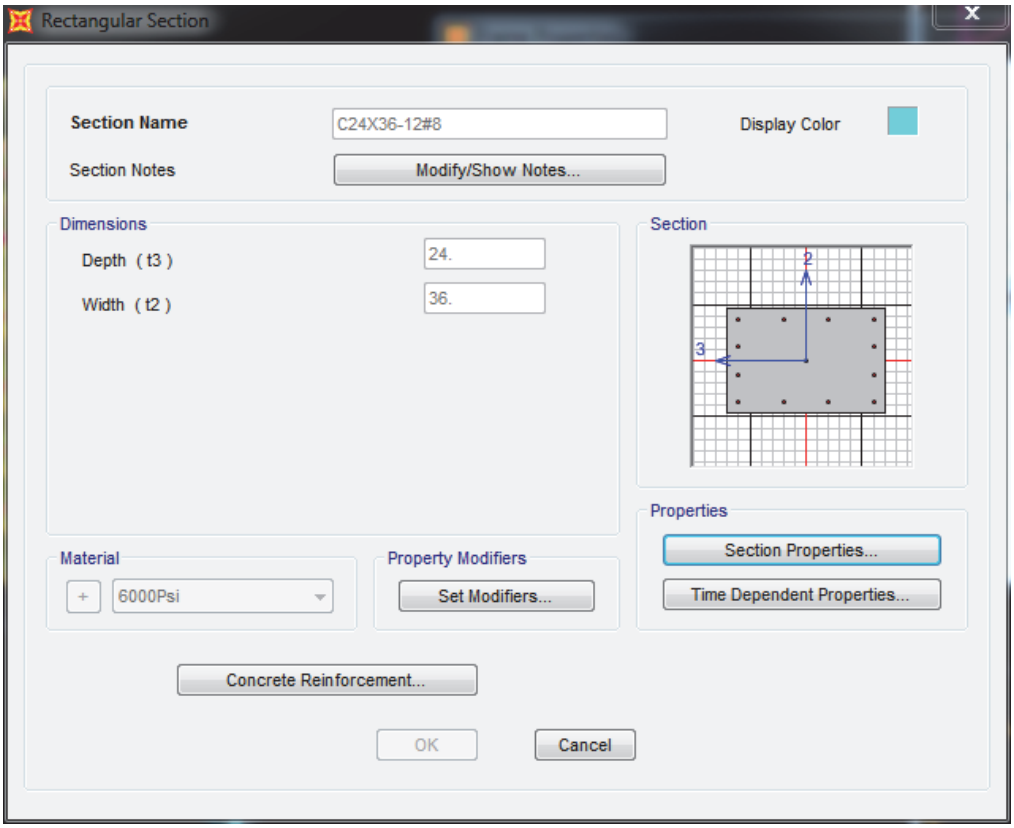

Figure B-13 Column geometry section input (CSI, 2015).

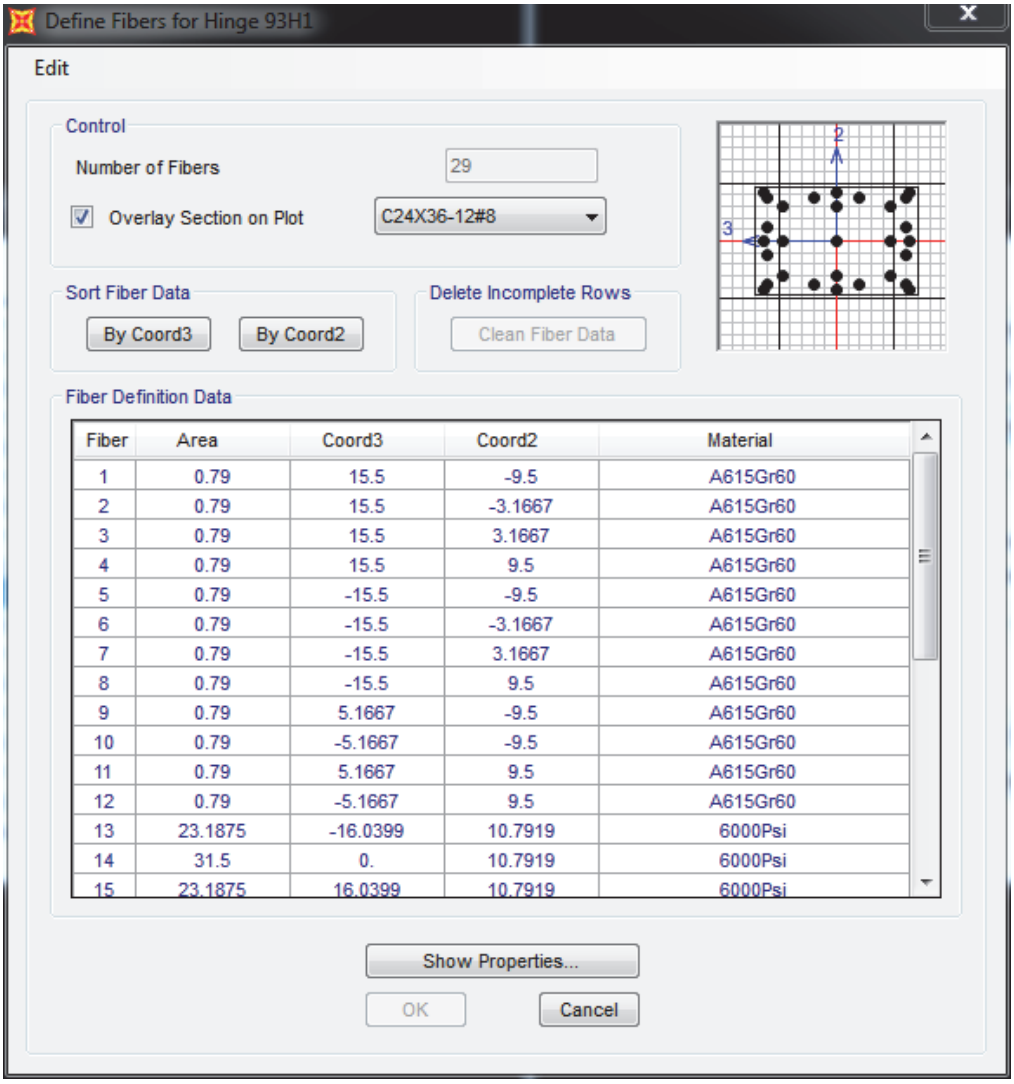

Figure B-14 Column fiber-section (CSI, 2015).

B.4.4 Beam-Column Panel Zone

In accordance with ASCE/SEI 41-13 Section 10.4.2.2, the beam-column panel zone is defined without explicitly modeling joint stiffness, but rather using the line elements extending from the beams and columns into the panel zone. The implicit modeling of the joint stiffness has the column offsets as rigid and beam offsets as flexible as new construction of moment frames have strong column-weak beam conditioned as prescribed by ACI 318-14.

B.4.5 Slab-Beam

The slab-beam elements represent the secondary moment frame composed of the "gravity" system. Similar to the primary beams, slab-beams are modeled using elastic line elements and zero-length rotational hinges to capture both the elastic deformation over the member length and inelastic deformations near the ends of the

members. Section 4.3 refers to ASCE/SEI 41-13 for nonlinear modeling of slab-beam line elements and concentrated moment hinges.

B.4.5.1 Slab-Beam Line Element

The effective beam width calculated per ASCE/SEI 41-13, as referenced in Section 3.6.2, for the slab-beams ranges from 105 to 210 inches. To simplify modeling, four representative slab-beam sections are defined with the widths of 105", 125", 160", and 210". The effective stiffness factor, β_{eff}, calculated per ASCE/SEI 41-13 (Eq. C10-4) is $^1/_3$ for all slab-beams in the model.

B.4.5.2 Slab-Beam Concentrated M3-θ Hinge

Condition *i* with $V_g/V_o = 0.2$ is assumed in determining the "*a*", "*b*", and "*c*" modeling parameters in ASCE/SEI 41-13 Table 10-15. The resulting parameters are as follows and the backbone curve is shown in Figure B-15.

a = 0.03

b = 0.04

c = 0.20

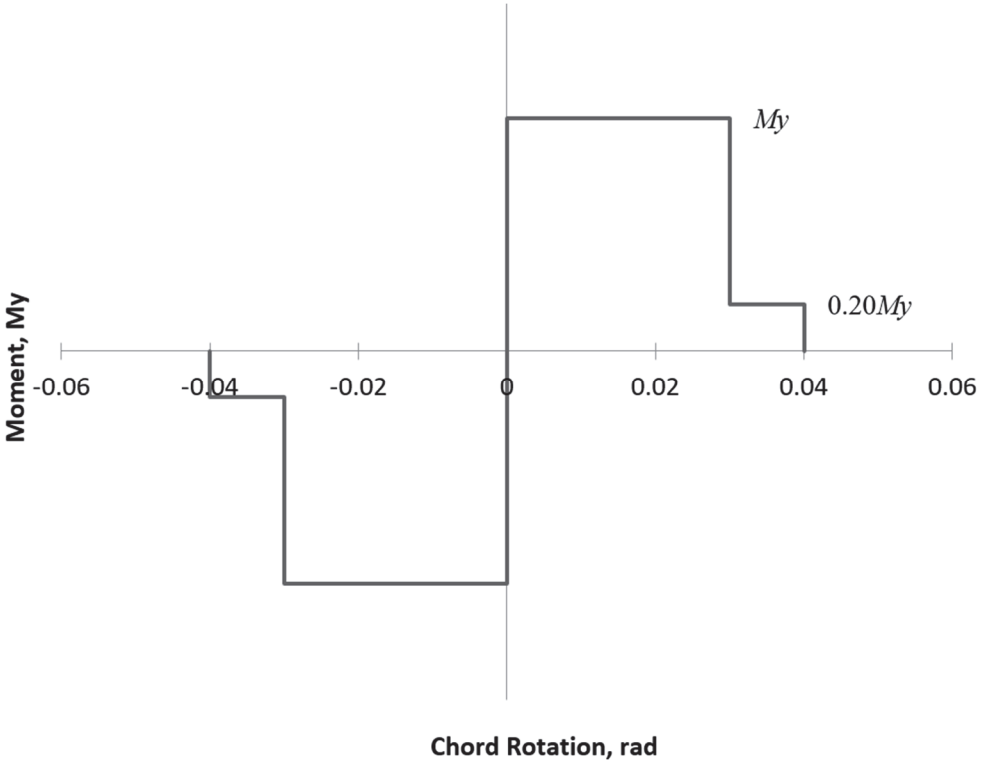

Figure B-15 Secondary slab-beam moment-rotation backbone curve.

B.4.6 Slab-Column Panel Zone

A rigid-plastic torsional spring, as recommended Section 3.6.2.1, is used to model the slab-column connection. From the slab design from the elastic analysis, the strength of the torsional spring is known based on the following parameters:

- Positive moment capacity = 1,530 k-in
- Negative moment capacity = 3,280 k-in
- γ = 0.6 for interior 1.0 for exterior

The resulting rigid-plastic backbone curve for the interior slab-column connection torsional spring is illustrated in Figure B-16.

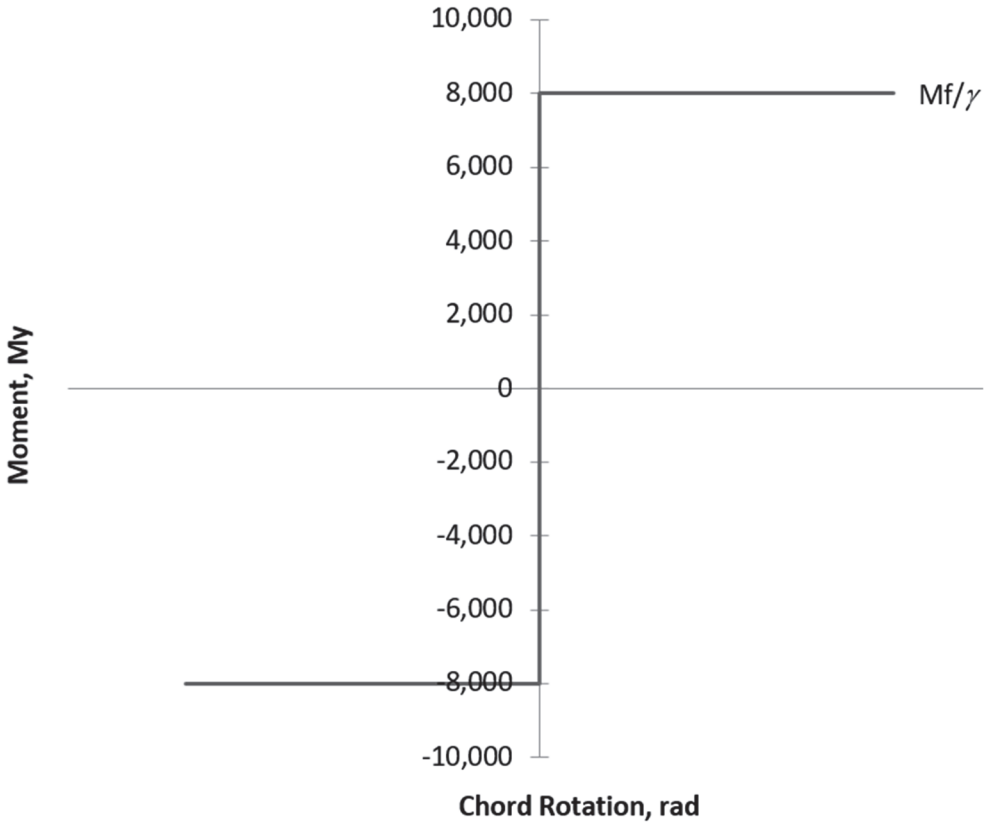

Figure B-16 Slab-column connection joint moment-rotation backbone curve.

B.4.7 Damping

Rayleigh damping is employed for the nonlinear direct integration analysis in SAP2000 (CSI, 2016a). The alpha and beta coefficients are chosen such that the damping ratio at periods equal to 1.5 and 0.25 times the first fundamental mode period is 2.5%. This represents the inherent damping typically provided for a concrete structure.

B.4.8 Ground Motions

Ground motions are developed based on the risk-targeted Maximum Considered Earthquake (MCE_R). The target response spectrum was developed per the Section 16.2.2.1 Method 1 of ASCE/SEI 7-16. Eleven horizontal ground motion pairs were selected. Vertical ground motion components were excluded from the analysis. Ground motions were selected from events within the same general tectonic regime and have generally consistent magnitudes and fault distances as those controlling MCE_R ground motion. The building site in San Francisco is located outside the near-fault zone and within the deterministic cap. Ground motions were scaled between the period range of 3.20 s and 0.10 s per 16.2.4.1 and 16.2.4.2. Figure B-17 shows the target and ground motion response spectra developed for this building site and Table B-4 lists the ground motion properties and scale factors.

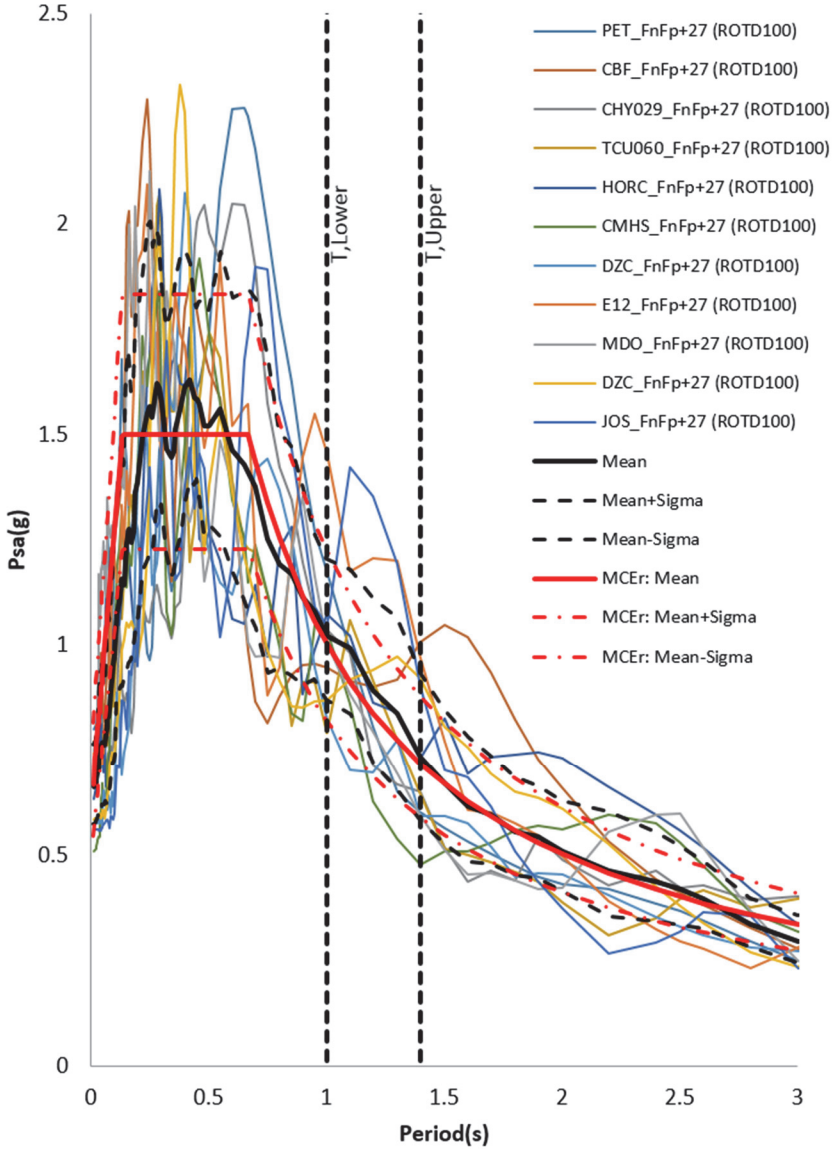

Figure B-17 Ground motion response spectra.

Table B-4 Ground Motion Set

Index	Event	Mw	Station	Site Class	Distance (km)	PGA (g)	PGV (cm/s)	Tpulse (s)	Scale Factor
1	Cape Mendocino	7.0	Petrolia	C	8.2	0.71	97	3.0	1.12
2	Cape Mendocino	7.0	Centerville Beach, Naval Facility	C	18.3	0.50	55	2.0	1.54
3	Chi-Chi, Taiwan	7.6	CHY029	C	11.0	0.27	38	--	2.24
4	Chi-Chi, Taiwan	7.6	TCU060	C	8.5	0.20	46	--	3.53
5	Darfield, New Zealand	7.0	HORC	D	7.3	0.47	105	9.9	1.14
6	Darfield, New Zealand	7.0	Christchurch Cashmere High School	E	17.6	0.25	49	--	2.03
7	Duzce, Turkey	7.1	Duzce	D	6.6	0.53	86	--	1.07
8	El Mayor-Cucapah	7.2	El Centro Array #12	D	11.3	0.39	74	8.7	1.7
9	El Mayor-Cucapah	7.2	Michoacan De Ocampo	D	15.9	0.48	72	--	1.39
10	Kocaeli, Turkey	7.5	Duzce	D	15.4	0.34	60	--	1.46
11	Landers	7.3	Joshua Tree	C	11.0	0.30	33	--	1.87

B.5 Nonlinear Response History Analysis

The example building is analyzed per requirements of Chapter 16 in ASCE/SEI 7-16. Table B-5 includes items required per Section 16.1.2. Formal design criteria are not explicitly included as part of this example however, the sections in this example provide a useful guide of relevant information to include in design criteria.

Table B-5 ASCE/SEI 7-16 Chapter 16 Analysis Requirements

Modeled Behavior: Elastic				
Item	*Action*	*Category*	*Acceptance Criteria*	*Capacity*
Non-Transfer Diaphragms	Force-Controlled	Ordinary	$V_n \geq 1.5Vu$	ACI 318
Transfer Diaphragms	Force-Controlled	Critical	$V_n \geq 2.0Vu$	ACI 318
Mat Foundation	Force-Controlled	Ordinary	$q_n \geq 1.5q_u$	Geotechnical Report & ASCE/SEI 41-13 Chapter 8
Modeled Behavior: Inelastic				
Item	*Action*	*Category*	*Acceptance Criteria*	*Capacity*
Beam Hinges	Deformation-Controlled	Ordinary	$\theta_u \leq \theta_{CP}$	ASCE/SEI 41-13 Table 10-7 & NIST GCR 17-917-45
Column Hinges	Deformation-Controlled	Ordinary	$\theta_u \leq \theta_{CP}$	ASCE/SEI 41-13 Table 10-8 & NIST GCR 17-917-45
Panel Zone	Deformation-Controlled	Ordinary	$\gamma_u \leq \gamma_{CP}$	ASCE/SEI 41-13 Table 10-10 & NIST GCR 17-917-45

B.5.1 Nonlinear Model Fundamental Periods

The computed periods and the modal response characteristics of the nonlinear building model for the first six modes are presented in Table B-6. It is of interest to note that the building periods are elongated compared to the elastic building model, even though the nonlinear model has additional elements to contribute in lateral stiffness. This is mainly because of the difference in the stiffness modifiers for the beam and column elements used in the nonlinear model versus the elastic model. The stiffness modifiers for beams and columns in the elastic model are 0.35 and 0.70, respectively, while those in the nonlinear model are 0.21 and 0.40 (based on a simplified approximation of stiffness modifiers, for a secant stiffness to the yield point, not fully exercising the equations of Section 4.2.1.2).

Table B-6 Computed Periods and Modal Response Characteristics – Nonlinear Model

Mode	Period (s)	Effective Mass Ratio *E-W*	Effective Mass Ratio *N-S*	Description
1	1.42	0%	82%	First Mode N-S
2	1.21	84%	0%	First Mode E-W
3	0.85	0%	0%	First Mode Torsion
4	0.45	0%	11%	Second Mode N-S
5	0.37	9%	0%	Second Mode E-W
6	0.32	0%	0%	Second Mode Torsion

B.5.2 Story Drift Check

In accordance with ASCE/SEI 7-16 Section 16.4.1.2, the mean story drift ratio is checked as a part of the global acceptance criteria. The allowable story drift limit is two times the limit employed for the elastic analysis. For the example building, which is Risk Category II and masonry-free, the allowable story drift ratio under nonlinear response history analysis is 4%. The mean story drift ratios in E-W and N-S directions are illustrated in Figures B-18 and B-19, respectively. It is observed that the building meets the drift criterion as the mean peak drifts at all levels and directions are less than 4%.

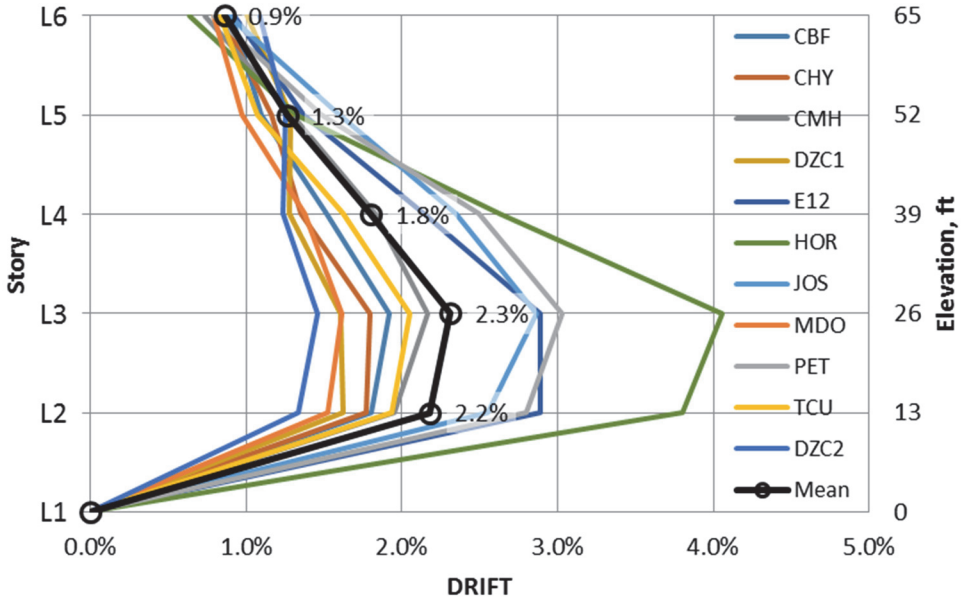

Figure B-18 Maximum peak story drift in east-west direction.

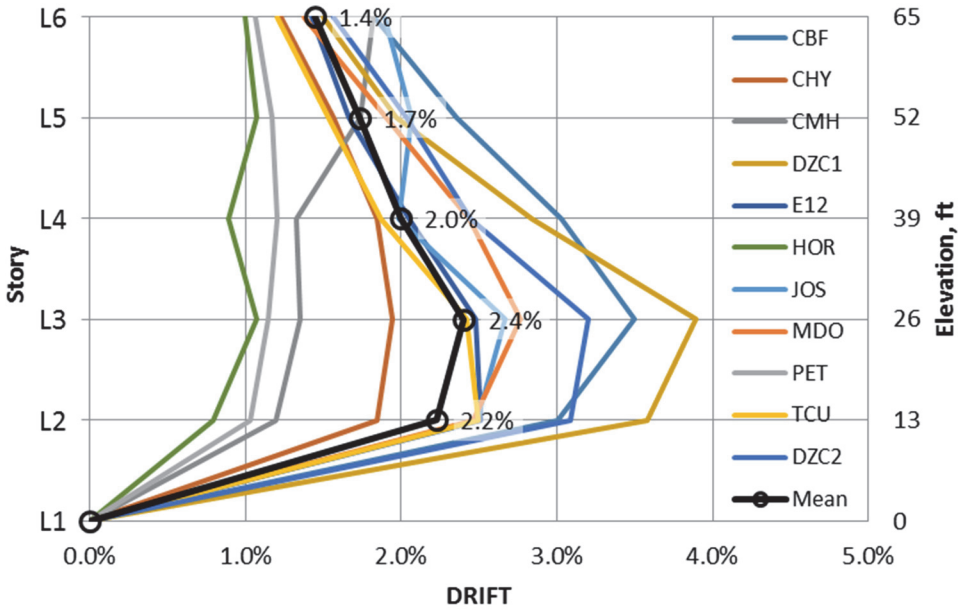

Figure B-19 Maximum peak story drift in north-south direction.

B.5.3 Story Shears and Overturning Moments

Mean peak building responses in story shears and overturning moments in each direction are illustrated in Figures B-20, B-21, B-22, and B-23.

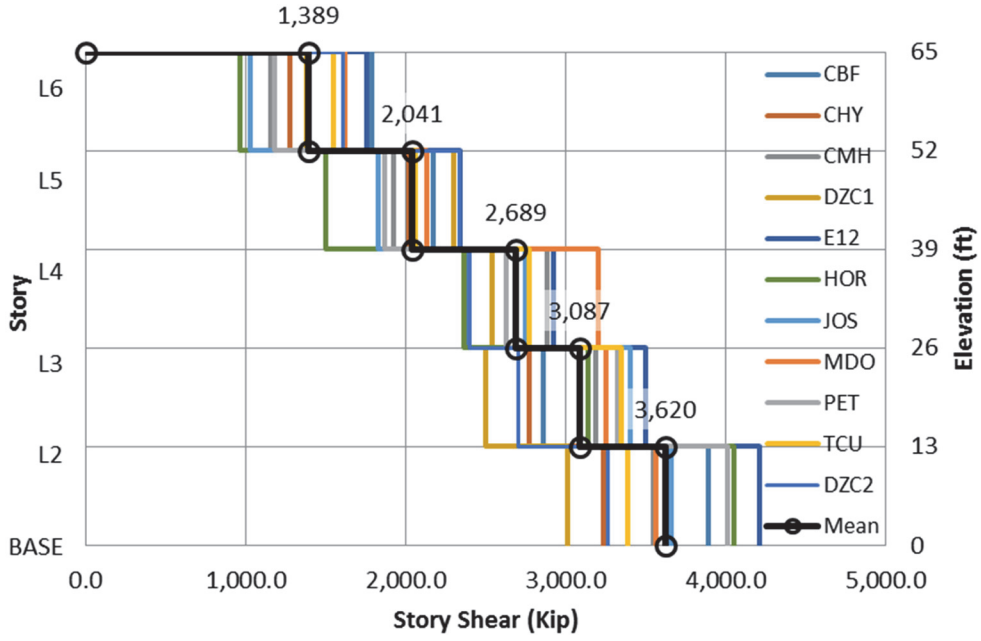

Figure B-20 Maximum peak story shear in east-west direction.

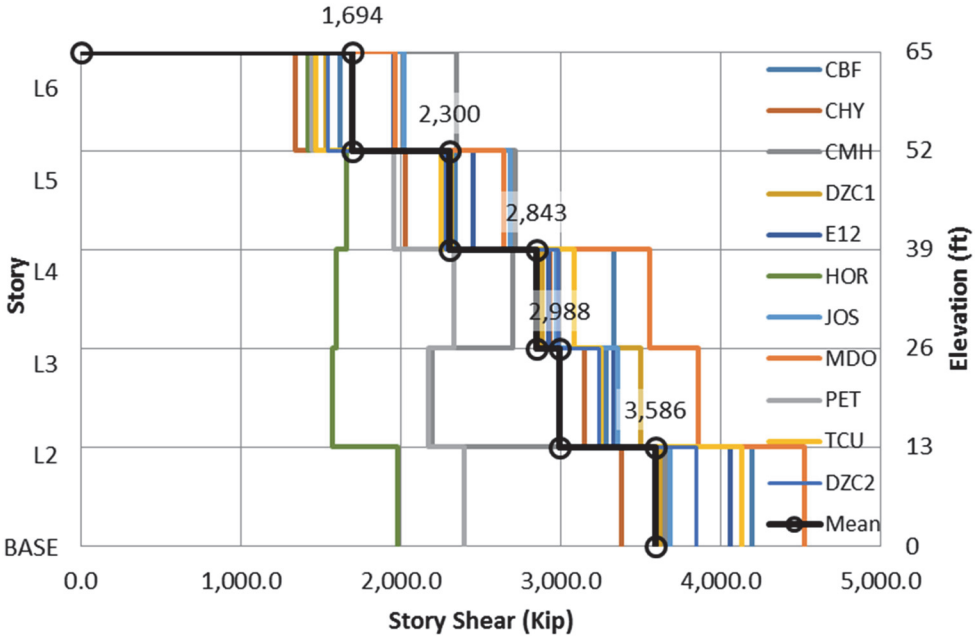

Figure B-21 Maximum peak story shear in north-south direction.

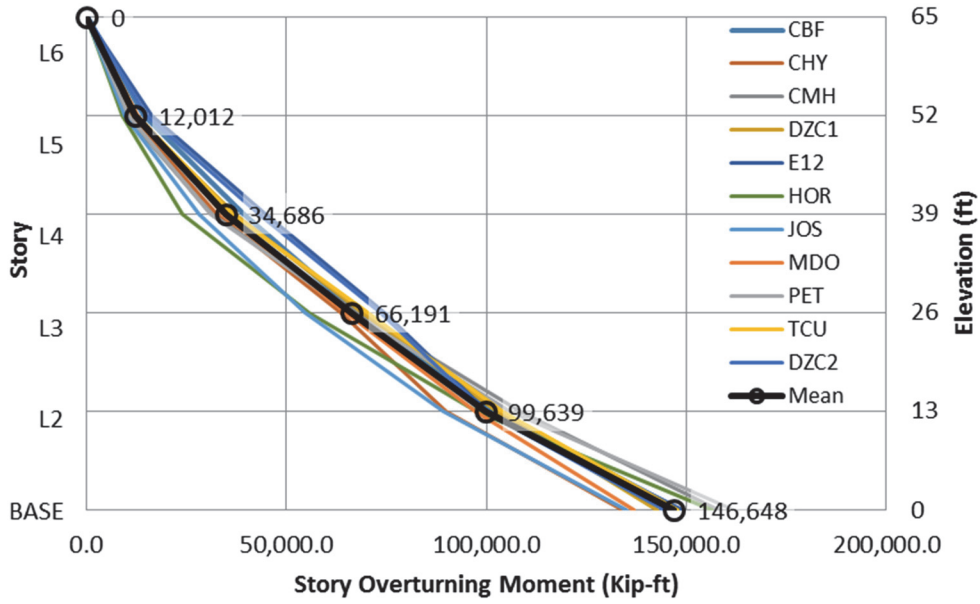

Figure B-22 Maximum peak story overturning moment about north-south axis.

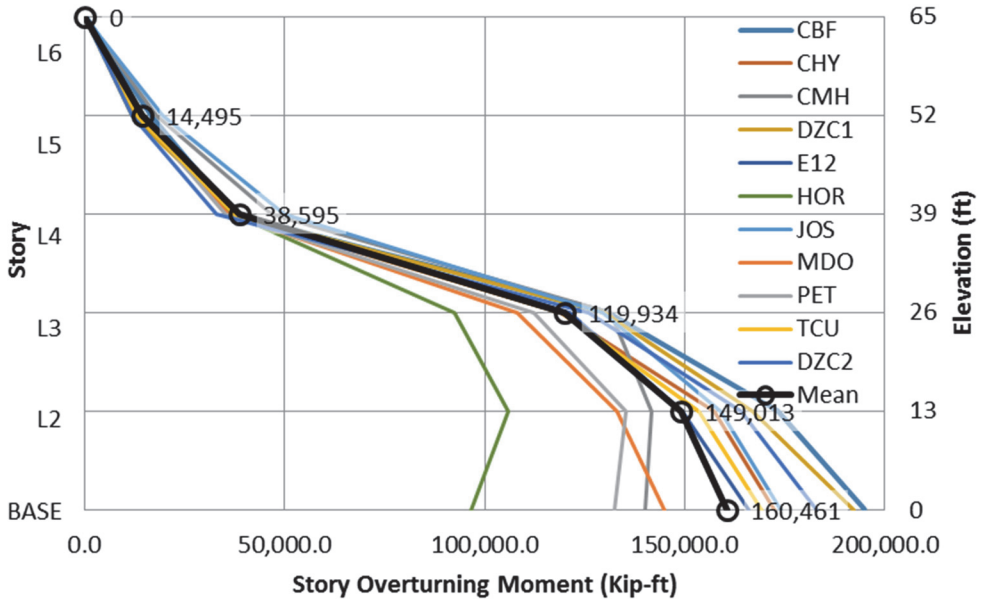

Figure B-23 Maximum peak story overturning moment about east-west axis.

B.5.4 Deformation-Controlled Action

For each beam or column element, there are two hinges associated to account for both ends of the line element.

B.5.4.1 Beam Hinge Rotation

The acceptable plastic rotation for the primary beams of the example building is determined based on the backbone curve of the beam hinges. Consistent with Table 10-7 of ASCE/SEI 41-13, the acceptable plastic rotations for beams at the performance level of collapse prevention is equal to the rotation at the onset of the strength loss, or $\theta_{cap,pl}$. The acceptable plastic rotation for the beams of the example building is equal to 0.033.

The plastic rotations for the beam hinges in MF-D and MF-1 are illustrated in Figures B-24 and B-25. It is observed that all beam hinges experience mean plastic rotations (shown with orange rectangles in Figures B-24 and B-25) less than 0.033, therefore the beam proportioning and design are all acceptable.

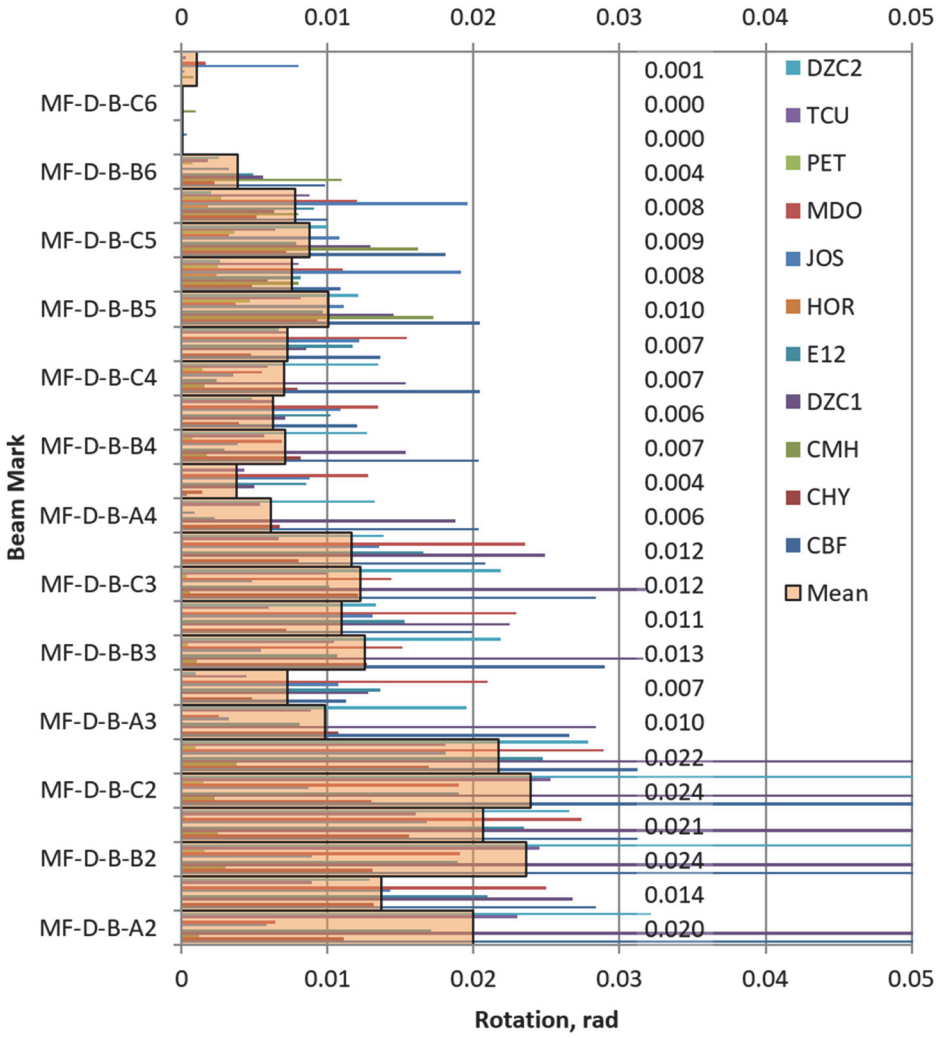

Figure B-24 MF-D: beam hinge rotations.

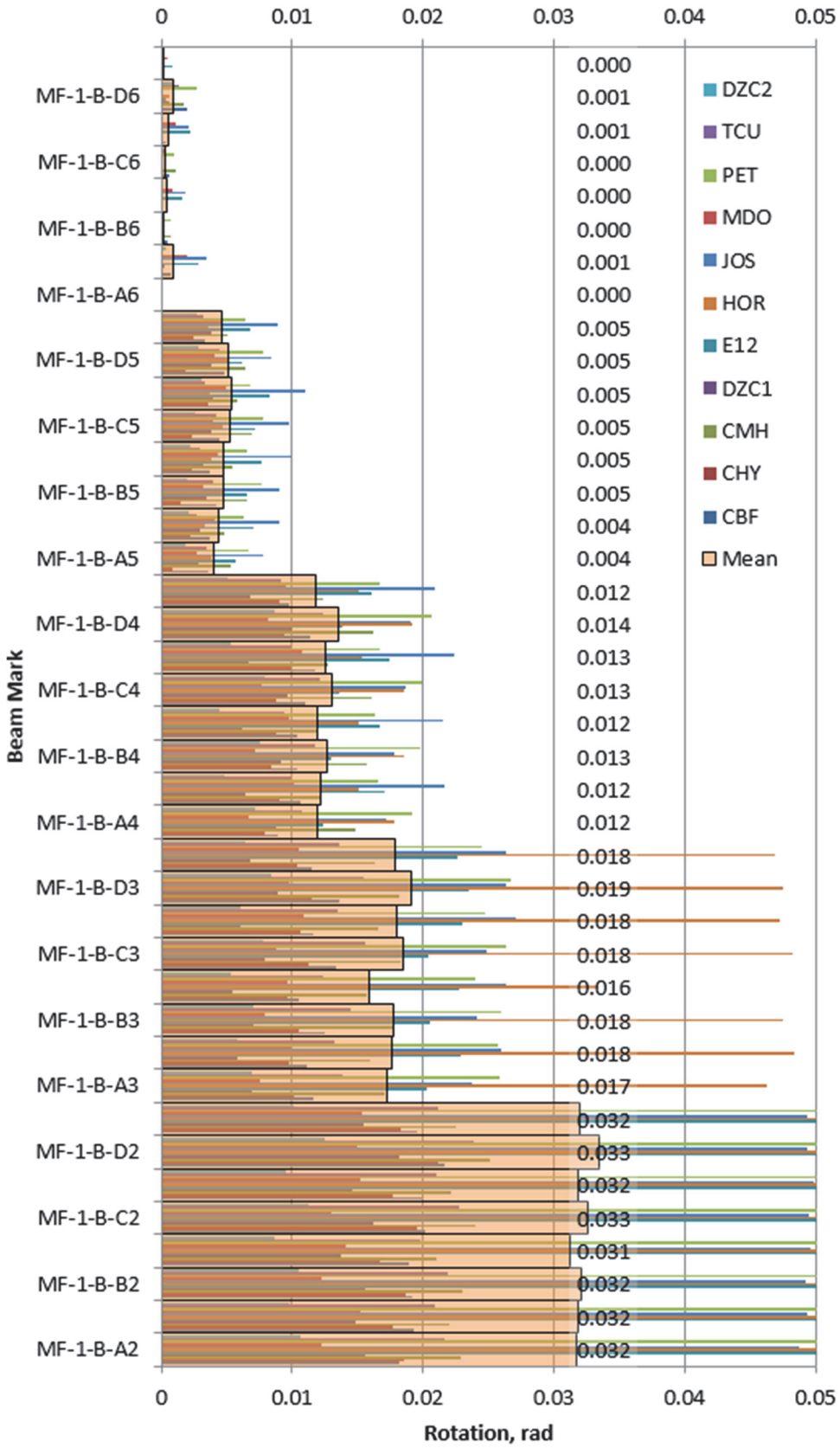

Figure B-25 MF-1: beam hinge rotations.

B.5.4.2 Column Hinge Rotation

The acceptable plastic rotation for the primary columns of the example building is determined from Table 10-8 of ASCE/SEI 41-13. The following parameters are assumed to determine the acceptance criteria:

- Condition = *i*
- Axial ratio = 0.25
- Confinement ratio ≥ 0.006

The resulting acceptable plastic rotation at the performance level of collapse prevention is 0.045.

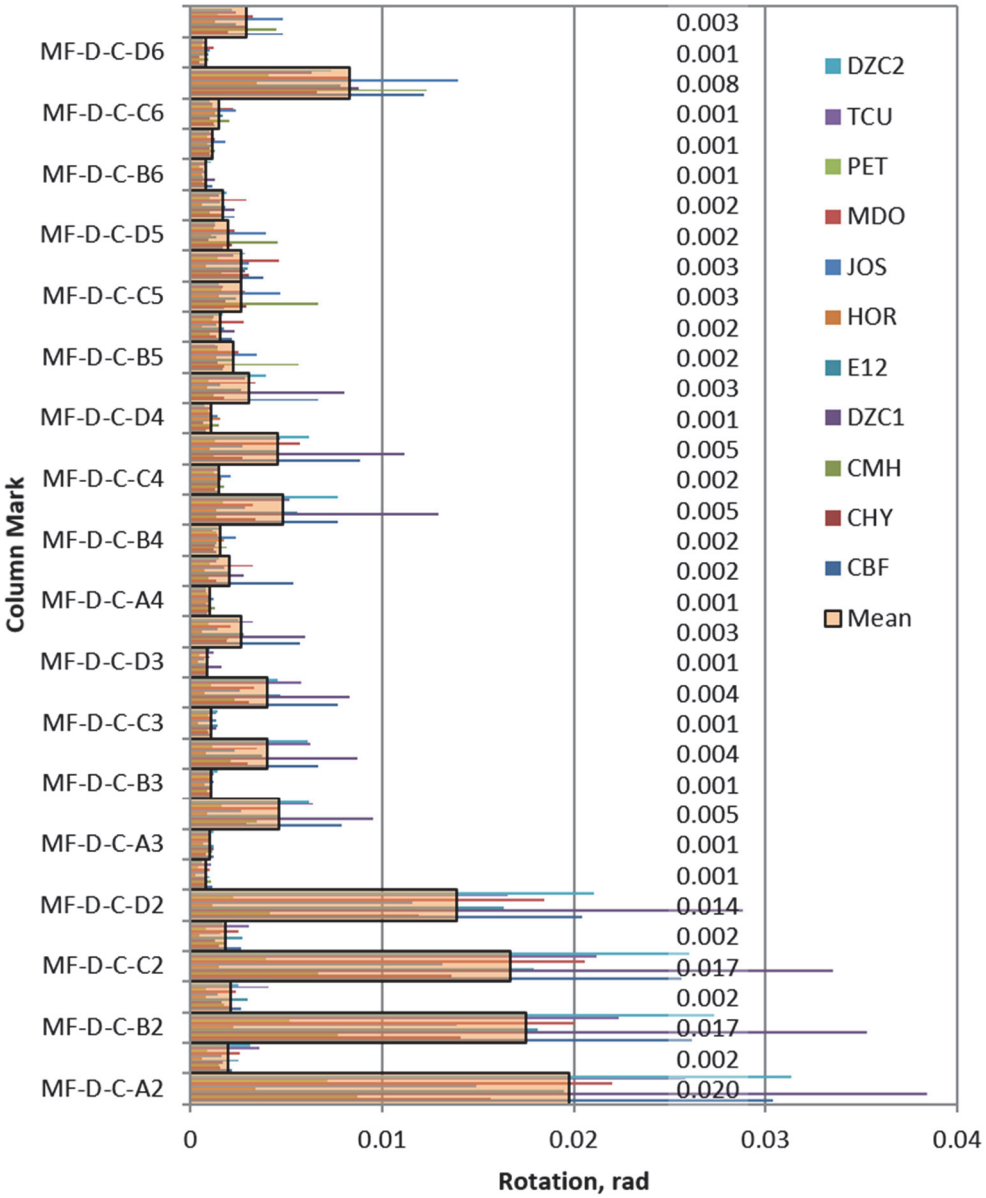

Figure B-26 MF-D: column hinge rotations.

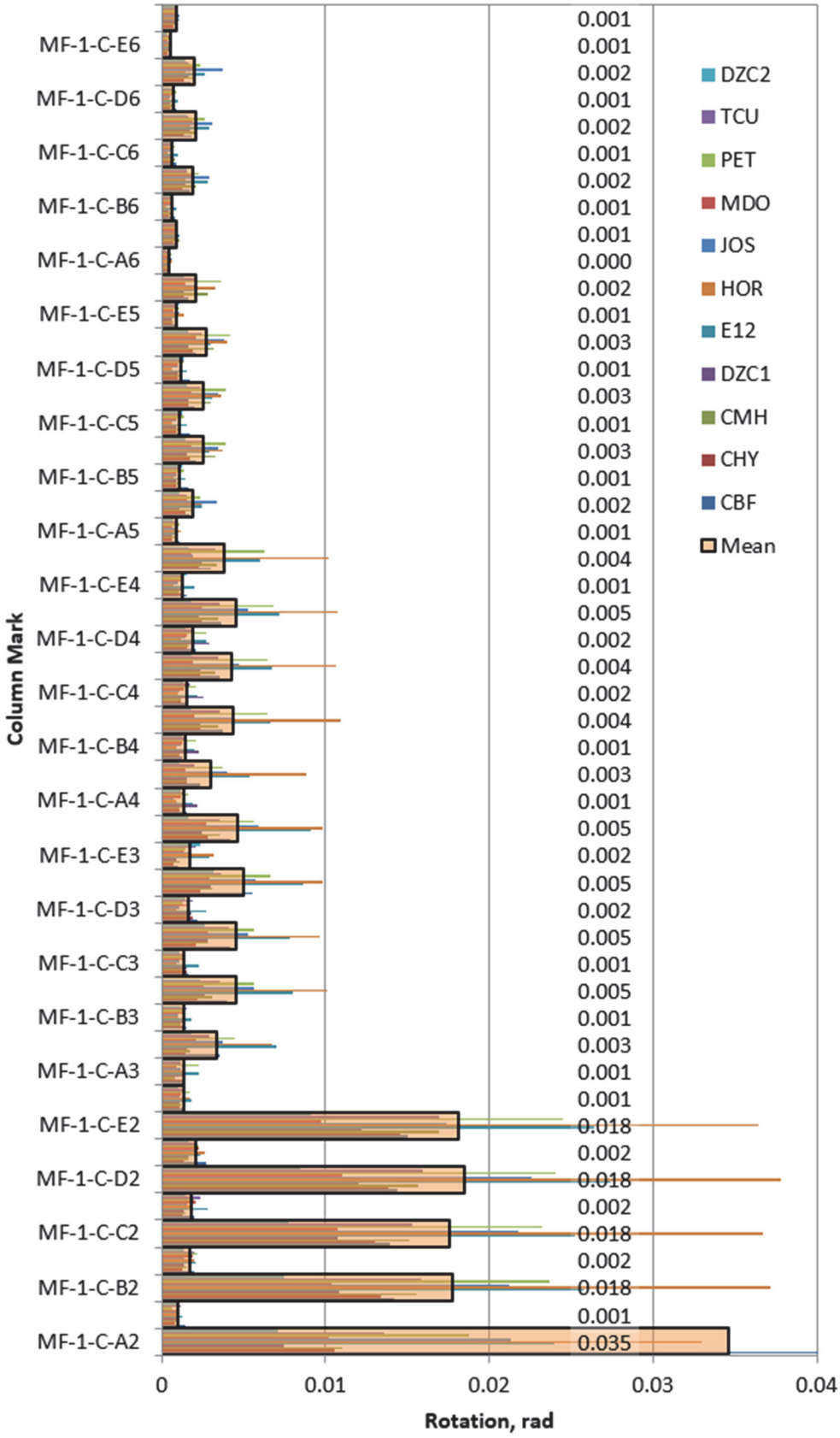

Figure B-27 MF-1: column hinge rotations.

B.5.4.3 Secondary Slab-Beam Hinge Rotation

The acceptable plastic rotation for the secondary slab-beams of the example building is determined from Table 10-15 of ASCE/SEI 41-13. The consistent parameters used to determine the backbone curve are assumed to determine the acceptance criteria:

- Condition = *i*
- V_g/V_o = 0.2
- Continuity reinforcement = Yes

The resulting acceptable plastic rotation at the performance level of collapse prevention is 0.040.

The plastic rotations for the slab-beam hinges around the columns at B3 and C3, as shown in Figure B-28, are illustrated in Figure B-29 and B-30. It is observed that all slab-beam hinges experience mean plastic rotations less than 0.040, therefore the slab proportioning and design are all acceptable.

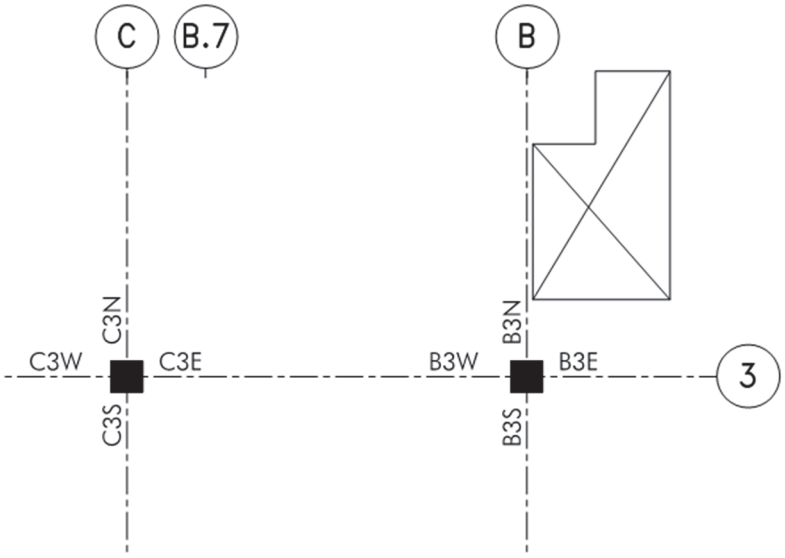

Figure B-28 Slab-beam hinges at column B3 and C3.

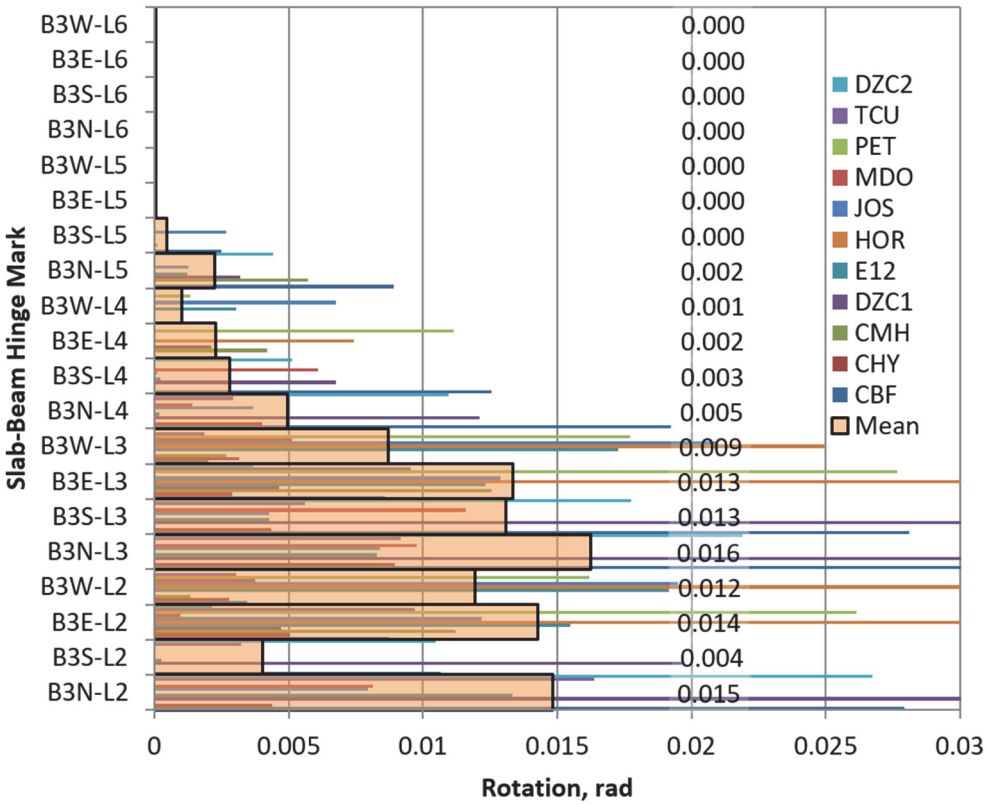

Figure B-29 Slab-beam hinge rotations at column B3.

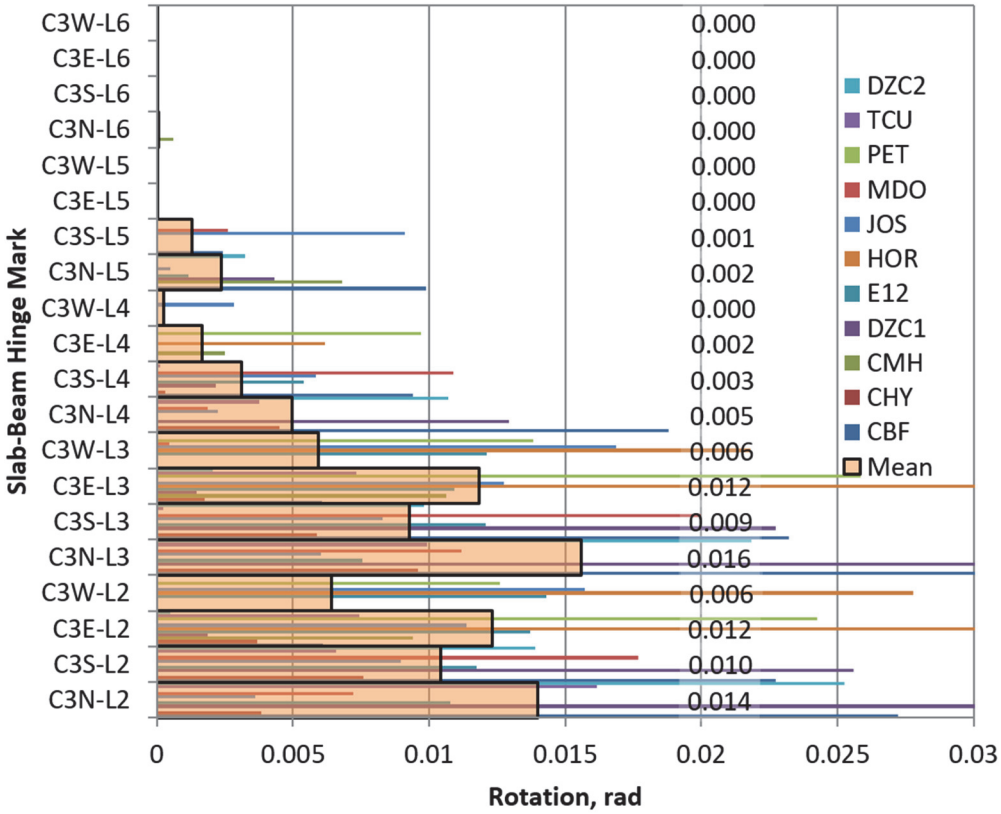

Figure B-30 Slab-beam hinge rotations at column C3.

B.5.5 Force-Controlled Action

Force-controlled actions typically found in a moment-resisting frame structure are beam and column shears. Beam shear actions are, however, typically capacity-designed against the shear corresponding to the maximum probable moment, since the beams are the main source of ductility in a moment-resisting frame structure. The same procedure is applicable to the columns, but the shear design value is often unrealistic as the column is designed against *P-M-M*, not just against major-axis moment. Therefore, it is recommended that, when nonlinear analysis is available, the demand from the analysis is used, in lieu of capacity-based approach, to design columns against the shear demand. It should be noted that the same design approach may be used for the beam shears, but it is not recommended as the capacity-design approach is less susceptible to the uncertainties associated with the ground motions. Refer to Section B.5.5.1 for the representative column shear design values for the example building.

Other elements that need to be designed as force-controlled actions are those expected to remain essentially elastic throughout the ground motion history. In the example building, the part of the moment frame that is also acting as a column transfer system is considered to remain elastic (and designed to remain that way under applied MCE_R ground motions) and therefore all its internal forces are considered force-controlled. Refer to Section B.5.5.2 for the representative transfer system design values for the example building.

B.5.5.1 Column Shear

The shear demand along the column B1 is representatively investigated to determine the adequateness of the column size and to design shear reinforcing. The peak shears for the column B1 are illustrated in Figure B-31.

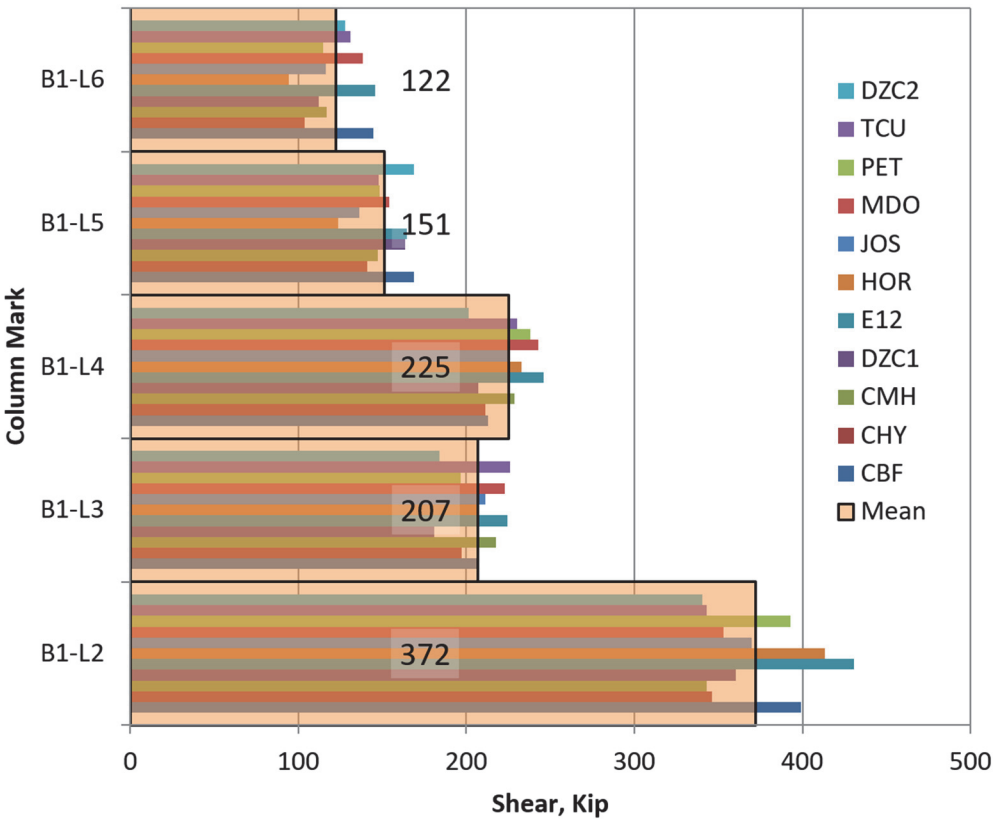

Figure B-31 Peak shears for column B1.

The design shear demand for the column is the observed mean peak shear multiplied by the critical load factor, $\gamma = 2.0$, and the importance factor, $I_e = 1.0$. The shear capacity calculation and check of the column is not shown in this section. However, it is observed that the B1 column and other columns at level 1 are not adequate against the design shear, therefore re-proportioning and re-iterations may be required.

B.5.5.2 Column Transfer

A beam transfer system is required as the column at grid intersection B4 is discontinued at level 1. This is illustrated in Figure B-32. The transfer system is assumed to remain elastic during an earthquake event and therefore modeled as such and designed as force-controlled elements.

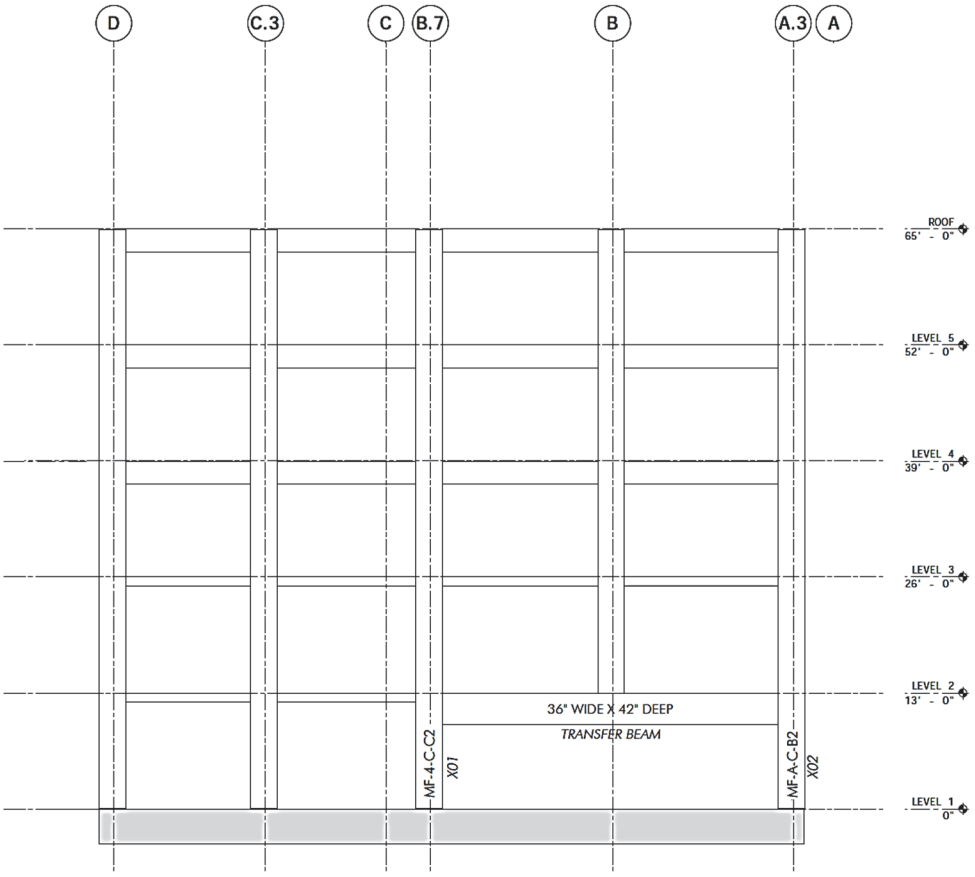

Figure B-32 Transfer system at grid 4.

Transfer Beam

The internal forces, shear and moment, along the transfer beam are illustrated in Figure B-33 and B-34. The design forces are the observed forces multiplied by the load factor and importance factor. The resulting design forces for the transfer beam are as follows. These transfer beams were then designed to remain elastic in accordance with the requirements of Section 6.3.1 of the *Part I Guidelines*.

- 600 × 2 = 1,200k for shear (Critical element)
- 4,350 × 1.5 = 6,500k-ft for positive moment (Ordinary element)
- 6,800 × 1.5 = 10,000k-ft for negative moment (Ordinary element)

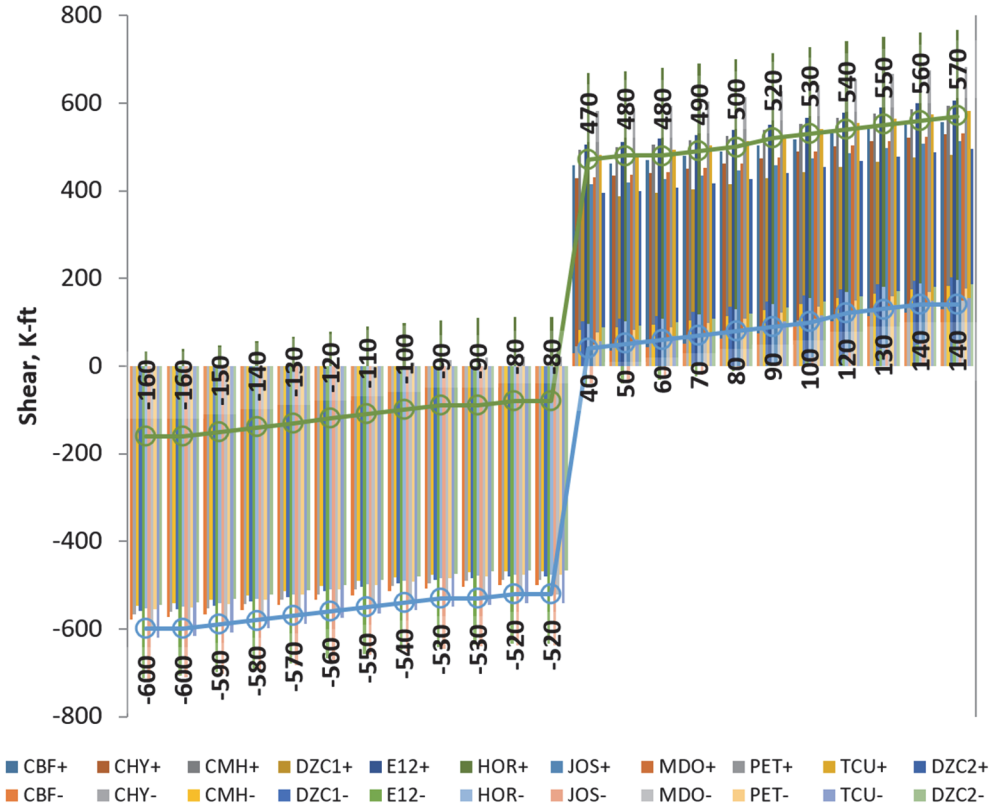

Figure B-33 Max and min peak shears for transfer beam on grid 4.

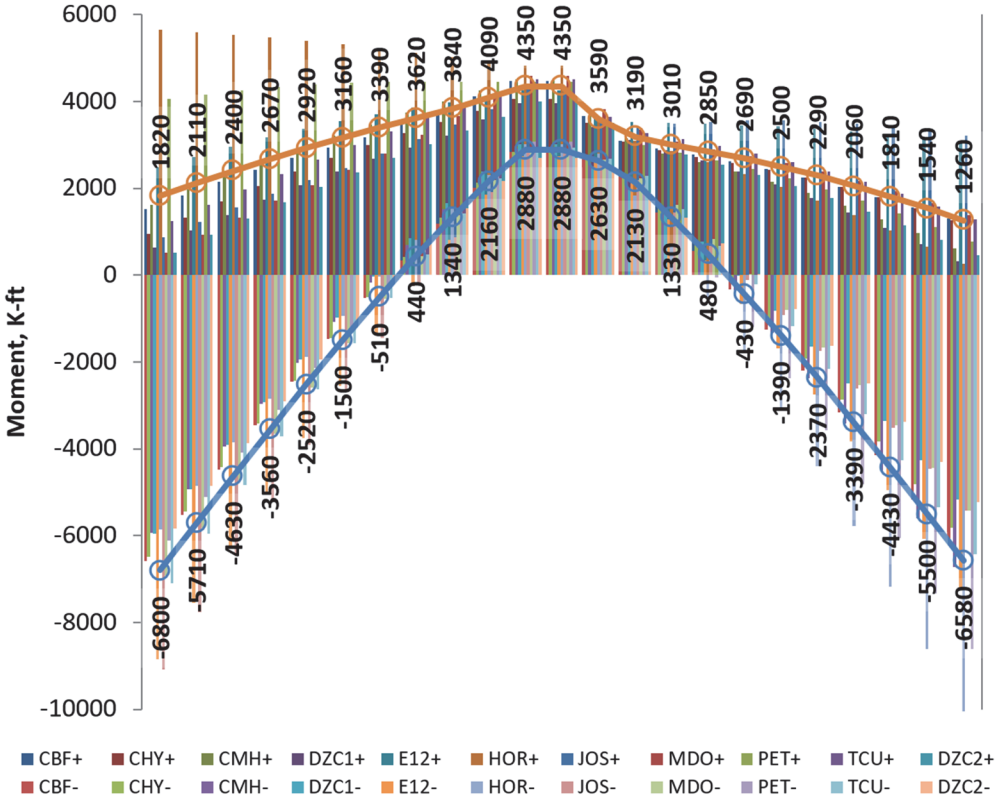

Figure B-34 Max and min peak moments for transfer beam on grid 4.

Transfer Columns

Because the column design against the simultaneous application of peak axial, peak moments is very conservative, the *P-M-M* check of the column is evaluated with internal forces corresponding to each time step. This results in DCR values for each step and the peak DCR is observed for each ground motion cases. The mean of the peak DCR values is then used to determine whether the column is adequate.

Before the DCR values are calculated for each time step, the internal forces due to the ground motion accelerations are amplified by the load and importance factors. This is done by subtracting the initial internal forces, which are purely due to gravity loadings corresponding to time step zero, from each time step and multiplying the results with the appropriate factors and then adding back the previously subtracted gravity induced forces.

The DCR check is evaluated using the column section design software spColumn by StructurePoint. The resulting DCR of all 11 ground motions for the transfer column at grid intersection of B.7 and 4 is plotted versus time in Figure B-35. The peak values for each ground motion and the mean DCR are also determined as shown in Table B-7 (which is the maximum DCR from each of the 11 ground motions, and acceptance criteria is then based on the average value of these maximum individual DCRs).

Table B-7 Mean DCR

GM	PEAK DCR
CBF	1.04
CHY	0.88
CMH	0.87
DZC1	0.86
E12	1.22
HOR	0.82
JOS	1.25
MDO	1.02
PET	0.87
TCU	0.96
DZC2	0.83
MEAN	0.97

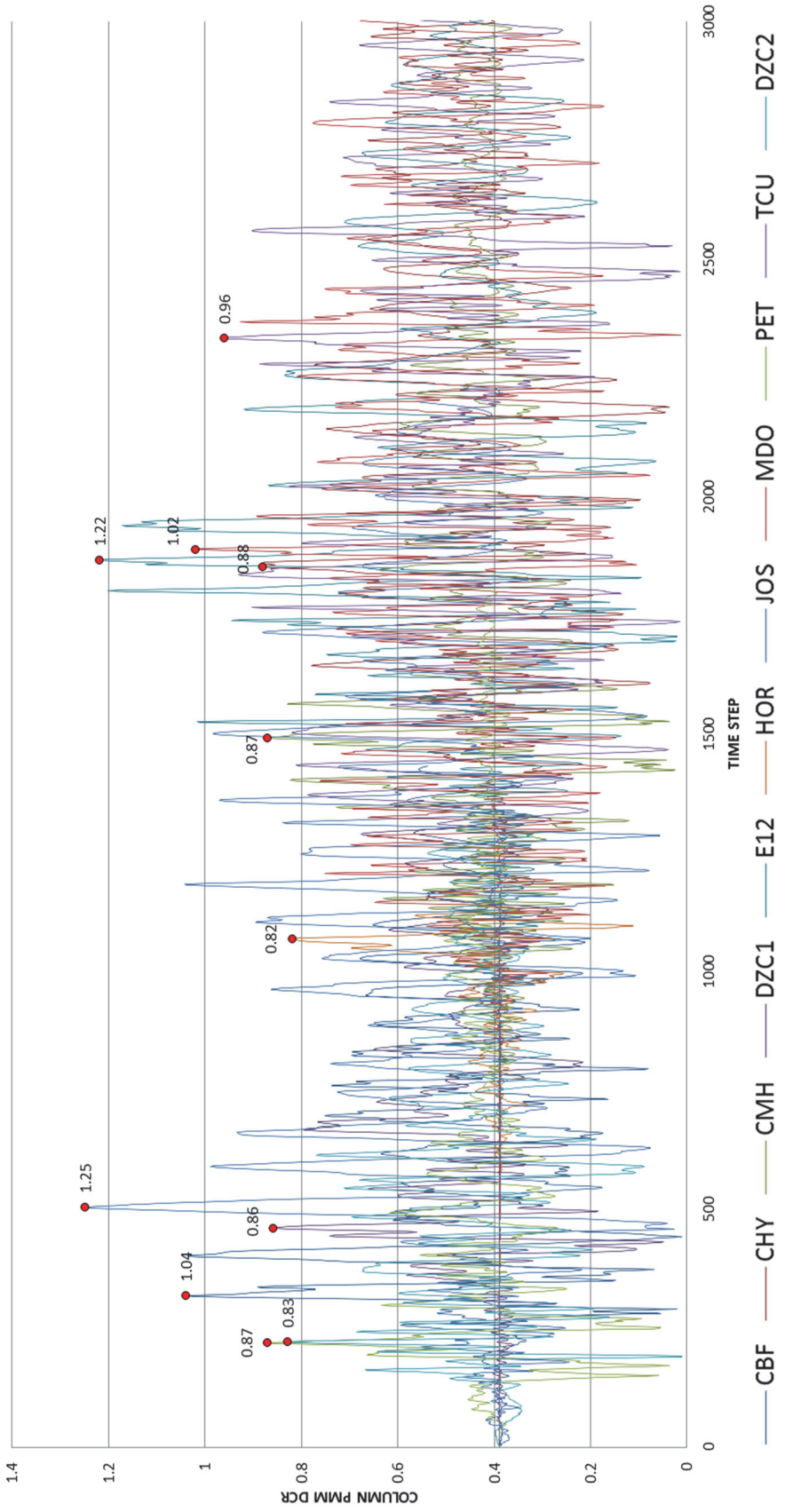

Figure B-35 DCR vs time for transfer column at grid B.7&4.

B.6 Conclusion

Nonlinear response history analysis is an improvement from simplified, elastic analysis methods as it is considered more rational and realistic. It should be noted though that with a more complex analysis, there are more opportunities to make errors and more parameters to be aware of. Before embarking on the task of nonlinear analysis of a building, a designer must identify/designate all elements expected to behave nonlinearly and also understand the characteristics of the nonlinearity in order to properly model the structure. Nonlinear analysis is time-consuming in both modeling and analysis often requires multiple iterations. To employ nonlinear analysis efficiently and effectively, the designer must start with a good baseline model and reasonable modeling of the nonlinear elements in order to avoid a large number of re-iterations and unmanageable analysis computing time due to overly complicated analysis. The following are some of tips and tricks discovered that may help engineers avoid the potential pitfalls.

- **Proportioning.** In order to take advantage of the ductility of the moment frame system, the designer should be careful not to over-design the elements that may delay the onset of yielding while limiting the drift ratio well below the acceptable range. This often results in a stiff building that develops high base shear and therefore high force demands in the lateral elements. It should be reminded that a high capacity structure does not necessarily mean a high performing structure.
- **Transfer System.** Lateral system that also holds significant gravity loads often require the system to remain elastic due to its force-controlled actions. This can yield an inefficient design and can also contribute to unnecessarily stiffening the building, so should be avoided in the design if possible.
- **Axial Ratcheting.** It should be noted that the column hinges that experience yielding in both sides of extreme fibers, grows taller as the residual tensile strain accumulates faster than that of compression strain. This is a real phenomenon and should not be considered as an analysis error.
- **Backbone Curve.** When defining the backbone curves of hinges or material stress-strain curves, designer should be aware of how the analysis method treats the unloading of internal forces. When a hinge experiences strength loss, the internal force it developed must be redistributed. It is observed from the example analysis that when redistribution is required, SAP2000 introduces temporary internal forces to unload the hinge, and then reverses that force to transfer the unloaded to the neighboring elements and hinges. This is an expensive event that requires large number of substeps when multiple hinges are experiencing strength loss simultaneously. This problem is exasperated when the strength loss for each hinge is a multi-event (i.e., progressive strength loss instead of sudden strength loss), because the complete unloading event requires a significant strain

development when progressive strength loss is employed, the analysis is required to perform the unloading event in small increments. During these small increments, however, the hinges are constantly competing to unload themselves and load others. This back-and-forth event is reduced when sudden strength loss is employed because the number of events required to unload a hinge is limited. It is understood that, as general rule, the designer should avoid modeling sudden strength loss in backbone curves as it is a rare event, and employ progressive strength loss, but analysis may never finish running if the hinges try to remain on the descending slope. It should be perhaps considered, depending on the unloading method used, that the strength loss be modeled with multiple sudden drops. This is illustrated in Figure B-36.

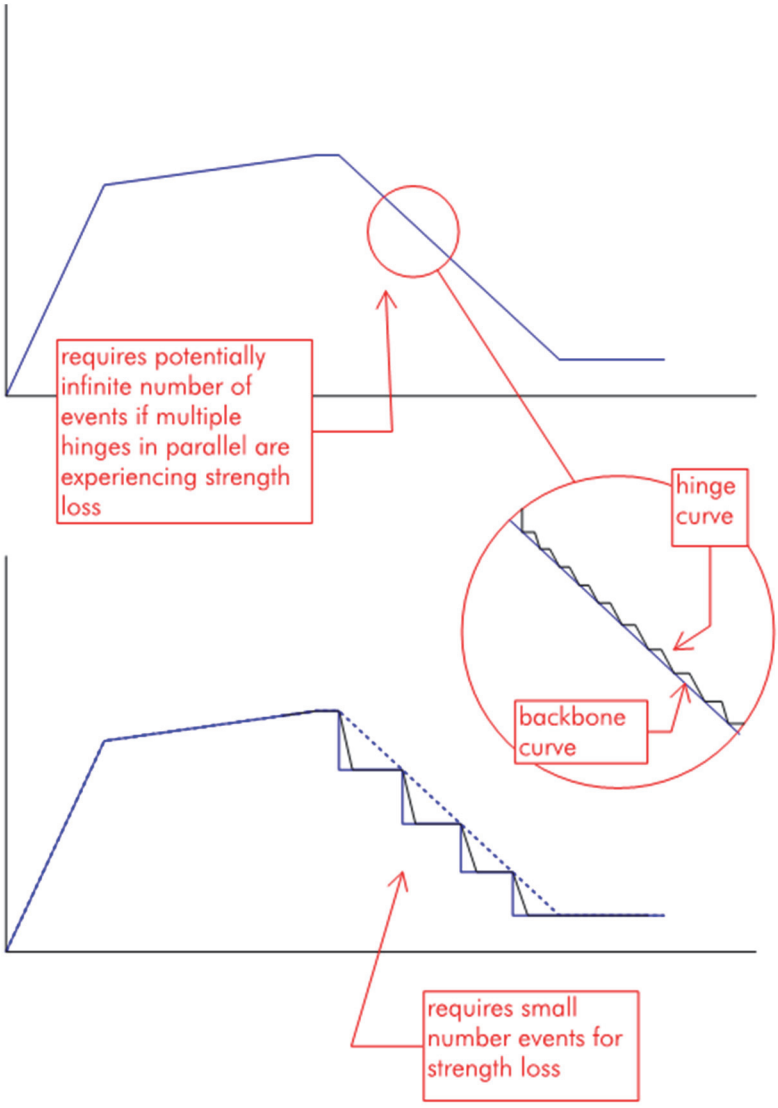

Figure B-36 Illustration of backbone curve and effects that negative stiffness have on some commercial software solution algorithms.

Finally, it should be emphasized that these observations are based on the one example building and software and that the observations and conclusions are not meant to generally apply to other buildings. Indeed, the intent of this *Guidelines* document is to facilitate the use of nonlinear analysis to investigate the specific characteristics of any building, and the purpose of this appendix is to illustrate application of the guidelines.

References

ACI, 2002, *Recommendations for Design of Beam-Column Connections in Monolithic Reinforced Concrete Structures*, ACI-ASCE 352-02, American Concrete Institute - American Society of Civil Engineers (ACI-ASCE) Joint Committee 352, American Concrete Institute, Farmington Hills, Michigan.

ACI, 2003, *Bond and Development of Straight Reinforcing Bars in Tension*, ACI 408R-03, ACI Committee 408, American Concrete Institute, Farmington Hills, Michigan.

ACI, 2005, *Acceptance Criteria for Moment Frames Based on Structural Testing and Commentary*, ACI 374.1-05, ACI Committee 374, American Concrete Institute, Farmington Hills, Michigan.

ACI, 2011, *Guide for Seismic Rehabilitation of Existing Concrete Frame Buildings and Commentary*, ACI 369R-11, American Concrete Institute, Farmington Hills, Michigan.

ACI, 2014, *Building Code Requirements for Reinforced Concrete*, ACI 318-14, ACI Committee 318, American Concrete Institute, Farmington Hills, Michigan.

ACI, 2017, *Guide for Seismic Rehabilitation of Existing Concrete Frame Buildings and Commentary*, ACI 369R-17, American Concrete Institute, Farmington Hills, Michigan.

Ahmad, S.H., and Shah, S.P., 1982, "Complete triaxial stress-strain curves for concrete," *Journal of the Structural Division*, Vol. 108, No. 4, pp. 728-742.

Alath, S., and Kunnath, S.K., 1995, "Modeling inelastic shear deformation in rc beam-column joints," *Proceedings*, 10th Conference on Engineering Mechanics Part 2 (of 2), Boulder, Colorado, pp. 822-825.

Alsiwat, J.M., and Saatcioglu, M., 1992, "Reinforcement anchorage slip under monotonic loading," *Journal of Structural Engineering*, Vol. 118, No. 9, pp. 2421-2438.

ASCE, 2014, *Seismic Evaluation and Retrofit of Existing Buildings*, ASCE/SEI 41-13, American Society of Civil Engineers, Reston, Virginia.

ASCE, 2017a, *Minimum Design Loads and Associated Criteria for Buildings and Other Structures*, ASCE/SEI 7-16, American Society of Civil Engineers, Reston, Virginia (forthcoming).

ASCE, 2017b, *Seismic Evaluation and Retrofit of Existing Buildings*, ASCE/SEI 41-17, American Society of Civil Engineers, Reston, Virginia (forthcoming).

ATC, 2015, *Seismic Evaluation of Older Concrete Frame Buildings for Collapse Potential*, ATC-78-3 report, prepared by the Applied Technology Council for the Federal Emergency Management Agency, Redwood City, California.

Beres, A., White, R.N., and Gergely, P., 1992, *Seismic Performance of Interior And Exterior Beam-to-Column Joints Related to Lightly Reinforced Concrete Frame Buildings: Detailed Experimental Results*, Structural Engineering, School of Civil and Environmental Engineering, Cornell University, Ithaca, New York.

Berry, M.P., Parrish, M., and Eberhard, M.O., 2004, *PEER Structural Performance Database User's Manual*, Pacific Earthquake Engineering Research Institute, Berkeley, California. Available at: http://nisee.berkeley.edu/spd/, last accessed April 17, 2017.

Berry, M.P., and Eberhard, M.O., 2008, *Performance Modeling Strategies for Modern Reinforced Concrete Bridge Columns*, PEER Report 2007/07, Pacific Earthquake Engineering Research Center, University of California, Berkeley, California.

Birely, A.C., Lowes, L.N., and Lehman, D., 2012, "Linear analysis of concrete frames considering joint flexibility," *Structural Journal*, Vol. 109, No. 3, pp. 381-92.

Caltrans, 2006, *Seismic Design Criteria*, Version 1.4, California Department of Transportation, Sacramento, California.

CEB, 1996, *RC Frames under Earthquake Loading – State of the Art Report*, Comité Euro-International du Béton, Convenor Michael N. Fardis, published by Thomas Telford, London.

Celik, O.C., and Ellingwood, B.R., 2008, "Modeling beam-column joints in fragility assessment of gravity load designed reinforced concrete frames," *Journal of Earthquake Engineering*, Vol. 12, No. 3, pp. 357-81.

Chang, G.A., and Mander, J.B., 1994, *Seismic Energy Based Fatigue Damage Ananlysis of Bridge Columns: Part 1 – Evaluation of Seismic Capacity*, NCEER Technical Report No. NCEER-94-0006, State University of New York, Buffalo, New York.

Collins, M.P., Bentz, E.C., Quach, P.T., and Proestos, G.T., 2015, "The challenge of predicting the shear strength of very thick slabs," *Concrete International*, Vol. 37, No. 11, pp. 29-37.

Corley, W.G., 1966, "Rotational capacity of reinforced concrete beams," *Journal of the Structural Division*, Vol. 92, No. 5, pp. 121-46.

CSI, 2015, *Integrated Analysis, Design, and Drafting of Building Systems*, ETABS, Computers and Structures, Inc., Walnut Creek, California.

CSI, 2016a, *Integrated Software for Structural Analysis and Design*, SAP2000, Version 18.1.1, Computers and Structures, Inc., Walnut Creek, California.

CSI, 2016b, *Nonlinear Analysis and Performance Assessment of 3D Structures*, PERFORM-3D, Computers and Structures, Inc., Walnut Creek, California.

Darvall, P., and Allen, F., 1983, "Lateral load effective width of flat plates with drop panels," *ACI Journal Proceedings*, Vol. 81, No. 6.

Dovich, L.M., and Wight, J.K., 2005, "Effective slab width model for seismic analysis of flat slab frames," *Structural Journal*, Vol. 102, No. 6.

Eligehausen, R., Popov, E.P., and Bertero, V.V., 1983, *Local Bond Stress-Slip Relationships of Deformed Bars under Generalized Excitations*, Report No. UCB/EERC-83/23, Earthquake Engineering Research Center, University of California, Berkeley.

Elwood, K.J., and Eberhard, M.O., 2009, "Effective stiffness of reinforced concrete columns," *Structural Journal*, Vol. 106, No. 4, pp. 476-484.

Elwood, K.J., Matamoros, A.B., Wallace, J.W., Lehman, D.E., Heintz, J.A., Mitchell, A.D., Moore, M.A., Valley, M.T., Lowes, L.N., Comartin, C.D., and Moehle, J.P., 2007, "Update to ASCE/SEI 41 concrete provisions," *Earthquake Spectra*, Vol. 23, No. 3, pp. 493-523.

Fardis, M. N., and Biskinis, D. E., 2003, "Deformation capacity of RC members, as controlled by flexure or shear," *Proceedings*, International Symposium on Performance-Based Engineering for Earthquake Resistant Structures, pp. 511-530.

FEMA, 2000, *Prestandard and Commentary for the Seismic Rehabilitation of Buildings*, FEMA 356, prepared by the American Society of Civil Engineers for the Federal Emergency Management Agency, Washington, D.C.

fib, 2008, *Practitioner's Guide to Finite Element Modelling of Reinforced Concrete Structures*, Fédération Internationale du Béton (fib), International Federation for Structural Concrete, Lausanne, Switzerland.

fib, 2013, *fib Model Code for Concrete Structures 2010*, Fédération Internationale du Béton (fib), International Federation for Structural Concrete, Ernst & Sohn, Berlin, Germany.

Ghannoum, W.M., 2017, "Updates to modeling parameters and acceptance criteria for non-ductile and splice-deficient concrete columns," *Proceedings*, 16th World Conference on Earthquake Engineering, Santiago, Chile.

Ghannoum, W.M., and Moehle, J.P., 2012a, "Dynamic collapse analysis of a concrete frame sustaining column axial failures," *Structural Journal*, Vol. 109, No. 3, pp. 403-412.

Ghannoum, W.M., and Moehle, J.P., 2012b, "Rotation-based shear failure model for lightly confined RC columns," *Journal of Structural Engineering*, Vol. 138, No. 10, pp. 1267-1278.

Ghannoum, W.M., and Sivaramakrishnan, B., 2012a, *ACI 369 Circular Column Database*, Network for Earthquake Engineering Simulation (NEES), DOI:10.4231/D39Z90B9T.

Ghannoum, W.M., and Sivaramakrishnan, B., 2012b, *ACI 369 Rectangular Column Database*, Network for Earthquake Engineering Simulation (NEES), DOI:10.4231/D36688J50.

Ghannoum, W.M., and Slavin, C.M., 2016, "Low-cycle fatigue performance of high-strength steel reinforcing bars," *ACI Materials Journal*, Vol. 113, No. 6, pp. 803-814.

Hachem, M.M., Mahin, S. A., and Moehle, J. P., 2003, *Performance of Circular Reinforced Concrete Bridge Columns under Bidirectional Earthquake Loading*, PEER Report 2003/06, Pacific Earthquake Engineering Research Center, University of California, Berkeley.

Harajli, M., 2009, "Bond stress-slip model for steel bars in unconfined or steel, FRC, or FRP confined concrete under cyclic loading," *Journal of Structural Engineering*, Vol. 135, No. 5, pp. 509-518.

Hardisty, J.N., Villalobos, E., Richter, B.P., and Pujol, S., 2015, "Lap splices in unconfined boundary elements," *Concrete International*, Vol. 37, No. 1.

Haselton, C.B., Liel, A.B., Taylor-Lange, S.C., and Deierlein, G.G., 2008, *Beam-Column Element Model Calibrated for Predicting Flexural Response Leading to Global Collapse of RC Frame Buildings*, PEER Report 2007/03, Pacific Engineering Research Center, University of California, Berkeley, California.

Haselton, C.B., Liel, A.B., Taylor-Lange, S.C., and Deierlein, G.G., 2016, "Calibration of reinforced concrete beam-columns for simulating seismic response to collapse," *Structural Journal*, Vol. 113, Issue 6, pp. 1141-1152.

Hassan, W.M., 2011, *Analytical and Experimental Assessment of Seismic Vulnerability of Beam-Column Joints without Transverse Reinforcement in*

Concrete Buildings, PhD. Dissertation, University of California, Berkeley, California.

Hwang, S.-J., and Moehle, J.P., 2000, "Models for laterally loaded slab-column frames," *Structural Journal*, Vol. 97, No. 2, pp. 345-352.

Ibarra, L.F., Medina, R.A., and Krawinkler, H., 2005, "Hysteretic models that incorporate strength and stiffness deterioration," *Earthquake Engineering and Structural Dynamics*, Vol. 34, No. 12, pp. 1489-1511.

Ichinose, T., 1995, "Splitting bond failure of columns under seismic action," *Structural Journal*, Vol. 92, No. 5.

Ingham, J.M., Lidell, D., and Davidson, B.J., 2001, "Influence of loading history on the response of a reinforced concrete beam," *Bulletin of the New Zealand Society for Earthquake Engineering*, Vol. 34, No. 2, pp. 107-124.

Jeon, J-S., Lowes, L.N., and DesRoches, R., 2014, *Numerical Models for Beam-Column Joints in Reinforced Concrete Building Frames*, Special Publication SP 297, American Concrete Institute, Farmington Hills, Michigan.

Kaklauskas, G., and Ghaboussi, J., 2001, "Stress-strain relations for cracked tensile concrete from RC beam tests," *Journal of Structural Engineering*, Vol. 127, No. 1, pp. 64-73.

Kang, T.H., and Wallace, J.W., 2005, "Dynamic responses of flat plate systems with shear reinforcement," *Structural Journal*, Vol. 102, No. 5, pp. 763-773.

Kang, T.H-K., Wallace, J.W., and Elwood, K.J., 2009, "Nonlinear modeling of flat-plate systems," *Journal of Structural Engineering*, Vol. 135, No. 2, pp. 147-158.

Kappos, A.J., 1991, "Analytical prediction of the collapse earthquake for R/C buildings: Suggested methodology," *Earthquake Engineering and Structural Dynamics*, Vol. 20, No. 2, pp. 167-176.

Kim, J., and LaFave, J.M., 2007, "Key influence parameters for the joint shear behaviour of reinforced concrete (RC) beam-column connections," *Engineering Structures*, Vol. 29, No. 10, pp. 2523-2539.

Kwak, H.G., and Filippou, F.C., 1990, *Finite Element Analysis of Reinforced Concrete Structures Under Monotonic Load*, Report No. UCB/SEMM-90/14, University of California, Berkeley, California.

Kwon, J., 2016, *Strength, Stiffness, and Damage of Reinforced Concrete Buildings Subjected to Seismic Motions*, University of Texas at Austin, Austin, Texas, p. 239.

Kwon, J., and Ghannoum, W.M., 2016, "Assessment of international standard provisions on stiffness of reinforced concrete moment frame and shear wall buildings," *Engineering Structures*, Vol. 128, pp. 149-60.

LeBorgne, M.R., and Ghannoum, W.M., 2014a, "Analytical element for simulating lateral-strength degradation in reinforced concrete columns and other frame members," *Journal of Structural Engineering*, Vol. 140, No. 7, pp. 1-12.

LeBorgne, M.R., and Ghannoum, W.M., 2014b, "Calibrated analytical element for lateral-strength degradation of reinforced concrete columns," *Engineering Structures*, Vol. 81, pp. 35-48.

Lehman, D., and Moehle, J.P., 2000, *Seismic Performance of Well-Confined Concrete Bridge Columns*, PEER Report No. 1998/01, Pacific Earthquake Engineering Research Center, University of California, Berkeley, California.

Leon, R.T., 1990, "Shear strength and hysteretic behavior of interior beam-column joints," *Structural Journal*, Vol. 87, No. 1.

Lowes, L., and Filippou, F., 2006, *Finite Element Analysis of Reinforced Concrete Structures*, SP-237, American Concrete Institute, Farmington Hills, Michigan.

Lowes, L.N., Moehle, J.P., and Govindjee, S., 2004, "Concrete-steel bond model for use in finite element modeling of reinforced concrete structures," *Structural Journal*, Vol. 101, No. 4.

Mander, J.B., Priestley, M.J.N., and Park, R., 1988, "Theoretical stress-strain model for confined concrete," *Journal of Structural Engineering*, Vol. 114, No. 8, pp. 1804-1826.

McKenna, F., Fenves, G.L., Scott, M.H., and Jeremie, B., 2000, *Open System for Earthquake Engineering Simulation*, Open System for Earthquake Engineering Simulation (OpenSEES), University of California, Berkeley.

Menegetto, M., and Pinto, P.E., 1973, "Method of analysis for cyclically loaded RC plane frames including changes in geometry and non-elastic behavior of elements under combined normal force and bending," *Proceedings*, Symposium on Resistance and Ultimate Deformability of Structures acted on by Well Defined Repeated Loads, International Association for Bridge and Strcutural Engineering (IABSE), pp. 15-22.

Mitra, N., and Lowes, L.N., 2007, "Evaluation, calibration, and verification of a reinforced concrete beam-column joint model," *Journal of Structural Engineering*, Vol. 133, No. 1, pp. 105-120.

Moehle, J.P., 2015, *Seismic Design of Reinforced Concrete Buildings*, 1st Edition, McGraw-Hill Education.

Nagae, T., Ghannoum, W.M., Kwon, J., Tahara, K., Fukuyama, K., Matsumori, T., Shiohara, H., Kabeyasawa, T., Kono, S., Nishiyama, M., Sause, R., Wallace, J.W., and Moehle, J.P., 2015, "Design implications of a large-scale shaking table tests on a four-story reinforced concrete building," *Structural Journal*, Vol. 112, No. 2, pp. 135-146.

Nilson, A.H., 1968, "Nonlinear analysis of reinforced concrete by the finite element method," *ACI Journal Proceedings*, Vol. 65, No. 9.

NIST, 2009, *Research Required to Support Full Implementation of Performance-Based Seismic Design*, NIST GCR 09-917-2, prepared by the Building Seismic Safety Council of the National Institute of Building Sciences for the National Institute of Standards and Technology, Gaithersburg, Maryland.

NIST, 2010, *NEHRP Seismic Design Technical Brief No. 4: Nonlinear Structural Analysis for Seismic Design, A Guide for Practicing Engineers*, NIST GCR 10-917-5, prepared by the NEHRP Consultants Joint Venture, a partnership of the Applied Technology Council and the Consortium of Universities for Research in Earthquake Engineering for the National Institute of Standards and Technology, Gaithersburg, Maryland.

NIST, 2012, *Soil-Structure Interaction for Building Structures*, NIST GCR 12-917-21, prepared by the NEHRP Consultants Joint Venture, a partnership of the Applied Technology Council and the Consortium for Universities for Research in Earthquake Engineering, for the National Institute of Standards and Technology, Gaithersburg, Maryland.

NIST, 2013, *Nonlinear Analysis Research and Development Program for Performance-Based Engineering*, NIST GCR 14-917-27, prepared by the NEHRP Consultants Joint Venture, a partnership of the Applied Technology Council and the Consortium for Universities for Research in Earthquake Engineering, for the National Institute of Standards and Technology, Gaithersburg, Maryland.

NIST, 2016a, *NEHRP Seismic Design Technical Brief No. 1: Seismic Design of Reinforced Concrete Special Moment Frames, A Guide for Practicing Engineers*, NIST GCR 16-917-40, prepared by the NEHRP Consultants Joint Venture, a partnership of the Applied Technology Council and the Consortium of Universities for Research in Earthquake Engineering for the National Institute of Standards and Technology, Gaithersburg, Maryland.

NIST, 2016b, *NEHRP Seismic Design Technical Brief No. 3: Seismic Design of Cast-in-Place Concrete Diaphragms, Chords, and Collectors, A Guide for Practicing Engineers*, NIST GCR 16-917-42 Second Edition, prepared by the NEHRP Consultants Joint Venture, a partnership of the Applied Technology Council and the Consortium of Universities for Research in Earthquake

Engineering for the National Institute of Standards and Technology, Gaithersburg, Maryland.

NIST, 2017, *Guidelines for Nonlinear Structural Analysis for Design of Buildings, Part I – General*, NIST GCR 17-917-46v1, prepared by the Applied Technology Council for the National Institute of Standards and Technology, Gaithersburg, Maryland.

Nojavan, A., Schultz, A.E., Chao, S-H., Haselton, C., Simasathien, S., Palacios, G., and Liu, X., 2014, "Preliminary results for NEESR full-scale RC column tests under collapse-consistent loading protocols," *Proceedings*, Tenth U.S. National Conference on Earthquake Engineering (10NCEE), Anchorage, Alaska.

Nojavan, A., Schultz, A.E., Chao, S., and Haselton, C.B., 2016, "Influence of cross sectional size on seismic performance of RC columns," *Structural Journal*, American Concrete Institute (in press).

Orangun, C.O., Jirsa, J.O., and Breen, J.E., 1977, "Re-evaluation of test data on development length and splices," *Journal of the American Concrete Institute*, Vol. 74, No. 3, pp. 114-122.

Panagiotakos, T.B., and Fardis, M.N., 2001, "Deformations of reinforced concrete members at yielding and ultimate," *Structural Journal*, Vol. 98, No. 2, pp. 135-148.

Panagiotou, M., Visnjic, T., Antonellis, G., Galanis, P., and Moehle, J.P., 2013, *Effect of Hoop Reinforcement Spacing on the Cyclic Response of Large Reinforced Concrete Special Moment Frame Beams*, Report No. 2013/16, Pacific Earthquake Engineering Research Center, University of California, Berkeley, California.

Pantazopoulou, S.J., 1998, "Detailing for reinforcement stability in RC members," *Journal of Structural Engineering*, Vol. 124, No. 6, pp. 623-632.

Park, R., Priestley, M.J., and Gill, W.D., 1982, "Ductility of square-confined concrete columns," *Journal of the Structural Division*, Vol. 108, No. 4, pp. 929-950.

Paulay, T., and Priestley, M. J. N., 1992, *Seismic Design of Concrete and Masonry Structures*, John Wilev and Sons, New York, New York.

Pecknold, D.A., 1975, "Slab effective width for equivalent frame analysis," *ACI Journal Proceedings*, Vol. 72, pp. 135-137.

PEER/ATC, 2010, *Modeling and Acceptance Criteria for Seismic Design and Analysis of Tall Buildings*, PEER/ATC 72-1, prepared by the Pacific Earthquake Engineering Research Center (PEER) and Applied Technology Council (ATC), Redwood City, California.

Pfister, J.F., 1964, "Influence of ties on the behavior of reinforced concrete columns," *ACI Journal Proceedings*, Vol. 61, No. 5, pp. 521-538.

Popovics, S., 1973, "A numerical approach to the complete stress-strain curve of concrete," *Cement and Concrete Research*, Vol 3, No. 5, pp. 553-599.

Priestley, M.J.N., and Park, R., 1987, "Strength and ductility of concrete bridge columns under seismic loading" *Structural Journal*, Vol. 84, No. 1.

Priestley, M.J.N., Verma, R., and Xiao, Y., 1994, "Seismic shear strength of reinforced concrete columns," *Journal of Structural Engineering*, Vol. 120, No. 8, pp. 2310-2328.

Razvi, S., and Saatcioglu, M., 1999, "Confinement model for high-strength concrete," *Journal of Structural Engineering*, Vol. 125, No. 3, pp. 281-289.

Saatcioglu, M., and Razvi, S.R., 1992, "Strength and ductility of confined concrete," *Journal of Structural Engineering*, Vol. 118, No. 6, pp. 1590-1607.

SEAOSC, 2017, *SEAOSC Design Guide - City of Los Angeles Mandatory Earthquake Hazard Reduction in Existing Non-Ductile Concrete Buildings*, Structural Engineering Association of Southern California, Los Angeles, California.

Sezen, H., and Moehle, J.P., 2006, "Seismic tests of concrete columns with light transverse reinforcement," *Structural Journal*, Vol. 103, No. 6, pp. 842-849.

Sezen, H., and Setzler, E.J., 2008, "Reinforcement slip in reinforced concrete columns," *Structural Journal*, Vol. 105, No. 3, pp. 280-289.

Sheikh, S.A., and Uzumeri, S.M., 1982, "Analytical model for concrete confinement in tied columns," *Journal of the Structural Division*, Vol. 108, No. 12, pp. 2703-2722.

Sokoli, D., and Ghannoum, W.M., 2016, "High-strength reinforcement in columns under high shear stresses," *Structural Journal*, Vol. 113, No. 3, pp. 605-614.

Sokoli, D., Shekarchi, W., Buenrostro, E., and Ghannoum, W.M., 2014, "Advancing behavioral understanding and damage evaluation of concrete members using high-resolution digital image correlation data," *Earthquakes and Structures*, Vol. 7, No. 5, pp. 609-626.

Stevens, N.J., Uzumeri, S.M., Collins, M.P., and Will, G.T., 1991, "Constitutive model for reinforced concrete finite element analysis," *Structural Journal*, Vol. 88, No. 1.

Torres, Ll., Lopez-Almansa, F., and Bozzo, L.M., 2004, "Tension-stiffening model for cracked flexural concrete members," *Journal of Structural Engineering*, Vol. 130, No. 8, pp. 1242-1251.

Vecchio, F.J., 1989, "Nonlinear finite element analysis of reinforced concrete membranes," *Structural Journal*, Vol. 86, No. 1.

Vecchio, F.J., and Palermo, D., 2001, "Nonlinear finite element analysis of reinforced concrete: look both ways before crossing," *Finite Element Analysis of Reinforced Concrete Structures*, Special Publication SP-205, American Concrete Institute, Farmington Hills, Michigan.

Wang, Y., 2014, *Effects of web reinforcement discontinuities on the seismic response of structural walls*, Purdue University, West Lafayette, Indiana.

William, K., and Tanabe, T., 2001, *Finite Element Analysis of Reinforced Concrete Structures*, Special Publication SP 205, American Concrete Institute, Farmington Hills, Michigan.

Project Participants

National Institute of Standards and Technology

Steven L. McCabe
Engineering Laboratory (MS8604)
National Institute of Standards and Technology
100 Bureau Drive
Gaithersburg, Maryland 20899

Matthew S. Speicher
Engineering Laboratory (MS8604)
National Institute of Standards and Technology
100 Bureau Drive
Gaithersburg, Maryland 20899

Jay Harris
Engineering Laboratory (MS8604)
National Institute of Standards and Technology
100 Bureau Drive
Gaithersburg, Maryland 20899

Kevin K. F. Wong
Engineering Laboratory (MS8604)
National Institute of Standards and Technology
100 Bureau Drive
Gaithersburg, Maryland 20899

Siamak Sattar
Engineering Laboratory (MS8604)
National Institute of Standards and Technology
100 Bureau Drive
Gaithersburg, Maryland 20899

Applied Technology Council

Jon A. Heintz (Program Manager)
Applied Technology Council
201 Redwood Shores Parkway, Suite 240
Redwood City, California 94065

Veronica Cedillos (Associate Project Manager)
Applied Technology Council
201 Redwood Shores Parkway, Suite 240
Redwood City, California 94065

Ayse Hortacsu (Associate Program Manager)
Applied Technology Council
201 Redwood Shores Parkway, Suite 240
Redwood City, California 94065

Program Committee on Seismic Engineering

Jon A. Heintz (Chair)
Applied Technology Council
201 Redwood Shores Parkway, Suite 240
Redwood City, California 94065

James R. Harris
J.R. Harris & Company
1775 Sherman Street, Suite 1525
Denver, Colorado 80203

Michael Cochran
Thornton Tomasetti
4551 Glencoe Avenue, Suite 350
Marina del Rey, California 90292

James Jirsa
Department of Civil, Architectural and
Environmental Engineering
University of Texas at Austin
301 E. Dean Keeton Street, Stop C1700
Austin, Texas 78712

Roberto Leon
Department of Civil and Environmental Engineering
Virginia Tech
102-D Patton Hall
Blacksburg, Virginia 24061

Stephen Mahin
Department of Civil and Environmental Engineering
University of California, Berkeley
721 Davis Hall
Berkeley, California 94720

James O. Malley
Degenkolb Engineers
375 Beale Street, Suite 500
San Francisco, California 94105

Donald Scott
PCS Structural Solutions
811 First Avenue, Suite 620
Seattle, Washington 98104

Andrew Whittaker
Department of Civil, Structural and Environmental Engineering
University at Buffalo
230 Ketter Hall
Buffalo, New York 14260

Project Technical Committee

Curt Haselton (Project Director)
Haselton Baker Risk Group, LLC
120 W 2nd Street, Suite 3
Chico, California 95928

Wassim Ghannoum
Dept. of Civil and Environmental Engineering
The University of Texas at San Antonio
Building: BSE Room 1.328
One UTSA Circle
San Antonio, Texas 78249

Mahmoud Hachem
Degenkolb Engineers
1300 Clay Street, Suite 900
Oakland, California 94612

John D. Hooper
Magnusson Klemencic Associates
1301 Fifth Avenue, Suite 3200
Seattle, Washington 98101

Santiago Pujol
Bowen Laboratory
Purdue University
1040 South River Road
West Lafayette, Indiana 47907

Project Review Panel

Tony Ghodsi
Englekirk Institutional
888 South Figueroa Street, 18th Floor
Los Angeles, California 90017

Yuli Huang
Arup
560 Mission Street, Suite 700
San Francisco California 94105

Michael Mehrain
Mehrain Naeim International, Inc.
100 Spectrum Center Drive, Suite 900
Irvine, California 92618

Farzad Naeim
Farzad Naeim, Inc.
100 Spectrum Center Drive, Suite 900
Irvine, California 92618

John Wallace
5731C Boelter Hall
Dept. of Civil and Environmental Engineering
University of California, Los Angeles
Los Angeles, California 90095

Kent Yu (ATC Board Contact)
SEFT Consulting Group
4800 SW Griffith Drive, Suite 100
Beaverton, Oregon 97005

Working Group Members

Dustin Cook
Haselton Baker Risk Group, LLC
120 W 2nd Street, Suite 3
Chico, California 95928

Ian McFarlane
Magnusson Klemencic Associates
1301 Fifth Avenue, Suite 3200
Seattle, Washington 98101

Hee Jae Yang
Magnusson Klemencic Associates
1301 Fifth Avenue, Suite 3200
Seattle, Washington 98101